

# ATOMKI

## ANNUAL REPORT

### 2010



INSTITUTE OF NUCLEAR RESEARCH  
OF THE HUNGARIAN ACADEMY OF SCIENCES  
DEBRECEN, HUNGARY

INSTITUTE OF NUCLEAR RESEARCH  
OF THE HUNGARIAN ACADEMY OF SCIENCES  
DEBRECEN, HUNGARY

ANNUAL REPORT  
2010



ATOMKI

*Postal address:*

P.O. Box 51  
H-4001 Debrecen,  
Hungary

*Editors:*

I. Rajta  
E. Leiter

HU ISSN0 0231-3596

## Preface

The Advisory Board of Atomki, appointed by the President of the Hungarian Academy of Sciences paid its first visit to the Institute in 2010. The expertise of the board members (Á. Kiss, A. Jánossy, M.N. Harakeh, J. Räsänen, E. Widmann) matches our main scientific fields. Chaired by Prof. Á. Kiss, the task of the Board is to overview the scientific activities of Atomki.

It is a great honour to Atomki as well that the Debrecen City Council awarded Prof. R.G. Lovas, former director of the institute, the title ‘Honorary Freeman of the City of Debrecen’.

Atomki researchers made significant contribution to almost all our research fields with a total number of publications above 400. The publication activity of nuclear and particle physics was especially strong in 2010.

We inaugurated recently our new meeting room capable of hosting 30 persons, equipped by a High-Definition Videoconference system, Wi-Fi, and beamer. This room is ideal for small-scale workshops as well. The first such workshop was organized on the astrophysical reaction  ${}^3\text{He}(\alpha,\gamma){}^7\text{Be}$  in November.

To promote scientific work among students, Atomki launched its new grant system for undergraduate students and students with BSc wishing to carry out research in the institute. The grant holders are entitled to use the Atomki scientific facilities for their own research, supervised by Atomki members.

The production of the Atomki movie entitled ‘Lab Love’ has been completed. It was presented at the Researchers’ Night in September followed by a round-table discussion with the film makers. It was also broadcast by one of the national TV channels (M1) in November. The movie using animation technique looks at the scientific work and instruments of Atomki from a viewpoint of ignorant helium atoms wandering in the institute. A DVD edition is planned in the near future.

The Atomki Annual Report features this year the Laboratory for Environmental Studies named after Dr. E. Hertelendi, the founder. This ISO certified laboratory is an excellent example of how nuclear analytical methods can help in understanding and protecting our environment.

Last but not least, based on my application the President of the Hungarian Academy of Sciences appointed me the director of Atomki for the period 2011-2015.

Further details of Atomki events, and the back issues of the Annual Reports can be found on our homepage: <http://www.atomki.hu/>

Debrecen, 25 August 2011



Zsolt Fülöp  
Director

# Organizational structure of ATOMKI

<b>Director</b>		
Dr. Zsolt Fülöp D.Sc.		
<b>Deputy Directors</b>		<b>Finance Officer</b>
Dr. Béla Sulik D.Sc.	Dr. József Molnár C.Eng.	Dr. Mária Pálincás
Scientific Secretary: Zoltán Máté, C.Sc. Scientific Secretary: Zsuzsa Trócsányi-Kiss, Ph.D. Knowledge and Technology Translator: Mátyás Hunyadi, Ph.D.		
<b>Scientific Sections</b>		
<ul style="list-style-type: none"> <li>▪ <b>Division of Nuclear Physics</b> (Head: Attila Krasznahorkay, D.Sc.)               <ul style="list-style-type: none"> <li>• Section of Experimental Nuclear Physics (Head: János Timár, D.Sc.)</li> <li>• Section of Ion Beam Physics (Head: István Rajta, Ph.D.)                   <ul style="list-style-type: none"> <li>◦ Nuclear Astrophysics Group</li> <li>◦ Laboratory of Ion Beam Applications</li> </ul> </li> <li>• Section of Theoretical Physics (Head: András Kruppa, D.Sc.)</li> </ul> </li> </ul>		
<ul style="list-style-type: none"> <li>▪ <b>Division of Atomic Physics</b> (Head: Ákos Kövér, D.Sc.)               <ul style="list-style-type: none"> <li>• Section of Atomic Collisions (Head: László Gulyás, D.Sc.)</li> <li>• Section of Electron Spectroscopy and Materials Science (Head: László Kövér, Ph.D.)                   <ul style="list-style-type: none"> <li>◦ Laboratory of Secondary Ion/Neutral Mass Spectrometry</li> </ul> </li> </ul> </li> </ul>		
<ul style="list-style-type: none"> <li>▪ <b>Division of Applied Physics</b> (Head: Sándor Mészáros, C.Sc.)               <ul style="list-style-type: none"> <li>• Section of Environmental and Earth Sciences (Head: Mihály Molnár, Ph.D.)                   <ul style="list-style-type: none"> <li>◦ Hertelendi Laboratory of Environmental Studies</li> <li>◦ Radon Group</li> <li>◦ K-Ar Laboratory</li> <li>◦ QMS Laboratory</li> </ul> </li> <li>• UD - ATOMKI Department of Environmental Physics (Head: István Csige, Ph.D.)</li> <li>• Section of Cyclotron Applications (Head: Ferenc Ditrói, Ph.D.)</li> <li>• Section of Electronics (Head: János Gál, C.Sc.)                   <ul style="list-style-type: none"> <li>◦ Computational Group</li> </ul> </li> </ul> </li> </ul>		
<ul style="list-style-type: none"> <li>▪ <b>Accelerator Centre</b> (Head: Sándor Biri, Ph.D.)               <ul style="list-style-type: none"> <li>• Cyclotron Laboratory</li> <li>• Laboratory of Electrostatic Accelerators</li> <li>• ECR Laboratory</li> <li>• Isotope Separator Laboratory</li> </ul> </li> </ul>		
<ul style="list-style-type: none"> <li>▪ <b>Services</b> <ul style="list-style-type: none"> <li>• Library (Librarian: Mária Nagy)</li> <li>• Accounting (Head: Ibolya Monostori)</li> <li>• Basic Services and Maintenance (Head: István Katona)</li> <li>• Mechanical Workshop (Head: Zoltán Pintye)</li> <li>• Radiation- and Environmental Protection Group (Head: Gábor Dajkó)</li> </ul> </li> </ul>		

## Data on ATOMKI

At present the Institute employs 198 persons. The affiliation of personnel to units of organization and the composition of personnel are given below.

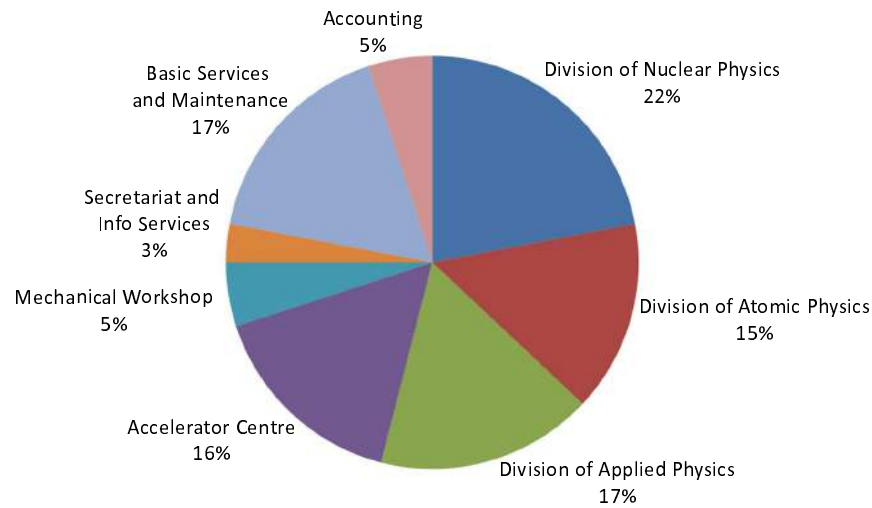


**Figure 1.** Affiliation of personnel to units of organization

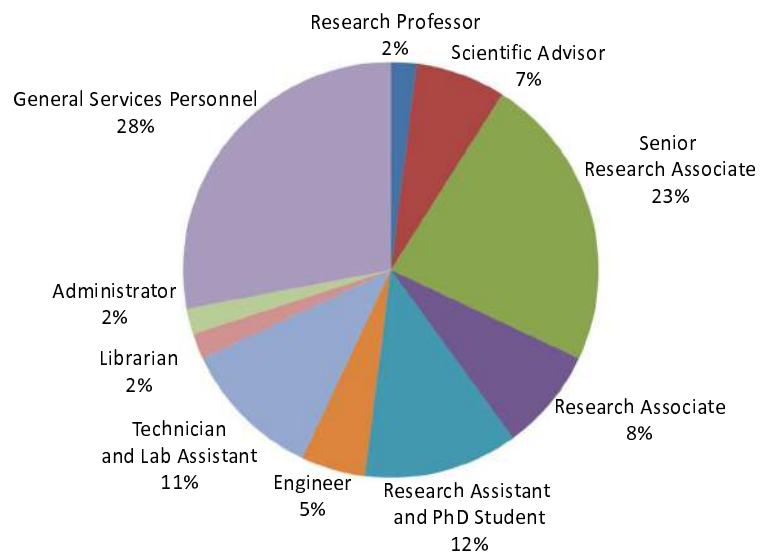


**Figure 2.** Composition of personnel

## **International connections**

Multilateral international programs: 14

Cooperations based on S&T (TÉT) bilateral intergovernmental agreements: 14

Cooperations based on HAS bilateral agreements: 19

Cooperations based on specific collaboration agreements between institutes:

- in nuclear physics and applications with 22 countries in 36 topics
- in atomic physics and applications with 21 countries in 39 topics
- in detection and signal processing technique with 5 countries in 6 topics
- in ion beam analysis with 6 countries in 7 topics
- in environmental research and dating with 11 countries in 13 topics

Membership in international scientific committees: 8

## **Running research projects, grants**

European Research Council (ERC) Starting Grant: 1

Other EU projects: 15

European Organization for Nuclear Research (CERN) projects: 2

International Atomic Energy Agency (IAEA) projects: 2

Intercomparison programs (EURATOM): 2

Hungarian National Research Foundation (OTKA) projects: 12

National Office for Research and Technology (NKTH) projects: 15

## **Higher education activity**

Number of researchers teaching at universities: 35

Number of researchers teaching in doctoral (PhD) schools: 7

Gradual and postgradual teaching: 64 courses, 1033 hours

Number of undergraduate students participating in research work (organized by the Student's Science Association, TDK): 7

Number of students making diploma work: 11

Number of PhD students: 14

Supervision activity by Atomki researchers: 1948 hours

## Finance

The total budget of the Institute for the year 2010 was 1397 million Hungarian Forints income, and 1352 million Hungarian Forints expenses. The composition of the budget and the share of personnel expenditure within the budget are shown below.

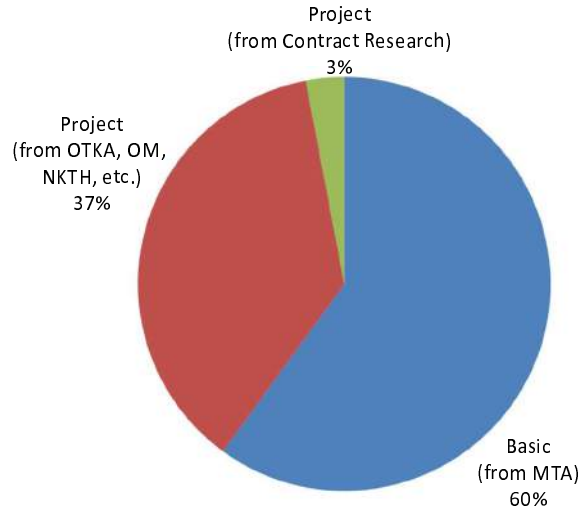


**Figure 3.** Composition of the budget of the Institute  
*MTA: Hungarian Academy of Sciences*  
*OTKA: Hungarian Scientific Research Fund*  
*OM: Ministry of Education*  
*NKTH: National Office for Research and Technology*

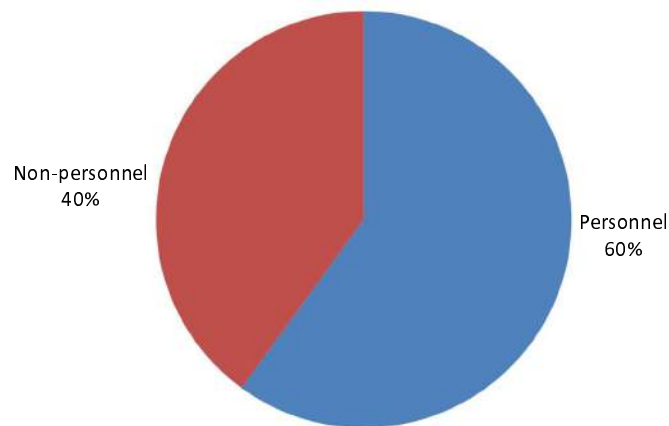


**Figure 4.** Breakdown of expenditure into personnel and non-personnel expenditures

# Table of contents

Preface . . . . .	i
Organizational structure of ATOMKI . . . . .	ii
Data on ATOMKI . . . . .	iii
International connections . . . . .	iv
Running research projects, grants . . . . .	iv
Higher education activity . . . . .	iv
Finance . . . . .	v
Table of contents . . . . .	vi

## Featured:

Hertelendi Laboratory of Environmental Studies . . . . .	1
--	---

## 1. General Physics

1.1 Asymptotic properties of solvable $\mathcal{PT}$ -symmetric potentials . . . . .	30
--	----

## 2. Particle Physics

2.1 Renormalization of $\text{QCD}_2$ . . . . .	31
2.2 Phase Structure and Compactness . . . . .	32

## 3. Nuclear Physics

3.1 Total reaction cross sections from elastic $\alpha$ -nucleus scattering angular distributions around the Coulomb barrier . . . . .	33
3.2 Nuclear structure study of $^{19,21}\text{N}$ nuclei by $\gamma$ spectroscopy . . . . .	34
3.3 Parameters of the isobar analog resonance in complex optical potential . . . . .	36
3.4 Towards a high precision astrophysical S-factor measurement for the $^3\text{He}+^4\text{He}$ reaction . . . . .	37
3.5 Alpha-induced reaction cross section measurements on $^{151}\text{Eu}$ for the astrophysical $\gamma$ -process . . . . .	38
3.6 Shell or cluster structure . . . . .	39
3.7 Observation of $\gamma$ -band structure in $^{104}\text{Pd}$ . . . . .	40
3.8 Rotational band structure of the chiral candidate $^{134}\text{Pr}$ . . . . .	41
3.9 Electric dipole moments in $^{230,232}\text{U}$ and implications for tetrahedral shapes . . . . .	42
3.10 High resolution study of SDR in $^{40}\text{Sc}$ isotope . . . . .	43
3.11 Determination of conversion coefficients in low-energy $\gamma$ rays of $^{132}\text{La}$ . . . . .	44
3.12 Mass and angular distribution of the fission fragments from $^{236}\text{U}$ hyperdeformed states studied with a new fission fragment detector called OBELISK . . . . .	45
3.13 Target structure induced suppression of the ionization cross section for very low energy antiproton-hydrogen collisions . . . . .	46
3.14 Ionization of the hydrogen atom by short half-cycle pulses: dependence on the pulse duration . . . . .	47
3.15 Ionization of the water by intense ultrashort half-cycle electric pulses . . . . .	48
3.16 The Newcomb–Benford law and nuclear half-lives . . . . .	49

<b>4. Atomic and Molecular Physics</b>	
4.1 Classical trajectory Monte Carlo model calculations for ionization of atomic hydrogen by 75 keV proton impact . . . . .	50
4.2 Two-electron cusp in the double ionization of helium . . . . .	51
4.3 L <sub>3</sub> -subshell alignment of Au and Bi in collisions with 12–55-MeV carbon ions . . . . .	52
4.4 Ab initio treatment of charge exchange in H <sup>+</sup> + CH collisions . . . . .	53
4.5 Studying the electron components of the ECR plasma by plasma photographs . . . . .	54
4.6 The development of an electrostatic spectrometer for low energy ions . . . . .	55
4.7 Effusive molecular gas jet target for molecule fragmentation experiments . . . . .	56
4.8 A new VdG-5 beamline for studying ion-atom and ion-molecule collisions . . . . .	57
4.9 Guided transmission of Ne <sup>7+</sup> ions through nanocapillaries in polymers: Dependence on the capillary diameter . . . . .	58
4.10 Ion guiding accompanied by formation of neutrals in PET polymer nanocapillaries: Further insight into a self-organizing process . . . . .	59
4.11 Emission of H <sup>-</sup> fragments from collisions of OH <sup>+</sup> ions with atoms and molecules . . . . .	60
<b>5. Condensed Matter</b>	
5.1 Determination of hydrogen concentration in a-Si and a-Ge layers by elastic recoil detection analysis . . . . .	61
5.2 Effect of temperature on the mutual diffusion in Ge/GaAs and GaAs/Ge systems . . . . .	62
5.3 Depth profile analysis of solar cells by Secondary Neutral Mass Spectrometry using conducting mesh . . . . .	63
5.4 AR-HAXPES for determining Effective Attenuation Length of electrons . . . . .	64
<b>6. Materials Science and Analysis</b>	
6.1 Transmission of electrons through a single glass macrocapillary: energy dependence . . . . .	65
6.2 Time dependence of electron transmission through a single glass macrocapillary . . . . .	66
6.3 Thin Layer Activation Technique under the Free Handling Limit . . . . .	67
6.4 Optical properties of silver thin films, derived from REELS . . . . .	68
6.5 Interaction potentials for fast atoms in front of Al surfaces probed by rainbow scattering . . . . .	69
<b>7. Earth and Cosmic Sciences, Environmental Research</b>	
7.1 Groundwater dating down to the milliliter level . . . . .	70
7.2 Rapid graphite target preparation with sealed tube zinc reduction method for C-14 dating by MICADAS . . . . .	71
7.3 Investigation of radioisotopes in different organisms around Paks NPP . . . . .	72
7.4 Development of procedure for the separation of <sup>107</sup> Pd from L/ILW radioactive waste material produced by the Hungarian NPP . . . . .	73
7.5 Advancing the use of noble gases in fluid inclusions of speleothems as a palaeoclimate proxy: method and standardization . . . . .	75
7.6 A 9-year old record and analysis of stable isotope ratios of precipitation in Debrecen . . . . .	76
7.7 Investigation of indoor aerosols at educational institutions in Debrecen, Hungary . . . . .	77
7.8 Study of emission episodes of urban aerosol by ion beam analytical techniques . . . . .	78
7.9 Study of the sap flow and related quantities of oak trees in field experiments . . . . .	79

<b>8. Developments of Methods and Instruments</b>	
8.1 Status Report on the Accelerators Operation . . . . .	80
8.2 Laboratory background in an escape-suppressed germanium $\gamma$ -ray detector at a shallow underground laboratory . . . . .	83
8.3 Beam divergence of the proton microprobe . . . . .	84
8.4 The CHARISMA project in ATOMKI . . . . .	85
<b>9. Appendix</b>	
9.1 Events . . . . .	86
9.2 Hebdomadad Seminars . . . . .	87
9.3 Awards . . . . .	89
9.4 List of Publications . . . . .	90
9.4.1 Highlights . . . . .	90
Nanochannel alignment analysis by scanning transmission ion microscopy . . . . .	91
Interference effect in the dipole and nondipole anisotropy parameters of the Kr $4p$ photoelectrons in the vicinity of the Kr $(3d)^{-1} \rightarrow np$ resonant excitations . .	92
An exactly solvable Schrödinger equation with finite positive position-dependent effective mass . . . . .	93
Reactor Decay Heat in $^{239}\text{Pu}$ : Solving the $\gamma$ Discrepancy in the 4-3000-s Cooling Period	94
Author index . . . . .	95

# Hertelendi Laboratory of Environmental Studies

É. Svingor, M. Molnár, L. Palcsu, I. Futó, L. Rinyu, M. Mogyorósi, Z. Major, Á. Bihari, G. Vodila, R. Janovics, L. Papp, I. Major

## 1 INTRODUCTION

The Hertelendi Laboratory for Environmental Studies (HEKAL) belongs to the Section of Environmental and Earth Sciences. It is a multidisciplinary laboratory dedicated to environmental research, to the development of nuclear analytical methods and to systems technology. During its existence of more than 15 years it has gained some reputation as a prime laboratory of analytical techniques, working with both radio- and stable isotopes [1]. It has considerable expertise in isotope concentration measurements, radiocarbon dating [2, 3, 4, 5], tritium measurements [6, 7, 8], in monitoring radioactivity around nuclear facilities and in modelling the movement of radionuclides in the environment. Many of its projects are within the scope of interest of the Paks Nuclear Power Plant [9].

Our research activity is mainly concerned with the so-called environmental isotopes. This term denotes isotopes, both stable and radioactive, that are present in the natural environment either as a result of natural processes or of human activities. In environmental research isotopes are generally applied either as tracers or as age indicators. An ideal tracer is defined as a substance that behaves in the system studied exactly as the material to be traced as far as the examined parameters are concerned, but has at least one property that distinguishes it from the traced material. The mass number of an isotope is such an ideal indicator.

In 2007 the laboratory assumed the name of Dr. Ede Hertelendi to honour the memory of the reputed environmental physicist who founded the group and headed it for many years [10]. The current core of the laboratory staff is made up of his pupils and coworkers. This team was like a family to him. The group owes it to his fatherly figure that it did not fall apart after his death, but advanced with intense work and tenacity during the last decade. One of his first pupils, Mihály Veres returned to the laboratory as a private entrepreneur and investor in 2005, and in the framework of a long-term cooperation contract he has significantly contributed to the progress of HEKAL. Its equipment is now as advanced as that of any modern environmental research centre in Europe, and it has been awarded the status of a strategically important research laboratory in the National Research Infrastructure Register (see HEKAL at <https://regiszter.nekifut.hu>).



## 2 METHODS

### 2.1 Stable isotope and noble gas mass spectrometry

The various isotopes of an element have slightly different chemical and physical properties due to their mass differences. For elements of low atomic numbers, these mass differences are large enough for many physical, chemical, and biological processes or reactions to “fractionate” or change the relative proportions of various isotopes. Two different types of

processes – equilibrium and kinetic isotope effects – cause isotope fractionation. As a result of fractionation processes, waters and solutes as well as living organisms often develop unique isotopic compositions (ratios of heavy to light isotopes) that may be indicative of their source or of the processes that formed them. These differences or changes are small but reliably detectable with specialised mass spectrometric techniques. They are normally reported as “delta” ( $\delta$ ) values in parts per thousand (‰) enrichments or depletions relative to a standard of known composition.  $\delta$  values are calculated by  $\delta(\text{in } \text{‰}) = (R_{\text{sample}}/R_{\text{standard}} - 1)1000$ , where “R” is the ratio of the heavy to light isotope in the sample or standard.



Stable isotope ratios of the life science elements carbon, hydrogen, oxygen and nitrogen vary slightly, but significantly in major compartments of the Earth. The small changes reflect natural fractionation processes that have left their signature in natural archives. Making us enable to investigate the climate of past times in order to understand how the Earth’s climatic system works and how it can react to external forces. In addition, studying contemporary isotopic change of natural compartments can

help to identify sources and sinks for atmospheric trace gases. Water isotope data provide key information about past and present global climate and the global water cycle. Quantitative evidence for past changes in global water balance and climate is found in the stable isotope chronologies preserved in non-marine archives, ranging from detailed time-series of paleoprecipitation stored in glaciers to the records of meteoric waters preserved in ground water, speleothems, lake sediments, tree rings and other materials. Crucial isotopic records of very recent and ongoing hydrologic and climatic change also exist in the form of contemporary observational data, derived from sampling and isotopic analysis of meteoric waters over the past few decades. These data provide fundamental information about the global water budget and help to validate atmospheric general circulation models (GCMs).

Biological processes are generally unidirectional and are excellent examples of “kinetic” isotope reactions. Organisms preferentially use the lighter isotopic species because of the lower energy “costs”, resulting in significant fractionations between the substrate (heavier) and the biologically mediated product (lighter). The magnitude of the fractionation depends on the reaction pathway utilized and the relative energies of the bonds being severed and formed by the reaction. For example, during photosynthesis, the carbon that becomes fixed in plant tissue is significantly depleted in  $^{13}\text{C}$  relative to the atmosphere. The  $\delta^{13}\text{C}$  of plants and organisms can provide useful information about sources of nutrients and food web relations, especially when combined with analyses of  $\delta^{15}\text{N}$  and/or  $\delta^{34}\text{S}$ .

Besides stable isotopes of the most abundant elements, noble gases can help us understanding special processes in geoscience. Although, noble gases are widely used in geochemistry, so far we use them only in several fields of isotope hydrology and palaeoclimate reconstruction. Since the solubility of gases are temperature dependent, the recharge temperatures at which water infiltrates the surface can be revealed with noble gas concentrations dissolved in groundwater samples. These so called noble gas temperatures can be used to reconstruct past prevailing temperatures from representative and dated groundwater samples of a suitable confined or semi-confined aquifer (see chapter 3.2.1). Recently, we try to apply this method for tiny water amount of fluid inclusions of speleothems (see chapter

3.2.2). Dating recent shallow groundwater or surface water layers, one of the most effective way is tritium and its daughter  $^3\text{He}$ , which method is known as  $^3\text{H}$ - $^3\text{He}$  dating. It requires precise tritium as well as helium isotope measurements. In our noble gas laboratory tritium concentrations of water, and recently, of other substances are determined via the mass spectrometric measurement of the daughter of tritium. This sensitive technique has been used for more than a decade. In fact, an isotope dilution procedure developed by us for low level tritium measurements has brought us to the frontline of the analytical community (see chapter 3.3.3). Noble gases can be used not only in geoscience but in nuclear industry as well. For many years we have been studying stable krypton and xenon isotopes of fission origin found in the primary circuit of the nuclear power plant. Examining these isotope abundances fuel element failures can be detected.

Our noble gas measurements are performed with a VG5400 (Fisons Instruments, now Thermo Scientific) noble gas mass spectrometer which is an allmetal, statically operated,  $90^\circ$  sector field mass spectrometer with 54 cm extended geometry. The mass spectrometer is suitable for determination of isotope ratios of all stable noble gases. This is the first noble gas mass spectrometer in Hungary which has the sensitivity, accuracy and resolution required by various important fields of research,

like environmental research, nuclear fission safety, waste disposal and geochronology. The sample inlet line is equipped with pneumatically activated high vacuum valves controlled by a computer. The line is made of stainless steel with UHV connections (VCR) with copper gaskets. The line includes two cryogenic cold heads, three turbomolecular pumps with fore-vacuum pumps for evacuating the purification section, and one ion pump for the inlet section. This provides a high vacuum in the system ( $<10^{-8}$  mbar). The sensitivity of the noble gas mass spectrometer is  $1 \cdot 10^{-3}$  A/mbar for Ar and  $2 \cdot 10^{-4}$  A/mbar for He. The resolution is adjusted to 600, which is sufficient for the resolution of  $^3\text{He}^+$ ,  $\text{H}_3^+$  and  $\text{HD}^+$  molecule ion beams. The abundance sensitivity measured as contribution from mass 40 at mass 39 is less than 0.5 ppm at  $10^{-7}$  mbar. The static vacuum level in the 1.7 l volume deflection chamber is  $1 \times 10^{-12}$  cm<sup>3</sup> STP/min at mass 40.



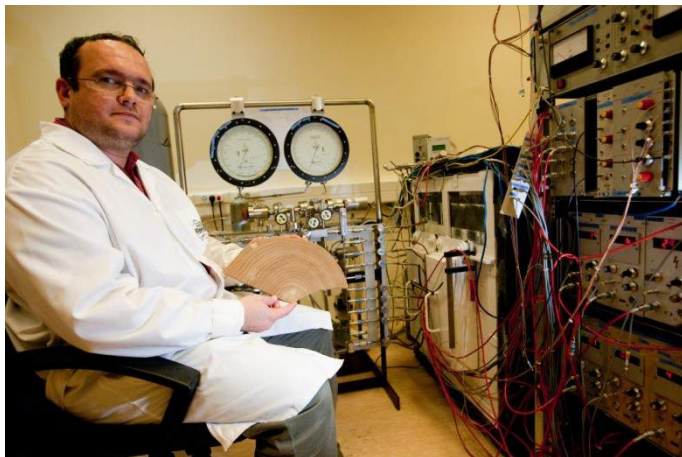
like environmental research, nuclear fission safety, waste disposal and geochronology. The sample inlet line is equipped with pneumatically activated high vacuum valves controlled by a computer. The line is made of stainless steel with UHV connections (VCR) with copper gaskets. The line includes two cryogenic cold heads, three turbomolecular pumps with fore-vacuum pumps for evacuating the purification section, and one ion pump for the inlet section. This provides a high vacuum in the system ( $<10^{-8}$  mbar). The sensitivity of the noble gas mass spectrometer is  $1 \cdot 10^{-3}$  A/mbar for Ar and  $2 \cdot 10^{-4}$  A/mbar for He. The resolution is adjusted to 600, which is sufficient for the resolution of  $^3\text{He}^+$ ,  $\text{H}_3^+$  and  $\text{HD}^+$  molecule ion beams. The abundance sensitivity measured as contribution from mass 40 at mass 39 is less than 0.5 ppm at  $10^{-7}$  mbar. The static vacuum level in the 1.7 l volume deflection chamber is  $1 \times 10^{-12}$  cm<sup>3</sup> STP/min at mass 40.

## 2.2 Radiocarbon dating and environmental studies ( $^{14}\text{C}$ )

Radiocarbon generated by cosmic rays in the atmosphere is a cosmogenic radioactive carbon isotope with a half-life of 5730 years. The formed  $^{14}\text{C}$  is rapidly oxidised to  $^{14}\text{CO}_2$  and enters the Earth's plant and animal lifeways via photosynthesis and the food chain. The rate of the dispersal of  $^{14}\text{C}$  into the atmosphere has been demonstrated by measurements of radioactive carbon produced from thermonuclear bomb testing.  $^{14}\text{C}$  also enters the Earth's oceans in an atmospheric exchange and as dissolved carbonate.

Plants and animals which utilise carbon in biological foodchains take up  $^{14}\text{C}$  during their lifetimes. They exist in equilibrium with the  $^{14}\text{C}$  concentration of the atmosphere, that is, the numbers of  $^{14}\text{C}$  atoms and non-radioactive carbon atoms stays approximately the same over time. As soon as a plant or animal dies, the metabolic function of carbon uptake ceases; there is no replenishment of radioactive carbon, only decay. Measuring the  $^{14}\text{C}$  concentration or residual radioactivity of a sample whose age is not known, comparing this with modern

levels of activity (1890 wood corrected for decay to 1950 AD) and using the known half-life it becomes possible to calculate a date for the death of the sample. This is the basis of the radiocarbon method developed by a team of scientists led by W. F. Libby in immediate post-WW2 years. Libby later received the Nobel Prize in Chemistry in 1960: *“for his method to use Carbon-14 for age determinations in archaeology, geology, geophysics, and other branches of science.”*



In the 1950s, measurements on samples of known ages, pointed to radiocarbon dates which were younger than expected. Researchers measuring the radioactivity of tree rings with known age found fluctuations  $^{14}\text{C}$  concentration up to a maximum of  $\pm 5\%$  over the last 1500 years. This necessitated the calibration of radiocarbon dates to other historically aged material. Radiocarbon dates of sequential dendrochronologically aged trees, then corals and speleothems

dated by U/Th method have been measured to produce a calendrical/radiocarbon calibration curve which extends back now over 50 000 years. This enables radiocarbon dates to be calibrated to solar or calendar dates. And, as a spin-off, we have got a database of the atmospheric radiocarbon over the last 50 000 years, which is a comprehensive source of data for atmospheric and ocean general circulation models. The  $^{14}\text{C}$  technique has become a very important and useful tool widely applied in environmental protection, archaeology, geology, hydrology, climatology, atmospheric science, oceanography and many other essential scientific fields all over the world. The radiocarbon method requires special techniques since very low and weak  $\beta$  activities have to be measured with very high precision. The major developments in the radiocarbon method involve improvements in measurement techniques and research into the dating of different materials.

### **2.3 Environmental monitoring of nuclear facilities**

An important aim of environmental research is to monitor and to study the impact of nuclear facilities on the environment. Nuclear power plants and radioactive waste disposals might emit radioactive isotopes which abundances exceed the natural level. To detect these increased levels creative sampling methods as well as state-of-the-art sample preparation and measurement techniques are required.

For more than 20 years radiocarbon and tritium content of atmospheric  $\text{CO}_2$ , water vapour, hydrocarbons and hydrogen have been continuously monitored around the nuclear power plant of Paks, Hungary (see chapter 3.2.6). Our laboratory developed the first differential radiocarbon and tritium samplers that take integrated samples from the ambient air. Nowadays, further developed samplers have been running for many years. Although the tritium content of these samples are measured by the laboratory of the nuclear power plant, radiocarbon concentrations are determined by our gas proportional counter system, since those low activities need to be measured by sensitive methods. In 2000, we purchased a high purity germanium detector with beryllium window which is able to detect low-energy gamma photons ( $>10$  keV). The gamma-detector has been placed into a low background laboratory; moreover it is shielded by a lead house making it possible to sensitively determine low level radioisotopes from environmental samples. Besides air monitoring, the groundwater has got into our interest. An automatic groundwater sampling device has been developed in order to

separately take anions and cations by means of ion exchange resins (see chapter 3.3.1). Having eluted the ions from the resins, cations are measured by gamma-spectrometry.

In 2000, we started investigating the impact of the radioactive waste disposal in Püspökszilágy on the groundwater. Since then thousands of groundwater and air samples for  $^3\text{H}$ ,  $^{14}\text{C}$ ,  $^{90}\text{Sr}$  and water chemistry have been measured. The results are the basis of a transport model that describes how radioisotopes could spread with the groundwater if they were getting out from the disposal. This work proceeds continuously in the next years which is essential for a safe operation of the radioactive waste disposal facility. In the frame of this work, a liquid scintillation counter was installed, firstly to determine tritium concentrations above natural level, although later on, due to methodological developments the measurements of additional radioisotopes have also been involved.

In addition to environmental samples, hardly-to-measure isotopes from low and intermediate level radioactive waste are also determined in our laboratory. These samples include ion exchange resins, evaporate residues from the primary circuit of the nuclear power plant. Numerous chemical extraction procedures have been adopted and developed to separate different radioisotopes of interest from the relatively high radioactive isotope abundance. The radioactivity of the final samples are measured either gamma-spectrometrically (for example:  $^{129}\text{I}$ ,  $^{60}\text{Co}$ ,  $^{134,137}\text{Cs}$ ) or with the liquid scintillation counters (e.g.  $^3\text{H}$ ,  $^{14}\text{C}$ ,  $^{36}\text{Cl}$ ,  $^{90}\text{Sr}$ ,  $^{99}\text{Tc}$ ). During the storage of low and intermediate level radioactive waste (L/ILW) significant quantities of gas may be produced, therefore, the measurement of gas mixing ratios from the headspace of radioactive waste drums was started by a quadrupole mass spectrometer (QMS). To obtain reliable estimations of the quantities and rates of the gas production in L/ILW, in 2000 a series of measurements was carried out on numerous waste packages produced and temporarily stored at the site of Paks Nuclear Power Plant (NPP). For further analysis, in 2004 additional ten drums filled with selected original L/ILW were placed into hermetic containers equipped with sampling valves for repeated sampling. The mass spectrometric measurements complemented with isotope analyses on specific compounds allowed us to determine gas generation rates, and to study which chemical and physical processes produce these gases, what sources and sinks are available (see chapter 3.2.8). Gas mixing ratio measurements with QMS have also been executed in the cooling ponds of the nuclear power plant since 2004, thus underwater gas generation, mainly hydrogen generation has been revealed (see chapter 3.3.8).



### 3 RECENT DEVELOPMENTS AND RESULTS

Here we give a report about our most relevant and important studies from the last decade using them as examples showing the wide range of research fields where the interdisciplinary research and development activity of HEKAL is focused.

### 3.1 Dating using different isotopes

#### 3.1.1 Archeology – New radiocarbon dates for the Baden culture

In 2001–2002, a settlement of the Baden culture was excavated in the vicinity of Balatonöszöd. During the rescue excavation along the M7 highway, in an area of 100,000 m<sup>2</sup>, 2800 pits dug into the subsoil, 320 hearths, and cultural layers rich in material were discovered. The material of the Baden culture represents phases IB–IC (Boleraz), IIA (Transitional), IIB–III (Early Classical) according to Němejcová-Pavúková's (1981, 1998) typological system. We took 20 samples from the large number of human and animal skeletons for radiocarbon dating, of which 16 measurements were successful. These results provide absolute dates for a Baden culture settlement with the longest occupation and the largest excavated surface in Hungary. This provides an opportunity to review the chronological position of the Baden culture, with special emphasis on its beginning and end (Figure 1) [11].

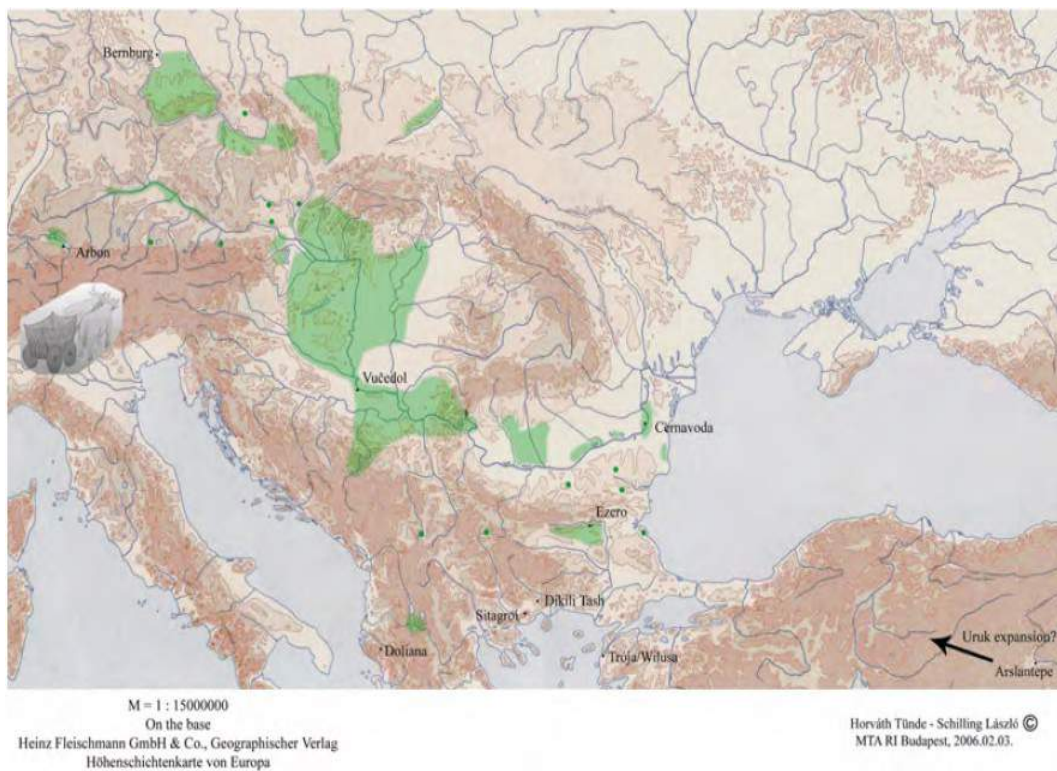


**Figure 1.** Distribution map of the Baden culture. Prepared by Tünde Horváth and László Schilling, based on the partial maps of Roman (2001).

#### 3.1.2 Archeometry - C-14 dating of the first permanent wooden bridge over the River Tisza

Given the non-monotonic form of the radiocarbon calibration curve, the precision of single <sup>14</sup>C dates on the calendar timescale is limited. However, radiocarbon dating combined with dendrochronology enabled us to date the timbers found in River Tisza during the dry period of summer 2003 (Figure 2).

Routine preparation of wood samples gave radiocarbon results spread over four centuries. Instead, dating alpha-cellulose two different, relatively narrow historical time periods were obtained: the first period (1505-1595 AD and 1612-1673 AD, respectively) coincides with the Turkish occupation period, while the second interval (1733-1813) obtained in case of two samples does not exclude the existence of another bridge constructed later.

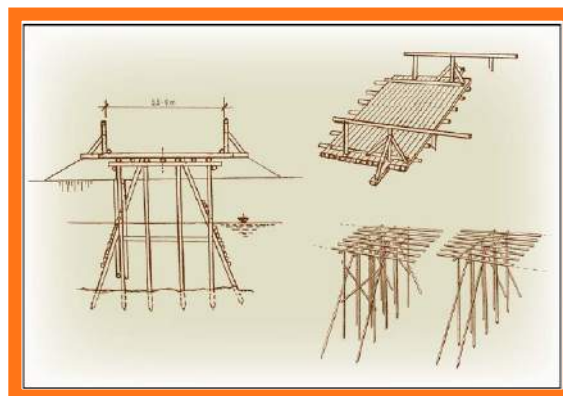


**Figure 2.** Engraving of Georgius Houfnaglius dated 1617 and representing the town of Szolnok with bridge over the River Tisza and the River Zagyva connecting at the same time both the town and the fortress

The dendrochronological data confirmed the bridge was constructed from oak timbers felled between 1558 and 1565. The radiocarbon and the dendrochronological dates harmonise with the date of the letter written in 1562 by Antal Verancsics, Bishop of Eger, mentioning the construction of the first bridge. As conclusion, the archaeological excavation revealed the proof of the first wooden bridge over River Tisza, Hungary [12]

### 3.1.3 Geological dating - Radiocarbon dating of the last volcanic eruption of the Ciomadul volcano.

The last volcanic eruption in the Carpathian-Pannonian Region occurred within the Ciomadul volcano, Southeast Carpathians. It is a lava dome complex active for about 900 ka. Following the effusive activity, at least two major explosive volcanic eruptions occurred forming two craters (Mohos and St. Anna). These eruptions resulted in pumiceous pyroclastic fall and flow deposits. In order to understand the behavior of this volcano and evaluate the possible renewal of the volcanic eruption, it is crucial to constrain the length of the active and repose periods and know the date of the last eruption.

The former K/Ar and radiocarbon data are controversial and give only a rough estimate for the active phases. The age data for the last eruption is in the range from 10000 and 40000 yr BC. In this study, we focus on the time of the last volcanic eruptions. We analyzed charcoal fragments found in pumiceous pyroclastic flow deposits from two localities. C14 dating from the first locality (Bx) was executed by GPC technique in the ATOMKI, and the following five dating (one repeated dating of the ATOMKI sample, with excellent match; one resampled charcoal from the first locality, and one sample from a second locality (Tf), and dating of NaOH-soluble fractions coming from sample prep for all the three charcoal samples) in NSF Lab in Tucson, Arizona (USA) by AMS technique [13].

The new radiocarbon data provided valuable information on the behaviour of the Ciomadul volcano and help to constrain the time of the last eruption of the volcano. The main conclusions are the following:

1. The last volcanic eruption occurred at about 27000 BP
2. The product of the youngest eruption is exposed at the southern margin of the volcano (Bx locality) and not at west (Tf locality) as was previously thought.
3. A striking new result is that there were at least two major explosive eruptions, not a single one, related to the formation of the St. Anna crater. The youngest one followed another subplinian eruption after about 10 ka quiescence period.
4. Further dating for the time of the older eruptions is crucial to understand the nature of the volcano and to evaluate the characteristic repose time of Ciomadul.

These data are consistent with the different composition of the volcanic products from the two localities. This study is part of the research project supported by the OTKA grant # K68587.



**Figure 3.** St. Anna crater lake (up), and the Ciomadul lava dome complex (down).

### 3.1.4 Ice-dating and ice-formation study using the tritium bomb-peak

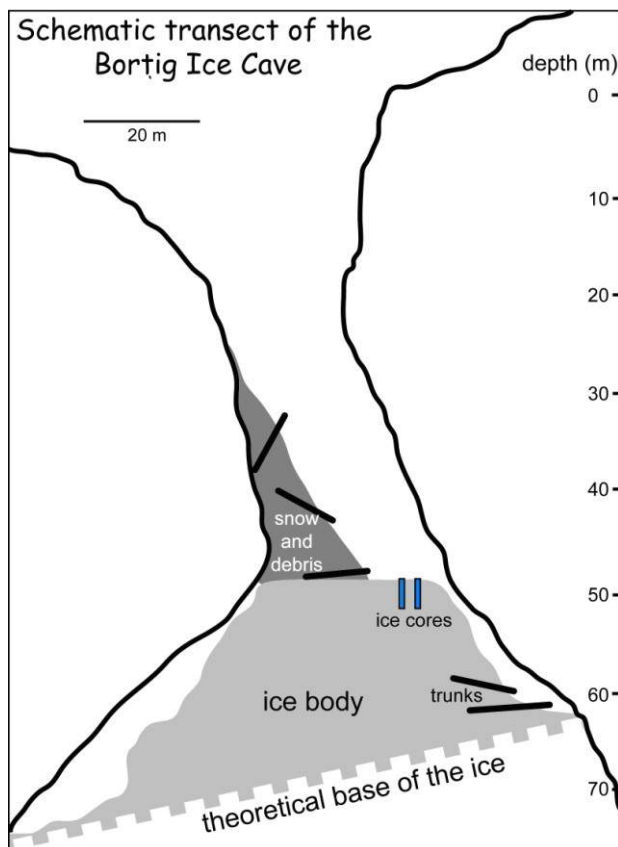


**Figure 4.** Schematic transect of the Bortig Ice Cave. Approximate place of extracted cores are indicated.

Validation of cave ice in paleoclimatology is mainly criticised due to the episodically appearing multiannual negative mass balance periods. Not only the total amount of increment is destructed during these periods but previously deposited ice could also be destroyed creating longer hiatus in the stratigraphy than the melting period. Bortig Ice Cave is the third largest ice cave of the Apuseni Mountains, Romania. The main shaft has approximately 45 m depth to the ice surface; the ice thickness is estimated to be 20 m (Figure 4). The cave contains about 25000 m<sup>3</sup> of ice. We decided surveying and estimating the age and ascertain the potential gaps of the upper ice layers in Bortig Ice Cave.

We have chosen the anthropogenic bomb-peak of tritium (<sup>3</sup>H) concentration as reference horizon, because it has a well-known and distinct maximum in the atmospheric precipitation at June of 1963 according the “nuclear silence” on the Northern Hemisphere. We extracted ice cores with approx. length of 2 metres from Bortig Ice Cave on 11<sup>th</sup> and 12<sup>th</sup> of December 2005.

Sequence of ice layers with different physical properties within the cores was recorded. The core profile suggested that a less dense, grainy ice and a denser, transparent ice layer coupling together and form one higher order stratigraphic unit. The tritium activity was measured on water melted from the twenty samples of BA core (from BA-1 to BA-20) using liquid scintillation technique in the ATOMKI. The resulted activities suggest the position of the raised tritium concentration from the year of 1963 is between 81 and 102 cm below the ice surface at the drilling date (Figure 5).

Following some calculation we predict that the position of the tritium peak is probably at 95 cm below the ice surface. In addition, we argue that the higher order stratigraphic units represents the annual increment at the Bortig Ice Cave. Finally, we have ascertained three periods since 1950 with different ice accumulation rates: 1 cm/a for 1992-2005; 2.8 cm/a for 1963-1992; and even higher than the latter during the 1953-1963 period [14].

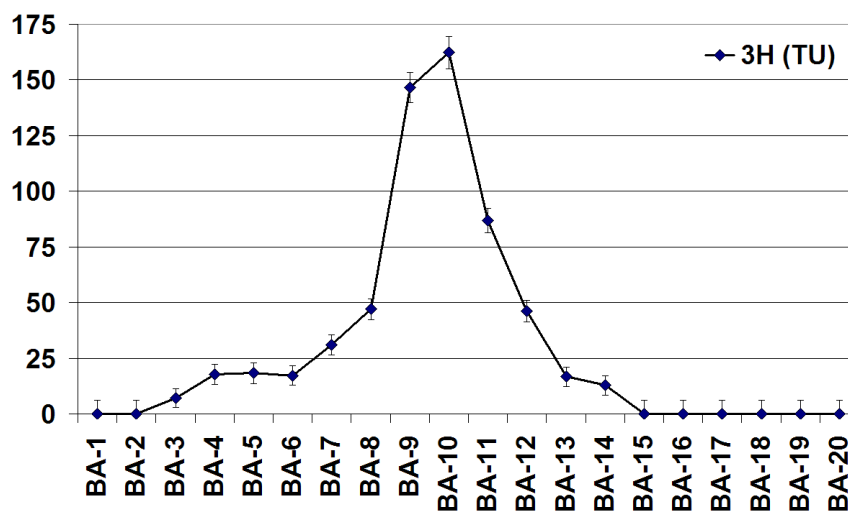
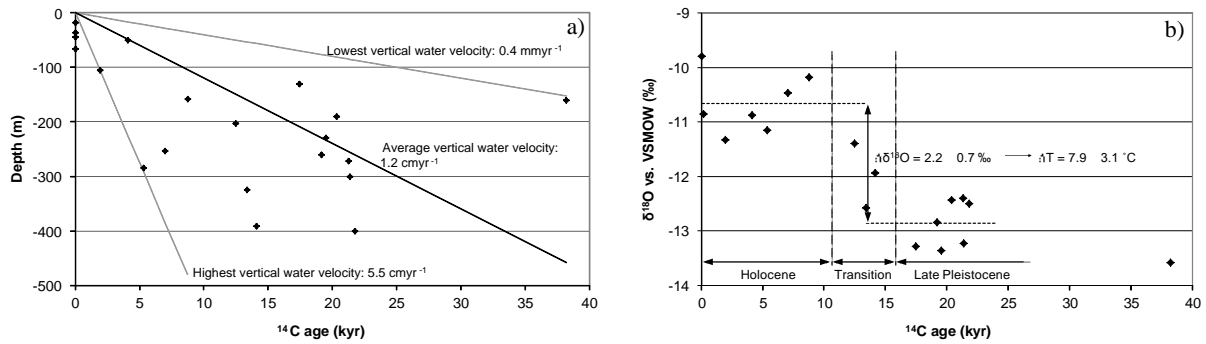


Figure 5. Tritium “bomb-peak” in the BA core.

### 3.1.5 Groundwater/aquifer dating and study by multi isotope techniques

In a frame of a large research project in Hungary to find the most suitable territory for a low and intermediate level radioactive waste repository, we investigated a fractured rock aquifer. A granite massif located near Bataapati, between Mecsek Mountains and Szekszardi Hills seems to be the best geological formation for the place of a potential repository. We performed isotope analyses and data interpretations to define the groundwater-flow system. The granite rock of Carboniferous age is covered by 30–70 metres thick Holocene and Pleistocene sediments. The sediment is mostly aquitard with several infiltration zones. The peripheral part of the granite body is more fractured than the inner part. The properties of the flow system were investigated by isotope measurements of groundwater samples from boreholes. Tritium content,  $\delta$ -values and radiocarbon ages show that Holocene waters appear in the upper and peripheral part of the granite body, and glacial, pre-glacial waters are present in the deeper part of the bulk. The vertical water movement is only a few  $\text{cm}\cdot\text{yr}^{-1}$  (Figure 6a).

Based on isotope examination of groundwater, one can conclude that this field is suitable for repository from hydrogeological point of view. Additionally, based on the stable isotope signatures and the ages of the groundwater samples, we also find that the warming due to climate change after the last ice age was  $7.9\pm 1.5$  °C (Figure 6b) [15].



**Figure 6.** a) Radiocarbon ages versus depth, and the vertical component of the groundwater velocity. b) The changing of  $\delta^{18}\text{O}$  during the transition of Holocene and Pleistocene can be used to calculate the climate cooling in the Last Glacial Maximum compared to the Holocene.

### 3.2 Environmental protection and research

#### 3.2.1 Palaeo-climate and palaeo-temperature study using noble gas measurements

To establish the increase in temperature and the time span of the transition between the Late Glacial Maximum (LGM) and the Holocene, the noble gas content, <sup>18</sup>O, <sup>2</sup>H, <sup>13</sup>C  $\delta$ -values, <sup>3</sup>H and <sup>14</sup>C activity and chemistry were studied in a groundwater flow system in Quaternary sediments in South-Hungary. The study area is a sub-basin of the Pannonian Basin, where the C isotope ratios are not influenced by carbonate reactions along the flow path, because the only water–rock interaction is ion exchange. The  $\delta^{18}\text{O}$  and  $\delta^2\text{H}$  values indicate a cold infiltration period, followed by warming, and finally, warm temperature conditions. The noble gas data show that the average infiltration temperature was 3.3 °C in the cold, 12.9 °C in the warm, and intermediate in the transitional stage. Using the noble gas temperatures, geochemical batch modelling was performed to simulate the chemical processes. Based on the geochemical model,  $\delta^{13}\text{C}$  and <sup>14</sup>C<sub>0</sub> (initial radiocarbon activity) in the recharging water were

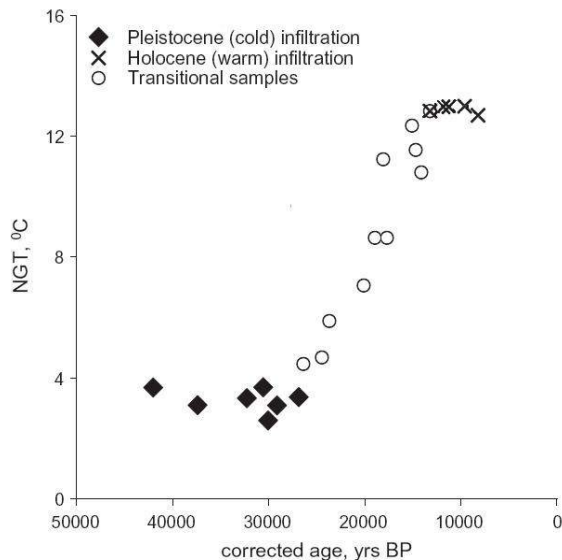


**Figure 7.** Noble gas temperatures (NGT) vs. radiocarbon ages of the groundwater samples.

calculated. Transport modelling was used to simulate the distribution of chemical components,  $\delta^{18}\text{O}$ ,  $\delta^2\text{H}$  and <sup>14</sup>C<sub>0</sub>, along the flow path.

It was found that the main processes determining the chemical composition of the groundwater were dissolution/precipitation of calcite and dolomite during infiltration near the surface, and ion exchange along the flow path. In the recharge area the  $\delta^{13}\text{C}$  and <sup>14</sup>C<sub>0</sub> were controlled by dissolution and precipitation of carbonate minerals, C speciation, and fractionation processes. All these processes were influenced by the recharge temperature. NGTs calculated from the dissolved noble gas concentrations showed an average of 3.3 °C for cold, and 12.9 °C for warm infiltration, i.e. for the LGM and for the Holocene (Figure 7).

The temperature difference was  $9.1 \pm 0.8$  °C, which is one of the largest degree of warming detected by noble gases so far. The alkalinity indicates that carbonate reactions were unimportant along the flow path. Due to the temperature dependence of the equilibrium constants, temperature conditions during infiltration have to be taken into consideration in radiocarbon age calculation. Dispersive transport along the flow path modified the chemical and isotopic composition of infiltrated water. The contribution of the old pore water, which was free of the  $^{14}\text{C}$  isotope, resulted in uncertainties in radiocarbon age determination. It was concluded that determination of the radiocarbon age or mean residence time requires detailed knowledge of the hydraulic conditions of groundwater [16].

### *3.2.2 Climate record revealed from noble gases in fluid inclusions of speleothems*

Stable isotopes, and recently, noble gases in fluid inclusions of speleothems are increasingly used to reveal past climate variations. Noble gases in groundwater have already been proven to be an absolute climate proxy; that is, solubility temperatures can be calculated from the noble gas concentration of groundwater samples. Recently, strong efforts have been made to adapt this technique for very tiny amounts of water such as fluid inclusions of speleothems or even coral skeletons. New studies have shown that noble gases dissolved in fluid inclusions can be extracted and then measured by sensitive noble gas mass spectrometers. In our research we have been developing a measurement process for tiny water filled inclusions. It includes the extraction of water from carbonates, determination of water amounts by the vapour pressure, mass spectrometric measurement of the released noble gases, calibration, and standardization with tiny, air equilibrated water samples enclosed in copper capillaries. The results of the performed calibration measurements (using well known air aliquots) show that measurements of most noble gas isotopes occur with a deviation of less than 2% or even better in some cases. However, we have found tiny different noble gas concentrations when measuring air equilibrated water samples enclosed in copper capillaries. Pre-treatment of the capillaries with helium purging can improve the noble gas signature of a standard water sample. Measurements of real soda straw stalactites show that special attention has to be paid to the sample preparation, although in some cases reasonable temperatures could be calculated from the obtained noble gas concentrations [17, 18, 19].

### *3.2.3 Groundwater protection - Study of old and fresh water mixing in a karstic aquifer*

The studied area is the part of the Aggtelek karst system, Hungary. The Pásnyag spring and the Lótusz spring are located one after the other nearby the Alsó-hill. The water of the Pásnyag spring is used as drinking water. From the local hydrogeological conditions it is possible that fresh and old ground water components are mixed in the springs (Figure 8). This fact is also confirmed by the water quality data.

The objective of this work was to determine the mixing ratio of the water of different origin in the springs. Repeated water sampling has been carried out around the site from the springs and two monitoring wells (F1 and F4) for two years. The F1 monitoring well is near at hand the Pásnyag spring, and the F4 well is between the two springs. The water quality of the Pásnyag spring and the nearby F1 well is significantly different. Helium content and isotope ratio, tritium concentration (by  $^3\text{He}$  ingrowth method), radiocarbon content of dissolved inorganic carbon (DIC), and  $\delta\text{D}$ ,  $\delta^{13}\text{C}$ ,  $\delta^{18}\text{O}$  isotope ratios were measured from the water samples. On the basis of isotope measurements the water of the springs and the observed monitoring wells are composed of fresh and old components in different ratios.

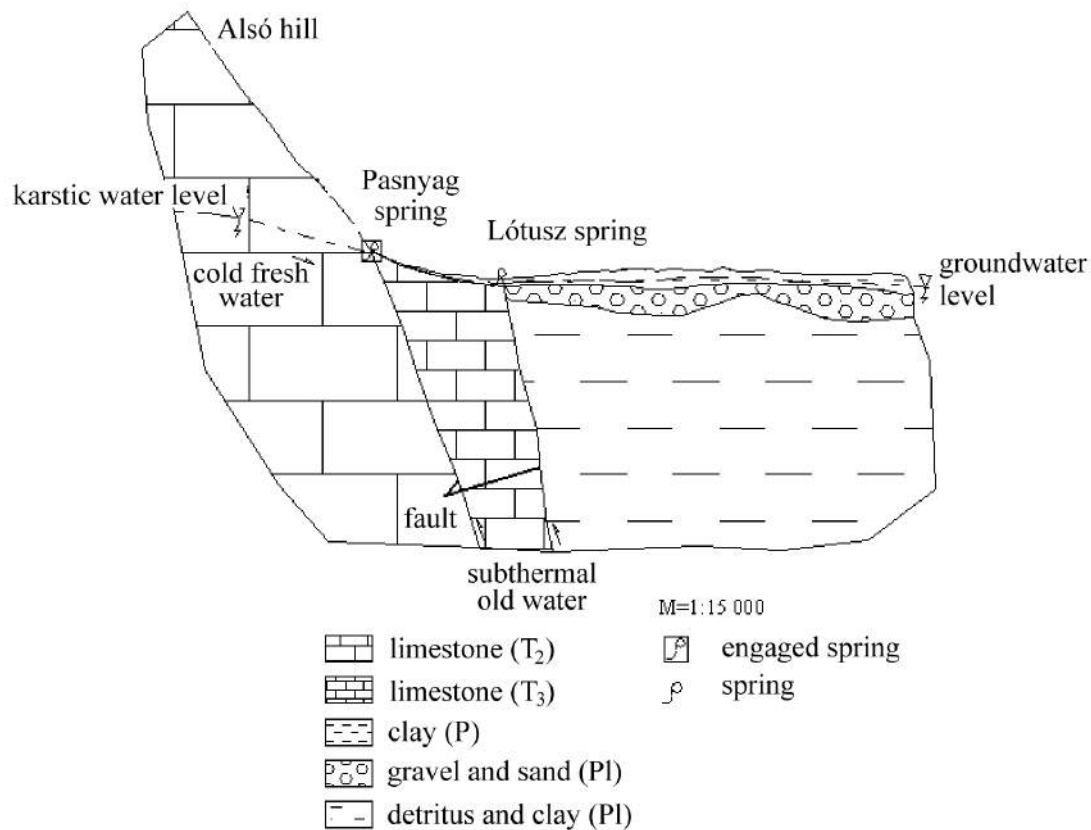


**Figure 8.** Presumed hydrogeological scheme of the area

The fresh component is dominant in the Pasnyag spring. The tritium and radiocarbon concentration of this water show that it is fresh, young water directly from the karstic system, with only small amount of DIC from the limestone. The helium concentration and isotope ratio in the water of this spring also shows that the subthermal water component is not significant. Higher ratio of the fresh karstic water also detectable in the far F4 monitoring well, but it has slightly lower tritium and <sup>14</sup>C content. In the Lótusz spring and the F1 well (nearby the Pasnyag spring) higher ratio of the subthermal water was observed. The low tritium and radiocarbon content show together that these waters contain high amount of old water. The higher helium content and the higher radiogenic <sup>4</sup>He ratio of the water also indicate subthermal origin in these cases [20].

### 3.2.4 Stable isotope composition of precipitation in Hungary between 2001 and 2009

The stable isotopic composition of hydrogen and oxygen of precipitation from Debrecen, Eastern Hungary was analysed in event based samples collected from the beginning of 2001 to the end of 2009.

The results showed that regional/local-scale processes control the isotopic composition of the local precipitation. During the monitoring period, the  $\delta^{18}\text{O}$  values varied between -22.3‰ and 6.64‰ and the  $\delta^2\text{H}$  values between -176.8‰ and 10.7‰. The local meteoric water line (LMWL) for the monthly based data is close to the global meteoric water line, but shows the effect of secondary evaporation of falling raindrops with lower intercept and slope. LMWL of each year shows highly different parameters due to differences in precipitation amount and summer temperatures, especially in the extreme years of 2002 and 2003. Based on our data it can be stated that  $\delta^{18}\text{O}$  values are more sensitive to indicate the extremities in the weather than  $\delta^2\text{H}$  values. Differences in the slopes and intercepts of the single years'

LMWL's are also a useful tool to monitor the given year regarding mainly secondary evaporation during the descent of precipitation from the cloud base to the ground. A very important result of our research was that due to the significant difference between the data of the other continental stations and Debrecen the extrapolation of the data of the surrounding stations to Debrecen would be misleading. On the basis of our data, deuterium-excess is considered to be the best parameter to reveal the extremities of dry and warm periods (Figure 9). Deuterium excess also proved to be a useful tool to show the different formation histories of certain precipitation events. Deuterium excess seems to be an even better way to see the effects of secondary evaporation in precipitation than  $\delta^{18}\text{O}$  values. The analyses of data suggest that the stable isotopic signature of the precipitation is strongly influenced by evaporation below the cloud base. Isotopic signatures ( $\delta^{18}\text{O}$ ,  $\delta^2\text{H}$ , d-excess, LMWL) of the extreme years of 2002, 2003 and 2007 deviate remarkably from the ones of the other six years. Good correlation of  $\delta^{18}\text{O}$  with temperature was obtained for the samples. The slope of the  $\delta^{18}\text{O}$ -T functions for the whole sampling period was  $0.32\pm 0.03\text{‰}/^\circ\text{C}$  for the monthly samples, however, a slope of  $0.37\pm 0.03\text{‰}/^\circ\text{C}$  was obtained if monthly mean temperatures were replaced with the monthly mean temperatures of the rainy days. Considering the temperature dependency of the  $\delta^{18}\text{O}$  values in the past, it can be concluded that  $\Delta\delta^{18}\text{O}/\Delta T$  relationship using monthly mean temperatures of the rainy days might be a better approach than monthly mean temperatures. The  $\delta^{18}\text{O}$ -T function has similar slope than reported from other continental stations, and is in the range characteristic for this climate [21].

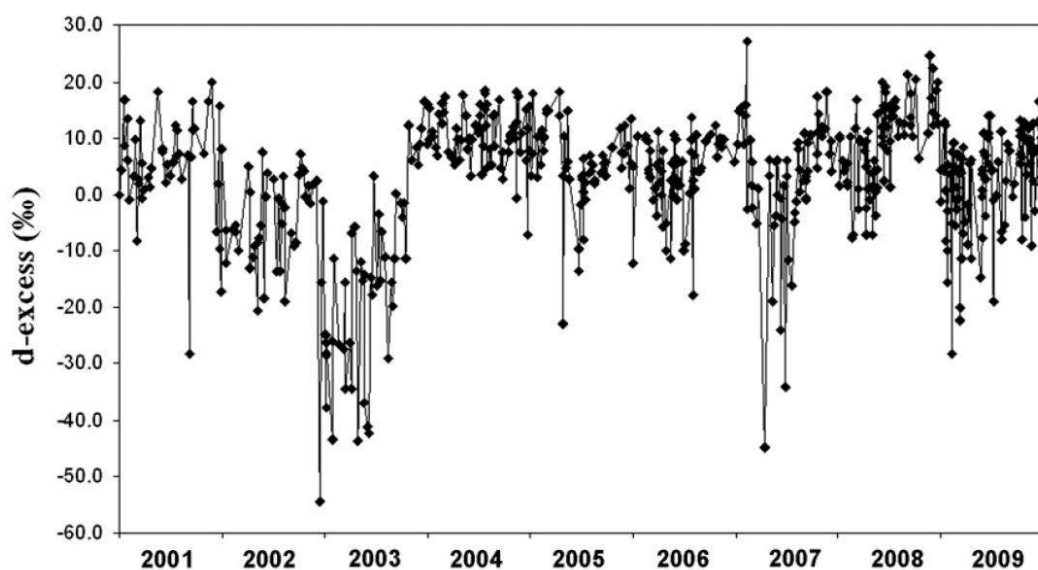


**Figure 9.** Deuterium excess values of precipitation at the sampling site: event based d-excess values of precipitation between 2001 and 2009 in Debrecen, Hungary.

### 3.2.5 Tritium washout by precipitation around a nuclear power plant

The impact of tritium is an important issue in environmental protection, e.g. in connection with the emissions from nuclear power plants. We have made an experimental and modelling work focusing on the rain washout of tritium emitted from the Paks Nuclear Power Plant. Rainwater collectors were placed around the plant and after a period of precipitation, rainwater was collected and analysed for tritium content. After the collectors had been positioned, data collection was delayed until the arrival of a 'good' rainfall period, that is, with wind from the southwest to northwest. The selected period fell during 7-8 June 2009.

Samples were analysed using low-level liquid scintillation counting, with some also subject to the more accurate  $^3\text{He}$ -ingrowth method. The results clearly show the trace of the tritium plume emitted from the plant; however, values are only about one order of magnitude

higher than environmental background levels. A washout model was devised to estimate the distribution of tritium around the plant. Based on emission and meteorological data, a reversible washout model was used to calculate the theoretical tritium concentration, which was then compared with the measured values. The model gives slightly higher concentrations than those measured in the field, but in general the agreement is satisfactory. The modelled values demonstrate that the effect of the plant on rainwater tritium levels is negligible over a distance of 5 kilometres (Figure 10) [22].

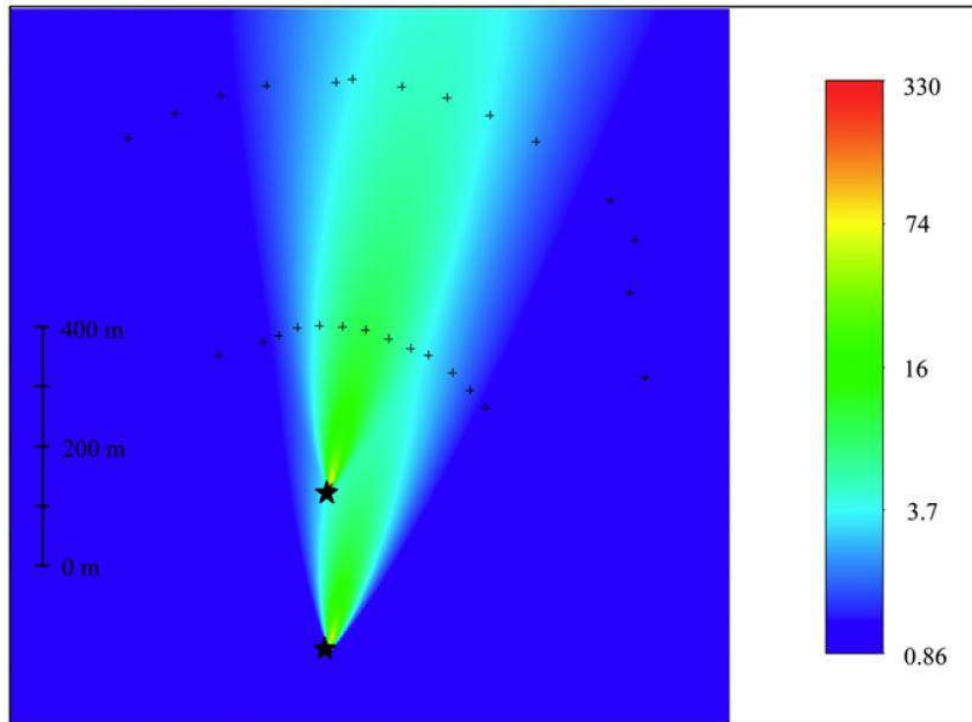


**Figure 10.** Concentration map around the power plant, calculated with the fitted mass transfer coefficient. The colour code shows the concentration on a logarithmic scale, in Bq/l. The stacks are shown with stars, and the samplers with plus signs.

### 3.2.6 *C-14 monitoring around a nuclear power plant*

The activity of  $^{14}\text{C}$  in  $^{14}\text{CO}_2$  and  $^{14}\text{C}_n\text{H}_m$  chemical forms is measured in the vicinity of the Paks Nuclear Power Plant (NPP), Hungary by sampling environmental air. Four differential sampling units (developed in ATOMKI) at different sites collected samples less than 2 km away from the 100-m-high stacks of the Paks NPP, and for reference a sampler was operated at a station ca. 30 km away from Paks NPP. We presented the results of the continuous observations at the five stations covering the time span from 2000 to 2005. The samples have been analyzed by proportional counting technique. During a cleaning tank incident at unit 2 of Paks NPP in April 2003 a significant release of radioactive isotopes took place from the damaged fuel assemblies and gaseous products escaped through the chimney. We evaluate the possible instant and long-term impact of this incident on the  $^{14}\text{C}$  content of the atmosphere in the surroundings of Paks NPP. Comparing our  $^{14}\text{CO}_2$  measurements with data sets from Jungfraujoch and Schauinsland as well as from Košetice (Czech Republic) we demonstrate that the incident had no definite influence on the  $^{14}\text{C}$  content of the atmosphere.

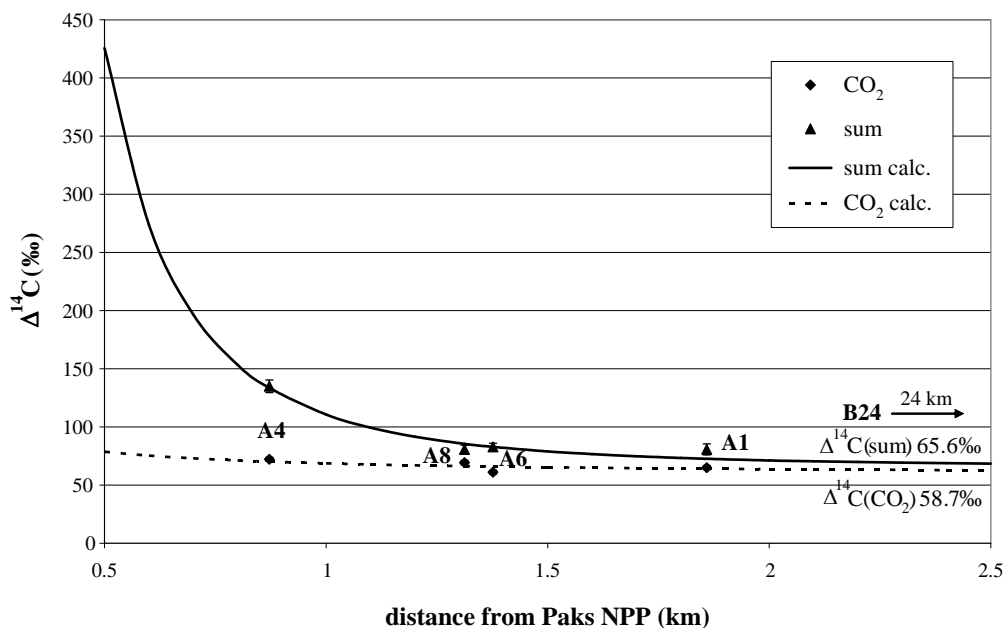


**Figure 11.** Average  $\Delta^{14}\text{C}$  values versus distance of the stations (A-1 to A-8) from the NPP.

Highest  $^{14}\text{C}$  values were measured at site A4, located less than 1km away from the Paks NPP (Figure 11). Here the excess  $\Delta^{14}\text{C}$  in the sum fraction fluctuated between 40–100‰ and the  $\Delta^{14}\text{C}$   $\text{CO}_2$  values fluctuated between 5 and 15‰. At the other stations (1.5–2km far from the plant) the excess  $\Delta^{14}\text{C}$  was on average  $13.0 \pm 2.6$ ‰. The influence of the  $^{14}\text{C}$  discharge in the environment decreases rapidly with the distance from the source and under normal operating conditions the effect of Paks NPP is negligible at a distance of 2.5km [23, 24, 25].

### 3.2.7 Atmospheric fossil $\text{CO}_2$ monitoring in a city

During the winter of 2008 we measured the mixing ratio and radiocarbon content of atmospheric  $\text{CO}_2$  at Debrecen city and a rural reference station (Hegyhátsál) simultaneously in Hungary to determine the fossil  $\text{CO}_2$  amount in the air of the city. The Debrecen observation station is a novel ATOMKI developed field deployable unit which can meet the requirements of fossil fuel monitoring in semi polluted areas (typical  $\text{CO}_2$  mixing ratio error is  $<0.3\%$  and  $\Delta^{14}\text{C}$  error is  $<0.5\%$ ).

It was concluded that  $\text{CO}_2$  mixing ratio showed a similar temporal variation at the two different sampling locations. Air quality in Debrecen during September of 2008 seemed to be relatively clean from the point of view of its  $\text{CO}_2$  content. When winter came in October, with lower outside temperature and less sunshine hours, the  $\text{CO}_2$  content of air increased in general at both sampling locations, but this effect was more intensive closer to the ground surface. According to our radiocarbon observations it was clearly indicated that there was not significant amount of fossil fuel  $\text{CO}_2$  in the air of Debrecen during September, 2008. But during the winter of 2008/09 the  $\Delta^{14}\text{C}$  value of atmospheric  $\text{CO}_2$  of Debrecen decreased with more than 40 ‰ relative to September's results, and according to our calculations it was caused by about 20 ppm fossil fuel  $\text{CO}_2$  which appeared as a surplus amount in the air above the September level (Figure 12) [26, 27, 28, 29]. This study was supported by the OTKA (F69029) and Isotoptech Zrt.

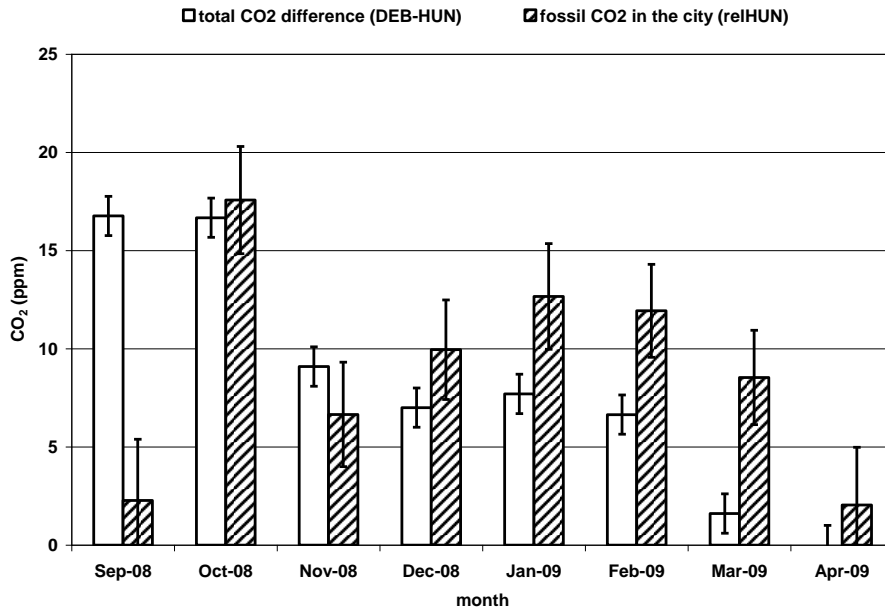


**Figure 12.** The total CO<sub>2</sub> surplus and the fossil fuel CO<sub>2</sub> in the city of Debrecen vs. the Hegyhátsál reference during the winter of 2008/09.

### 3.2.8 Study of gas generation in radioactive wastes

During the storage of low and intermediate level radioactive waste (L/ILW) significant quantities of gas may be produced. It is likely that a small proportion of the generated gas will be radioactive as the isotopes <sup>3</sup>H and <sup>14</sup>C are present within the waste.

To obtain reliable estimates of the quantities and rates of the gas production in L/ILW a series of measurements were carried out on waste packages produced and temporarily stored at the site of Paks Nuclear Power Plant (NPP). Ten drums filled with selected original L/ILW were placed into hermetic containers equipped with sampling valves for repeated sampling (Figure 13). These hermetic containers were stored at the same site where the L/ILW is stored primarily in the Paks NPP.

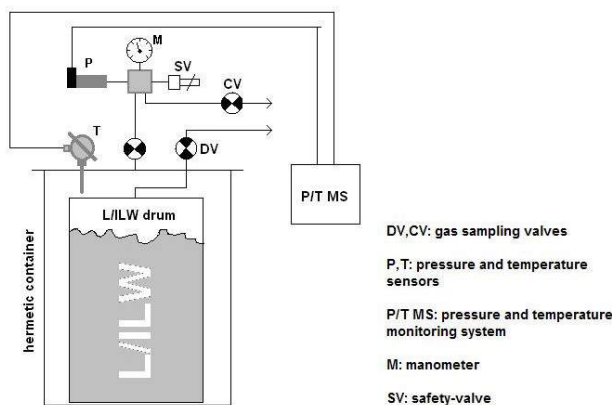


**Figure 13.** Hermetic containers designed for gas generation measurements of drum L/ILW.

Our results showed that the main generated gases in L/ILW are carbon-dioxide, methane, hydrogen and nitrogen. The typical rates were 0.05-0.2 normal litre gas/day for CO<sub>2</sub> and CH<sub>4</sub> generation, and less than 0.02 normal litre gas/day for H<sub>2</sub>. Because of the typical vanishing of the O<sub>2</sub> from the headspace gases no explosive gas mixture was indicated in the L/ILW drums during the investigated storage period. The stable carbon isotope results show

that the main source of the CO<sub>2</sub> gas is the degradation of organic matter in the waste. The low <sup>13</sup>C content indicates microbial degradation processes as the main sources of CH<sub>4</sub> gas. The He isotope ratios represent <sup>3</sup>He enrichment in the headspace gases produced by tritium decay in the waste. Significant variation of the tritium content in individual drums with time was typical. The maximal value was more than 20 Bq <sup>3</sup>H/litre. The typical tritium activity concentrations were between 0.1 and 10 Bq <sup>3</sup>H/litre. The main tritium content always was related to the vapour fraction, but when the methane became the main component in the headspace gas it also could contain significant amount of <sup>3</sup>H. The radioactivity of the carbon in the gas phase of the L/ILW drums are always significantly higher (10 or 100 times) than in the air. This <sup>14</sup>C enrichment also appears in the methane fraction if it has been the main component in the headspace gas. Maximal measured radiocarbon activity was about 3.0 Bq/litre. Typical <sup>14</sup>C activity values of the headspace gases were between 0.1 and 2.0 Bq/litre [30, 31, 32, 33, 34, 35, 36, 37, 38, 39, 40].

### 3.3 Development of sampling, sample preparation and measurement methods

#### 3.3.1 An automatic groundwater sampling unit for monitoring wells of nuclear facilities

Automatic water sampling unit was developed for monitoring the radioactive emission from nuclear facilities into the groundwater (Figure 14). The efficiency of existing and renewed geometry units and the reproducibility of survey data have been examined in the course of this work.

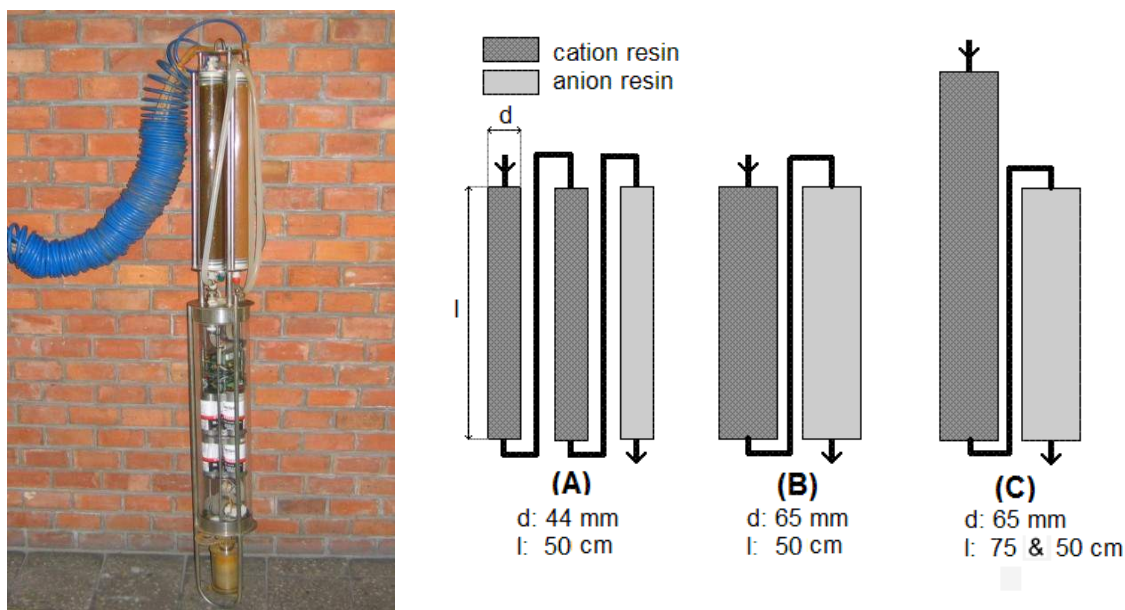


**Figure 14.** Picture of automatic ground-water sampling unit and schematic drawings of the tested three different resin geometries.

A testing method was developed for this purpose, and ion binding efficiencies of ion exchange resins were analysed for different ion concentrations. These efficiencies have to be taken into consideration when we estimate the amount of the contamination got into the groundwater on the basis of the proportion of ions gained back from the resin.

The model tests were executed under controlled laboratory circumstances. These circumstances were tried to be formed similar to nature. It has been found during the chain of tests that the sampling unit is suitable for well reproducible sampling. It can be told that all the tested different geometrical lay-outs (A, B, C in Figure 14) can be used and work with proper efficiency in small/low range of concentration as well. The “A”-lay-out showed some

ion loss in the last period but this phenomenon hardly has an influence on the effective and valid applicability of the existing system in the intended task. Taking the different efficiencies into consideration the activities can be corrected in the case of every element if it is necessary. A correction factor should be introduced in the  $^{14}\text{C}$  anion exchange sampling because samples taken show systematically lower radiocarbon content than the real one. We are working on continuing the tests. The gamma activity measurement of existing gained back cation samples and giving the exact value of  $^{14}\text{C}$  correction can give more reliable picture and direction to developing existing and possibly new systems [41, 42].

### 3.3.2 Preparation and measurement process for noble gases dissolved in groundwater samples

Previous studies of the last three decades have shown that noble gases dissolved in groundwater are a powerful tool for palaeoclimate reconstruction. Additionally, tritiogenic  $^3\text{He}$ , accompanied with tritium, can be used for dating of young waters. In the last few years, we successfully adapted the mass spectrometric measurement technique of dissolved noble gases of groundwater. Water samples for noble gas analyses are placed in copper tubes. We followed the method of sample preparation and measurement that has been developed in the Institute of Environmental Physics, University of Heidelberg, Germany, with a few modifications.

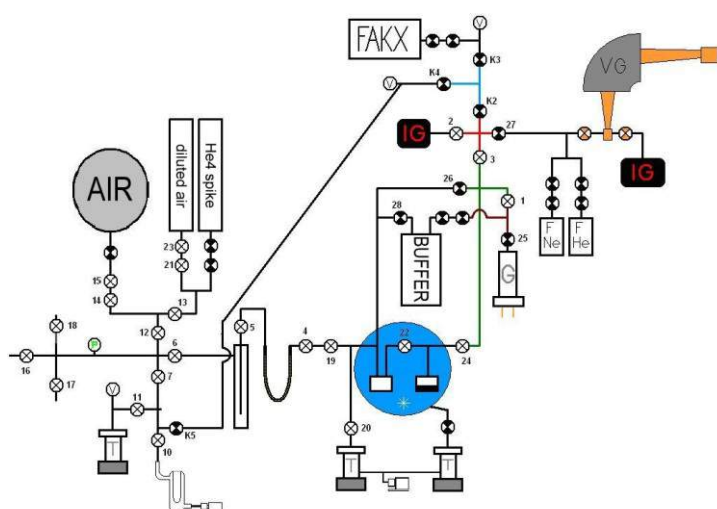


**Figure 15.** Left: schematic drawing of the preparation line;  
Right: picture of the preparation line and the cryogenic system.

The dissolved gases are extracted from the samples in the copper tubes on a preparation vacuum line. While the water vapour is kept back with a trap held at  $-70\text{ }^\circ\text{C}$ , all of the gases are collected in two cryo traps (Figure 15). With the exception of He and Ne, the gases are trapped in a stainless steel trap consisting of a polished metal surface held at 25 K. Helium and Ne are absorbed in a charcoal trap at 8 K. To admit the He fraction into the mass spectrometer, it is released from the charcoal at 42 K, while most of the Ne remains absorbed. After measuring the He, the Ne fraction is released from the charcoal trap at 90 K and admitted to the mass spectrometer. The gas fraction trapped in the stainless steel trap is released at 150 K, and a tiny split is purified by a getter trap. The heavier noble gases, namely Ar, Kr and Xe, are measured simultaneously in the VG5400 noble gas mass spectrometer. Calibrations are performed by repeated measurements of air aliquots of different sizes, covering the range found in the samples. The so-called fast calibration procedure is also applied. The standard deviations of the air calibrations vary between 0.5–0.7% for  $^4\text{He}$  and Ar, and around 1.5% for  $^3\text{He}$ , Ne, Kr and Xe. In the noble gas fitting procedure, these

uncertainties allow us to determine noble gas temperature by an uncertainty of 0.5–0.8°C. To check the precision of the measurements, air equilibrated water samples (AEW) have been measured. These artificial water samples were equilibrated with air of known temperature and pressure, hence the expected noble gas concentrations dissolved in the AEW samples were known. During the measurement runs, noble gas concentrations of AEW samples have been found to be as good as expected [8, 16, 43].

### 3.3.3 Using an ultrapure $^4\text{He}$ -spike for high precision helium isotope ratio measurements

The most sensitive method to measure tritium amounts in water is based on the mass spectrometric measurement of  $^3\text{He}$ , the daughter of tritium. The method consists of three major steps: (1) the water sample is put into a container and the dissolved gases including helium are then removed from the water by vacuum pumping; (2) the samples are stored for several months or years so that  $^3\text{He}$  atoms are produced by tritium decay; (3) the helium fraction is admitted to a dual collector noble gas mass spectrometer, and the abundance of the tritiogenic  $^3\text{He}$  is then measured applying the peak height method.

Numerous laboratories have adopted this method and we did so. However, the mass spectrometric measurements of such small amounts of helium are always hard to perform precisely. We have developed a new technique that is based on an unusual isotope dilution technique. Using this new method we could improve our precision for the measurement of low tritium concentrations in environmental water samples. These measurements are usually calibrated by means of known air aliquots, which can be compared in size with the amount of helium from the tritium sample.

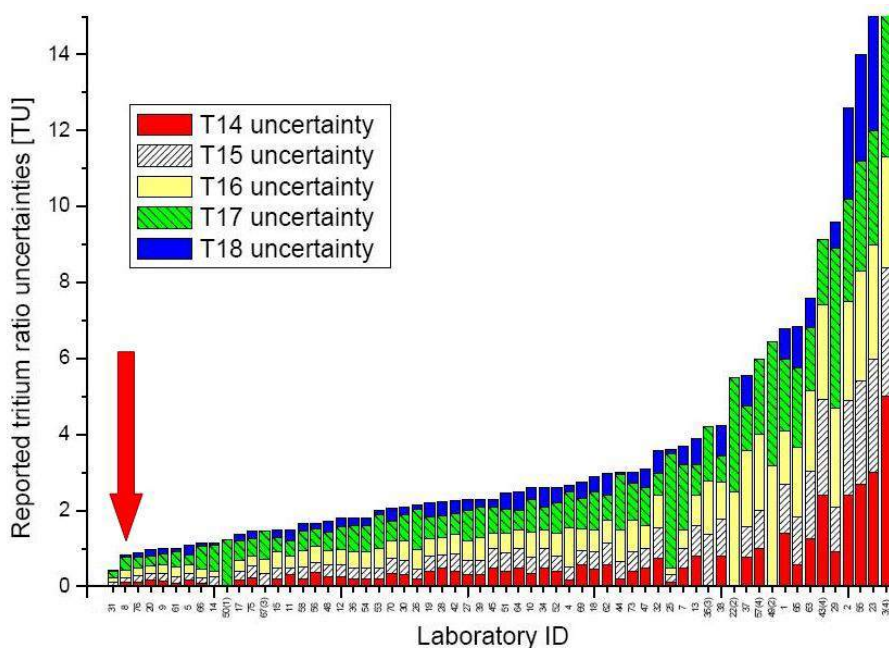


**Figure 16.** Cumulative uncertainties for tritium concentrations of samples T14 to T18 as reported by laboratories involved in TRIC2008. Our laboratory (ID 8) is marked by the red arrow.

However, the  $^3\text{He}/^4\text{He}$  ratio of samples can differ considerably from that of the air used for calibration of the mass spectrometric measurement. The mass spectrometric sensitivities of the different helium isotopes depend on the pressure in the ion source. In the case of tritium measurements, the overall pressure of the helium in the mass spectrometer is much lower than that of the helium from the air calibration, and therefore the accurate calibration that is effective for both  $^3\text{He}$  and  $^4\text{He}$  isotopes always has to be determined. Usually, low amounts of air aliquots are used for calibration as their helium content can be compared with that of a

tritium sample. However, only the  $^4\text{He}$  contents can be estimated in these cases. To solve this sensitivity problem, we increased the helium pressure in the ion source for a tritium sample by adding ultrapure  $^4\text{He}$  spikes to each tritium sample during the inlet stage. Taking aliquots from this spike, we add  $7.6 \cdot 10^{-8} \text{ cm}^3\text{STP}$  of  $^4\text{He}$  to the tritium samples in a normal measurement process from now on. In this way the helium pressures from either a sample or a calibration are always of the same order of magnitude. To test the overall precision of this technique in tritium measurement, we measured 29 tritium standard samples of known concentrations. The measured tritium concentrations of the artificial standard samples are scattered around the expected values within a  $1\sigma$  relative standard deviation of 2.3%. The average of the ratio of the measured and the expected values is 1.0 (actually: 1.000092), which means there is no longer a systematic error. To test our precision and accuracy, we participated in the TRIC2008 (Tritium Intercomparison 2008) Proficiency Test of the IAEA (Figure 16). We have measured the tritium content of six water samples received from the Isotope Hydrology Laboratory of the IAEA. The two data sets are equal within the  $1\sigma$  uncertainty limits, and the correlation factor ( $\chi^2$ -test) between the measured and reference data sets is 0.999334. With respect to precision and sensitivity, our laboratory is one of the best laboratories of tritium measurements [43].

### 3.3.4 *Measurements of dissolved gas in the liquid of cooling ponds in a nuclear power plant*

Changes of the composition or content of the dissolved gas in the coolant, especially of the noble gases and the hydrogen, are really significant indicators of the alterations in state parameters of the nuclear reactors during the working or the shutdown periods. The aim of this work was the investigation of the effect of nuclear fuel rods to the composition of the dissolved gas in the cooling water of the cooling ponds and service pool No.1 of reactor No. 2 of Paks Nuclear Power Plant (Paks NPP). The dissolved gases in coolant were measured for surveying the kilter of the nuclear fuel remained in service pool No.1 after the incident in April of 2003.

For dissolved gas measurements the gas must be representatively retrieved from the coolant of the cooling ponds and service pool No. 1. Two different experimental ways were applied in parallel for ensuring the better reliability of the results. The basis of the first method is gas sampling with degassing of the coolant on the site and the measurements are carried out later from these gas samples in the lab. Gamma activity of the gas samples in the ampoules was measured by HPGe detector. The other way means in-situ measurement of the dissolved gas directly from the coolant with membrane inlet quadrupole mass spectrometer on the site. Noble gas isotope measurements were carried out by a noble gas mass spectrometer from the gas in ampoules.

The concentration of the total dissolved gas is similar in the coolant of all the investigated cooling ponds and service pool No. 1. On the other hand the compositions of the dissolved gas in the systems of reactor No. 2 and in the other cooling ponds were completely different. In the cooling ponds of reactors No. 1, 3 and 4 the dissolved gas in the coolant is air, with only little  $\text{H}_2$  and  $\text{CO}_2$  surplus, and these values were relatively stable during the whole sampling period. The composition of the dissolved gas in the cooling pond and service pool No. 1 of reactor No. 2 differs from the air and strongly varied during the sampling period. The hydrogen content of the coolant of the service pool No.1 continuously increased till the fifth sampling in 2004, and reached a value of  $2,4 \text{ cm}^3 \text{ H}_2 / \text{litre coolant}$ . That time the portion of  $\text{CO}_2$  was also significantly higher than in the other investigated coolants. But before the  $\text{H}_2$  concentration increased over the  $1 \text{ cm}^3 / \text{litre}$  value, the oxygen content in the coolant drastically decreased (fourth sampling in 2004 of the service pool).

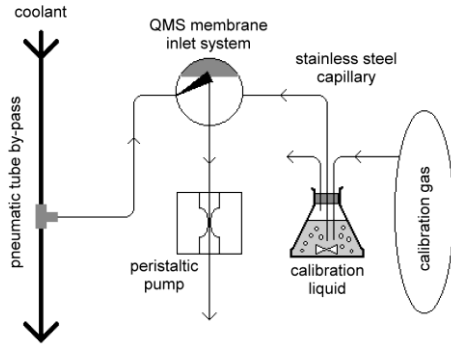


**Figure 17.** Measurement by QMS with membrane inlet.

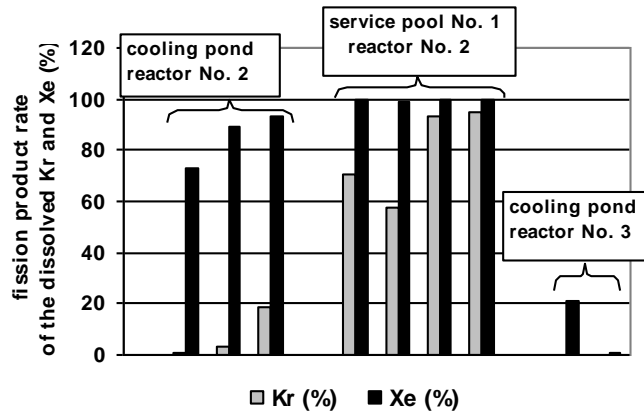


**Figure 18.** The rate of fission product Kr and Xe in the dissolved Kr and Xe in the coolants.

In the samples from the cooling ponds of reactors No. 1, 3 and 4 the noble gas contents were very similar to each other and to the dissolved air. Noble gas content in these systems was varying and a little bit lower than the typical values of the water saturated with air. In the cooling water of service pool No. 1 of reactor No. 2 the amount of dissolved Xe and Kr is significantly higher than in the other investigated cooling ponds. This difference is two or three orders of magnitude. In the cooling pond of reactor No. 2 the Xe content was also ten times higher than in the others of Paks NPP. The gamma analytical results from the degassed samples showed that only  $^{85}\text{Kr}$  isotopes gave measurable activity and only for the samples from reactor No. 2. All the other samples had no detectable radioactivity. The measured  $^{85}\text{Kr}$  activities showed similar trends in time, but the values were 10-100 times higher in the case of the service pool. At the time of the last sampling in 2004 the  $^{85}\text{Kr}$  activity was more than 10 kBq/litre for the coolant of the cooling pond and more than 1000 kBq/litre in the case of service pool No. 1 [44, 45].

### 3.3.5 Refining the $\text{CO}_2$ absorption method for low background C-14 liquid scintillation counting

A new method of chemical sample preparation for liquid scintillation  $^{14}\text{C}$  measurements was implemented in HEKAL.

The developed absorption method is quick, inexpensive and simple. In a special preparation line  $\text{CO}_2$  samples are absorbed in CarboSorb absorbent. The developed line consists of a gas-bag  $\text{CO}_2$  container (PG), a freezing finger for easier  $\text{CO}_2$  transport, a fine-regulation valve (VG), a bubbler filled Hg for gas-flow control (Hg), a buffer bulb for initial pressure reduction (PB), and the vial containing CarboSorb (CS) (Figure 19).

For the exact determination of the amount of the absorbed  $\text{CO}_2$  gas two independent techniques were applied (direct weighing of vial and measuring of the amount of the rest  $\text{CO}_2$  gas). Several tests were executed with old borehole  $\text{CO}_2$  gas (Linde Hungary Ltd. Répcelak, Hungary) without significant  $^{14}\text{C}$  content). This gas has been used as background gas in our gas proportional counter (GPC) system.

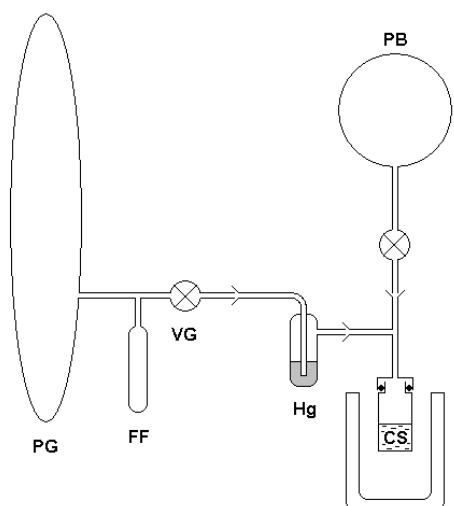


**Figure 19.** Schematics of the new design of CO<sub>2</sub> absorption line.

Tests were also performed on samples of known <sup>14</sup>C activities between 29 and 7000 pMC, previously measured by GPC. The <sup>14</sup>C activities of all prepared samples were measured by liquid scintillation counter (LSC) including quenching parameter (tSIE). The observed agreement between LSC and GPC data was very good in the case of several samples. We demonstrated the reproducibility of the sample preparation and the stability of the prepared counting mixture. We have determined parameters for measurements in our TRI-CARB 3170 TR/SL liquid scintillation counter (LSC) including optimised <sup>14</sup>C window with counting efficiency (65.3 %) and the corresponding <sup>14</sup>C dating limit (31,200 yr BP). The combined uncertainty of the determination was about 2 % for recent carbon samples. Thus, the presented method is suitable for <sup>14</sup>C determination and dating of geological, hydrological, and environmental samples [46].

### 3.3.6 A field deployable atmospheric fossil CO<sub>2</sub> monitoring station

The aim of the project supported by Hungarian NSF (ref No. F69029) is the determination of atmospheric fossil fuel CO<sub>2</sub> concentration in major cities or average industrial regions in Hungary using together measurement of CO<sub>2</sub> mixing ratio and radiocarbon (<sup>14</sup>C) content of the air. For this aim we developed a high precision atmospheric CO<sub>2</sub> monitoring station in ATOMKI (Figure 20). The station's measuring system is based on an Ultramat 6F (Siemens) infrared gas analyser. To help continuous, unattended run and autocalibration we built up an automatic gas handling line for the analyzer. For radiocarbon measurements we applied an integrating sampling system. One was installed in Debrecen station and two independent <sup>14</sup>CO<sub>2</sub> sampling line were installed 400 km far from Debrecen at Hegyhátsál station as background references.



**Figure 20.** The developed mobile observation station for monitoring of atmospheric fossil fuel CO<sub>2</sub>.

During several tests of the measuring and sampling systems we demonstrated that uncertainty of individual CO<sub>2</sub> mixing ratio results is less than 0.5 ppm and the applied radiocarbon sampling system developed by ATOMKI works with good reproducibility. Using the developed mobile and high-precision atmospheric CO<sub>2</sub> monitoring station we plan to determine the atmospheric fossil fuel CO<sub>2</sub> trend in next winters in Debrecen [47].

### 3.3.7 A simplified and rapid C-14 AMS graphite target preparation method

In most cases the last step of the sample preparation for <sup>14</sup>C dating by AMS is to produce graphite from the pure CO<sub>2</sub> gas samples. Catalytic reaction is generally used to produce graphite for which stabilized temperature reaction cells are developed in certain laboratories. The properties (e.g. purity, conductivity) of the produced graphite vitally influence the quality of the AMS measurement. Although the internationally validated hydrogen reduction graphitization line of HEKAL is able to produce high quality graphite for AMS C-14 analyses, the throughput of the prepared targets is highly limited [48, 49, 50].



**Figure 21.** The developed new sealed-tube graphitization gas-preparation line in HEKAL

We were looking for a rapid production and low cost graphitization method, whereby we are capable to handle numerous biomedical and environmental samples per day. The sealed tube zinc reduction method mostly suits these criteria (Figure 21). We have adapted the method in ATOMKI and the goal of our study was to find out the proper conditions of the graphitization process. We have analyzed how does the graphitization time (240 – 3720 min) and the amount of zinc (30, 50 and 80 mg) and titanium hydride (7, 10 and 12 mg) reagents influence the value of the <sup>12</sup>C ion current and the measured radiocarbon content of the sample and how big the caused isotope fractionation.

We have also investigated the reproducibility of graphitization process and examined the radiocarbon content of graphite targets made of oxalic acid standard (NIST-SRM-4990c). All of the graphite targets were prepared in ATOMKI laboratory and the AMS measurements were carried out on the MICADAS type accelerator mass spectrometer, developed and hosted in ETHZ, Zürich. The amount of TiH<sub>2</sub> we have examined does not have any kind of influence on the important features of the produced graphite. On the other hand the smaller volume of the zinc decreased the ion current and increased the  $\delta^{13}\text{C}$  shifts of the sample. We have also observed that higher volume of the zinc increased the stability of the graphite target.

### 3.3.8 A new method for groundwater C-14 AMS analyses

In this study we investigated the applicability of a new method to prepare samples from dissolved inorganic carbonate (DIC) in ground-water for radiocarbon AMS analysis. The pretreatment method developed does not require sample preparation under vacuum, which significantly reduces the complexity. Reaction time and conditions can be easily controlled as the CO<sub>2</sub> content of a water sample is extracted by acid addition in a He atmosphere using a simple septum sealed test tube. A double needle with flow controlled He carrier gas is used to remove CO<sub>2</sub> from the test tube (Figure 22). The CO<sub>2</sub> extraction yield is less than 80% mainly because a large portion of the gas remains in solution in accordance with Henry's Law. CO<sub>2</sub> is then trapped on zeolite without using liquid N<sub>2</sub> freezing.

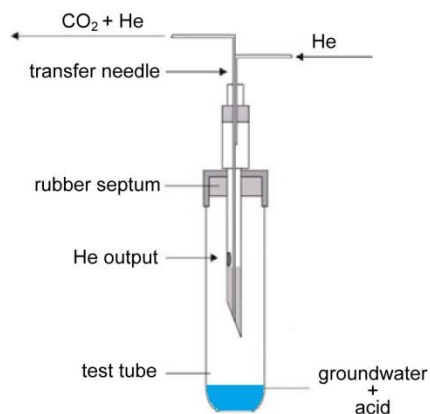


**Figure 22.** CO<sub>2</sub> transfer method using He carrier gas flushing through a double needle (Thermo, Gasbench) in a septum sealed test tube.

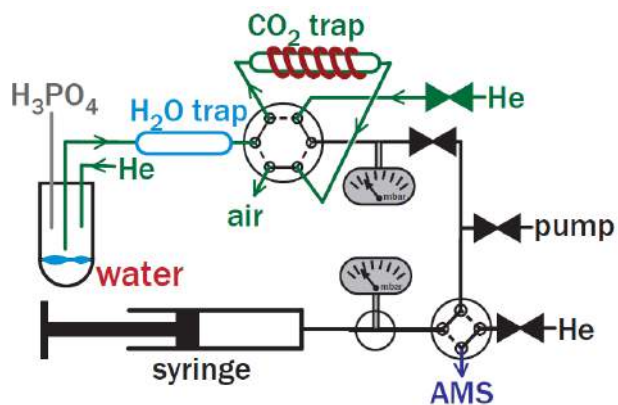


**Figure 23.** Layout of the connection of ground-water preparation line to the AMS gas ion source interface

The new method can be combined with an automated graphitization system like AGE from ETHZ [1] to have a fully automated water preparation line for AMS graphite targets. In this case, about 5-12 ml of water is needed for an AMS sample. The greatest advantage of the new groundwater pretreatment method is the possibility to connect the extraction line directly to an AMS system using gas ion source interface (Figure 23).

With our MICADAS AMS system we demonstrated that the <sup>14</sup>C content in 1 ml of water could be routinely measured with better than 1% precision (for a modern sample). The AMS measurement of one water sample including sample preparation takes only about 20 minutes.

### 3.3.9 Radiochemistry: separation of <sup>79</sup>Se from radioactive waste

The low- and intermediate-level liquid wastes produced by the Paks NPP contain routinely measurable gamma-emitting (e.g. <sup>54</sup>Mn, <sup>60</sup>Co, <sup>110m</sup>Ag, <sup>125</sup>Sb, <sup>134</sup>Cs and <sup>137</sup>Cs) as well as many so-called “difficult-to-measure” isotopes. Despite of their low specific activity compared to the total, the reliable determination of these isotopes is an important issue of nuclear waste management.

Selenium-79 is a beta emitter produced by the fission of <sup>235</sup>U. It is one of the radionuclides of interest in the management of nuclear waste repositories because of its long half life ( $2.95 \cdot 10^5$  y) and its potential migration ability from the repository to the environment. Typical overall activity concentration of low and intermediate level (L/ILW) liquid wastes as well as spent ion exchange resins of Paks NPP meant to deposition is in the range of  $10^5 - 10^7$  Bq/l and  $10^6 - 10^9$  Bq/kg, respectively. Measurement of <sup>79</sup>Se is particularly difficult due to its low activity (about  $10^{-3}$  Bq/l and  $10^{-1}$  Bq/kg) in such waste matrixes. One of the main difficulty of the development of a separation procedure is that <sup>79</sup>Se is not available as a standard either in liquid or solid form. As a consequence, a “step by step” methodology was implemented to achieve the validation of the protocol where stable Se and <sup>75</sup>Se (gamma emitter) were used as carrier and tracer to estimate the chemical yields of the different steps. The estimated chemical form of selenium in the samples is selenite (Se(IV)) due to strongly basic matrix. This way we expected that it must be concentrated on anion exchange as well as mixed bed resins while cation exchange resin does not adsorb it. This theory has been tested on the resins using the stable selenite as carrier. The concentrations of selenium were measured by ICP-OES. The spent anion ion exchange resin samples already contained <sup>75</sup>Se therefore the measurement of the chemical yields was made by this way too. The resin samples were washed with 100 times the resin bed volume of 10 w% NaNO<sub>3</sub> solution. The Se

content of the resulting elutes proved our theory. However, they also contained various contaminants depending on the original sample. The ratios of the separation for the other radioisotopes (e.g.  $^{54}\text{Mn}$ ,  $^{60}\text{Co}$ ,  $^{106}\text{Ru}$ ,  $^{125}\text{Sb}$ ,  $^{137}\text{Cs}$ , etc.) were also carried out by the measurement of their activity in each steps of the procedure. The elutes were transferred in to 1:1 HCl matrix and selenite was reduced to elemental selenium by  $\text{H}_2\text{S}$ . The precipitated Se was filtered and was additionally cleaned by digestion in hot 1:1 HCl solution. After the required number of cleaning cycles, the selenium precipitate can be measured with liquid scintillation counting if  $^{79}\text{Se}$  standard reference material is available [51].

#### 4 OUTLOOK – C-14 AMS IN ATOMKI FOR ENVIRONMENTAL STUDIES

In the recent past, impressive progress has been made to simplify the Accelerator Mass Spectrometry (AMS) measurement technique, and to provide easier-to-operate instruments and high-performance commercial AMS spectrometers to the AMS user community [52, 53]. However, the ultimate goal of having AMS instrumentation with tabletop dimensions and a system complexity similar to those of conventional mass spectrometers has not been reached yet. To take a next step forward at ETHZ (Zürich, Switzerland) they have focused on pushing the AMS technique, in particular that of radiocarbon, towards lower beam energies. It has been demonstrated that the destruction of the molecular interferences using multiple ion gas collisions can be applied at energies as low as 240 keV and a novel design for the acceleration stage became possible resulting in a new generation of AMS spectrometers [54]. The MICADAS spectrometer is a very compact instrument of  $2.5 \times 3 \text{ m}^2$  overall dimensions (Figure 24).

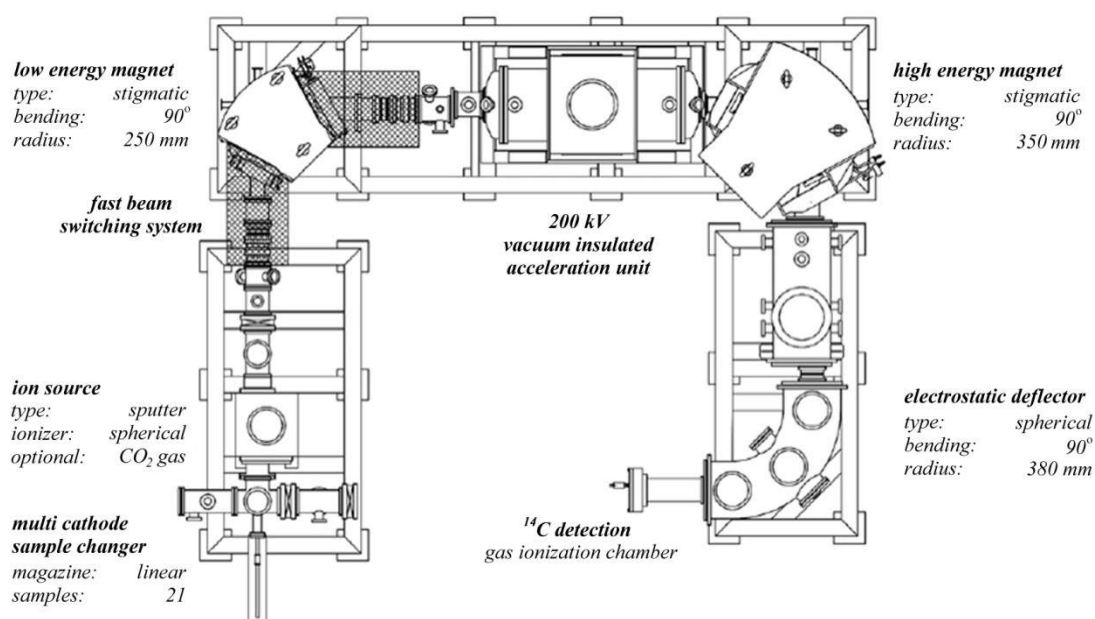


**Figure 24.** The layout of MICADAS. The system design avoids open high voltage potentials. Operation procedures, in particular sample and magazine exchanges can be carried out without interrupting the measurement process.

The novel feature of this instrument is the acceleration unit. In contrast to other AMS spectrometers, which use conventional particle accelerators, a vacuum-insulated high voltage platform is utilized to generate energetic ions. Neither a pressure vessel to insulate the high voltage terminal nor acceleration tubes is needed for beam transport. A first prototype of this class of instruments has been finalized in 2004 at the ETH Laboratory of Ion Beam Physics in Zürich. This system now serves under routine operation conditions for radiocarbon dating measurement at ETH. In 2006 a dedicated version for biomedical application, the

BioMICADAS, instrument has been developed. This system is now being operated by a commercial service provider for biomedical AMS work (Vitalea Science) in Davis, CA, USA. An improved version of the MICADAS instrument dedicated for high performance radiocarbon dating has been developed in Zürich in 2008/2009. This instrument is at present routinely run at ETH Zürich and will finally be operated by the Reiss-Engelhorn-Stiftung in Mannheim, Germany. The novel class of very compact AMS spectrometers shows a superb performance and ultra-high-precision radiocarbon dating measurements at the uncertainty level below 2‰.

#### 4.1.1 Research collaboration between ETHZ and ATOMKI

In 2009 research collaboration was officially started between the Laboratory of Ion Beam Physics of Swiss Federal Institute of Technology Zurich (ETH), Isotopech Zrt. and the Hertelendi Laboratory (HEKAL) of ATOMKI aiming at the development of a dedicated  $^{14}\text{C}$  AMS system for Hungary. In this project we have identified the need for a further improved AMS machine dedicated for radiocarbon studies in connection with environmental research, in particular equipped with a gas inlet system to handle  $\text{CO}_2$  sample material and agreed to undertake a collaboration to develop such a further optimized AMS machine for environmental radiocarbon dating studies, referred to as “EnvironMICADAS” by the end of 2010. This unique EnvironMICADAS for Hungary developed first in the world could ensure the continuing of the reputed Hungarian traditions and knowledge in  $^{14}\text{C}$  studies not only in the Eastern-Europe region but world-wide, as well.

The new developed AMS called EnvironMICADAS will be installed during the summer of 2011 in a new measurement hall of the ATOMKI (Figure 25).



**Figure 25.** The EnvironMICADAS is under construction at ETH Zürich, Switzerland.

## 5 ACKNOWLEDGEMENTS

We express our gratitude to the former members of the Section and its predecessors who helped to establish this line of research in ATOMKI, and contributed to the research work in the field during many years: Zoltán Elekes, József Hakl, Zoltán Köllő, Róbert Rozinai and Andrea Zsuzsanna Szántó.

To our technicians: Renáta Gönczi, Etelka Orbánné Pető, László Szőke, István Tóth, Ferenc Túri and technicians during the years: Mariann Kállai, László Katona, Éva Küss, Ágnes Szűcs and László Újkéri.

To the former heads of ATOMKI, of our Division and of our Section who helped significantly the survival of the Laboratory after we lost Ede: Sándor Bohátka, Árpád Zoltán Kiss, Rezső Lovas and Sándor Mészáros.

To the engineers: János Gál, Gyula Hegyesi, Zsolt Kertész, Zoltán Pintye and János Szádai to the staff of the workshops, and to all helpful colleagues.

To Mihály Veres and the staff of Isotoptech Zrt: Ágnes Czébely, Andrea Czébely, Zoltán Dezső, Enikő Heim, Mihály Jakab, Norbert Karacs, Zoltán Moór, Tamás Nagy, Csaba Pintér, Gyula Rác, Sándor Szabó and Csaba Vilmányi.

Last but not least we express our thanks for all our external collaborators and a partners.

## 6 REFERENCES

- [1] E. Hertelendi, J. Gál, A. Paál, S. Fekete, M. Györffi, I. Gál, Zs. Kertész, S. Nagy: Stable isotope mass spectrometer, *Fourth working meeting isotopes in nature* **1** (1987) 323
- [2] É. Csongor, E. Hertelendi: Radiokarbon kormeghatározásra alkalmas alacsony háttérű mérőrendszer (Low level radiocarbon dating system), *Annual Report of ATOMKI* **23** (1981) 189 (in Hung)
- [3] É. Csongor, I. Szabó, E. Hertelendi: Preparation of counting gas of proportional counters for radiocarbon dating, *Radiochemical and Radioanalytical Letters* **55** (1982) 303
- [4] É. Csongor, E. Hertelendi: Low-level counting facility for  $^{14}\text{C}$  dating, *Nuclear Instruments and Methods in Physics Research Section B: Beam Interactions with Materials and Atoms* **17** (1986) 493
- [5] E. Hertelendi, É. Csongor, L. Záborszky, J. Molnár, G. Dajkó, M. Györffi, S. Nagy: A counter system for high-precision  $^{14}\text{C}$  dating, *Radiocarbon* **31** (1989) 399
- [6] K. Balogh, E. Hertelendi: Természetes trícium koncentrációk mérésének lehetősége tömegspektrométerrel (Potential of mass spectrometric measurement of natural tritium concentrations), *Hydrology Report* **12** (1981) 553 (in Hung)
- [7] I. Futó, M. Molnár, L. Palcsu, É. Svingor, Zs. Szántó: Application of a noble gas mass spectrometric system in environmental studies, *Vacuum* **61** (2001) 441
- [8] L. Palcsu, M. Molnár, Zs. Szántó, É. Svingor, I. Futó: Metal container instead of glass bulb in tritium measurement in helium-3 ingrowth method, *Fusion Sciences and Technology* **41** (2002) 532
- [9] E. Hertelendi, G. Uchrin, P. Ormai:  $^{14}\text{C}$  release in various chemical forms with gaseous effluents from Paks Nuclear Power Plant, *Radiocarbon* **31** (1989) 754
- [10] É. Svingor: Ede Hertelendi (1950-1999), *Radiocarbon* **41** (1999) vii-x
- [11] T. Horváth, É. Svingor, M. Molnár: New radiocarbon dates for the Baden culture, *Radiocarbon* **50** (2008) 447
- [12] Zs. Szántó, R. Kertész, A. Morgós, D. Nagy, M. Molnár, M. Grabner, L. Rinyu, I. Futó: Combined techniques to date the first Turkish bridge over the river Tisza, Hungary, *Radiocarbon* **49** (2007) 515
- [13] Sz. Harangi, M. Molnár, A. P. Vinkler, B. Kiss, A. J. T. Jull, A. G. Leonard: Radiocarbon dating of the last volcanic eruptions of Ciomadul Volcano, Southeast Carpathians, Eastern-Central Europe, *Radiocarbon* **52** (2010) 2-3: 1498
- [14] Z. Kern, M. Molnár, É. Svingor, A. Perşoiu, B. Nagy: High resolution, well preserved tritium record in the ice of Borţig Ice Cave, Bihor Mountains, Romania, *The Holocene* **19** (2009) 729
- [15] L. Palcsu, É. Svingor, M. Molnár, Zs. Szántó, L. Rinyu, I. Horváth, Gy. Tóth: Isotope studies of a groundwater-flow system in granite, Middle Hungary, *IAH Selected Papers* **9** (2007) 343
- [16] I. Varsányi, L. Palcsu, L. Ó-Kovács: Groundwater flow system as an archive of palaeo-temperature: Noble gas, radiocarbon, stable isotope and geochemical study in the Pannonian Basin, Hungary, *Applied Geochemistry* **26** (2011) 91

- [17] L. Palcsu, Z. Major, W. Aeschbach-Hertig: A múltbeli barlanghőmérséklet meghatározása a cseppkövek vízzárvaiban oldott nemesgázok koncentrációja alapján (Determination of past temperature based on noble gas concentration of fluid inclusions in speleothems), *Proceedings of the Conference on Karst Development* (2006) 47 (in Hung)
- [18] L. Palcsu: Cseppkövek folyadékzárvaiban oldott nemesgázok, mint a múltbeli klíma vizsgálatának új lehetősége (Noble gases in fluid inclusions of speleothems as a new palaeoclimate proxy), *Proceedings of the 4<sup>th</sup> Carpathian Basin Conference on Environmental Science* (2008) 263 (in Hung)
- [19] L. Papp, L. Palcsu, Z. Major, O. Bak: Karbonátok folyadékzárvaiban oldott nemesgázok mérés technikája (Measurement technique of noble gases dissolved in fluid inclusions of carbonates), *Proceedings of the 6<sup>th</sup> Carpathian Basin Conference on Environmental Science* (2010) 271 (in Hung)
- [20] L. Palcsu, L. Rinyu, Z. Major, M. Molnár, I. Futó, Zs. Szántó, É. Svingor: A Pásnyag-forrás karsztvízrendszerének izotóphidrológiai vizsgálata (Isotope hydrological study of karts aquifer of Pásnyag spring), *Proceedings of the 9<sup>th</sup> Conference on Karst Development* (2004) 91 (in Hung)
- [21] G. Vodila, L. Palcsu, I. Futó, Zs. Szántó: A 9-year record of stable isotope ratios of precipitation in Eastern Hungary: Implications on isotope hydrology and regional palaeoclimatology, *Journal of Hydrology* **400** (2011) 144
- [22] Z. Köllő, L. Palcsu, Z. Major, L. Papp, M. Molnár, T. Ranga, P. Dombóvári, L. Manga: Experimental investigation and modelling of tritium washout by precipitation in the area of the nuclear power plant of Paks, Hungary, *Journal of Environmental Radioactivity* **102** (2011) 53
- [23] I. Svetlík, L. Tomáshová, M. Molnár, É. Svingor, I. Futó, T. Pintér, P. Rulík, V. Michálek: Monitoring of atmospheric  $^{14}\text{CO}_2$  in Central European countries, *Czechoslovak Journal of Physics* **56** (2006) 291
- [24] M. Molnár, T. Bujtás, É. Svingor, I. Futó, I. Svetlík: Monitoring of atmospheric excess  $^{14}\text{C}$  around Paks Nuclear Power Plant, Hungary, *Radiocarbon* **49** (2007) 1031
- [25] I. Svetlík, P. P. Povinec, M. Molnár, M. Vána, A. Sivo, T. Bujtás: Radiocarbon in the air of Central Europe: long-term investigations, *Radiocarbon* **52** (2010) 823
- [26] I. Svetlík, M. Molnár, M. Vána, V. Michálek, P. Stefanov: Estimation of  $^{14}\text{CO}_2$  amount in the atmosphere, *Journal of Radioanalytical and Nuclear Chemistry* **281** (2009) 137
- [27] M. Molnár, I. Major, L. Haszpra, I. Svetlík, É. Svingor, M. Veres: Fossil fuel  $\text{CO}_2$  estimation by atmospheric  $^{14}\text{C}$  measurement and  $\text{CO}_2$  mixing ratios in the city of Debrecen, Hungary. *Journal of Radioanalytical and Nuclear Chemistry* **286** (2010) 471
- [28] M. Molnár, L. Haszpra, É. Svingor, I. Major, I. Svetlík: Atmospheric fossil fuel  $\text{CO}_2$  measurement using a field unit in a Central European city during the winter of 2008/09, *Radiocarbon* **52** (2010) 835
- [29] I. Svetlík, P. P. Povinec, M. Molnár, F. Meinhardt, V. Michálek, J. Simon, É. Svingor: Estimation of long-term trends in the tropospheric  $^{14}\text{CO}_2$  activity concentration, *Radiocarbon* **52** (2010) 815
- [30] M. Molnár, L. Palcsu, É. Svingor, Zs. Szántó, I. Futó, P. Ormai: Gas formation in drum waste packages of Paks NPP, *Proceedings of International Conference, Nuclear Energy in Central Europe* (CDROM) (2001) 1008
- [31] Zs. Szántó, Z. Szűcs, É. Svingor, M. Molnár, L. Palcsu, I. Futó, N. Vajda, Zs. Molnár, É. Kabai: Determination of  $^{129}\text{I}$  in low level radioactive waste by two different methods, *Proceedings of International Conference, Nuclear Energy in Central Europe* (CDROM) (2001) 802
- [32] Zs. Szántó, É. Svingor, M. Molnár, L. Palcsu, I. Futó, Z. Szűcs: Diffusion of  $^3\text{H}$ ,  $^{99}\text{Tc}$ ,  $^{125}\text{I}$ ,  $^{36}\text{Cl}$  and  $^{85}\text{Sr}$  in granite, concrete and bentonite, *Journal of Radioanalytical and Nuclear Chemistry* **252** (2002) 133
- [33] M. Molnár, L. Palcsu, É. Svingor, Zs. Szántó, I. Futó: Headspace gas analysis of closed radioactive waste vaults in a near surface disposal facility of Hungary, *Proceedings of International Conference, Nuclear for New Europe* (CDROM) (2002) 1
- [34] Zs. Szántó, É. Svingor, M. Molnár, L. Palcsu, I. Futó: Approach to assessing the radiological impact of the Püspökszilágy RWTF, *International Conference on Issues and Trends in Radioactive Waste Management, Contributed Papers* (2002) 25
- [35] Zs. Szántó, É. Svingor, L. Palcsu, M. Molnár, I. Futó: Near field issues: Investigation of gas generation in situ, *Proceedings of International Conference, Management of Radioactive Waste from Non-Power Applications – Sharing the Experience* (CDROM) (2002) 397
- [36] M. Molnár, L. Palcsu, I. Futó, É. Svingor, Z. Major, M. Veres, P. Ormai, I. Barnabás: Study of gas generation in real L/ILW containers, *Journal of Radioanalytical and Nuclear Chemistry* **286** (2010) 745
- [37] Zs. Szántó, É. Svingor, I. Futó, Z. Major, L. Rinyu, M. Veres: A hydrochemical and isotopic case study around a near surface radioactive waste disposal, *Radiochimica Acta* **95** (2007) 55
- [38] G. Vodila, M. Molnár, M. Veres, É. Svingor, I. Futó, I. Barnabás, S. Kapitány: Mapping of tritium emissions using absorption vapour samplers, *Journal of Environmental Radioactivity* **100** (2009) 120
- [39] L. Palcsu, M. Molnár, Z. Major, É. Svingor, M. Veres, I. Barnabás, S. Kapitány: Detection of tritium and alpha decaying radionuclides in L/ILW by measurements of helium isotopes, *Journal of Radioanalytical and Nuclear Chemistry* **286** (2010) 483

- [40] É. Svingor, M. Molnár, L. Palcsu, M. Veres, T. Pintér, L. Köves: Monitoring system with automatic sampling units in the surroundings Paks NPP, *Czechoslovak Journal of Physics* **56** (2006) 133
- [41] R. Janovics, M. Molnár, I. Futó, L. Rinyu, É. Svingor, M. Veres, I. Somogyi, I. Barnabás: Development of an automatic sampling unit for measuring radiocarbon content of groundwater, *Radiocarbon* **52** (2010) 1141
- [42] W. Aeschbach-Hertig, H. El-Gamal, M. Wieser, L. Palcsu: Modeling excess air and degassing in groundwater by equilibrium partitioning with a gas phase, *Water Resource Research* **44** (2008) W08:449
- [43] L. Palcsu, Z. Major, Z. Köllő, L. Papp: Using an ultrapure  $^4\text{He}$  spike in tritium measurements of environmental water samples by the  $3\text{He}$ -ingrowth method, *Rapid Communications in Mass Spectrometry* **24** (2010) 698
- [44] M. Molnár, L. Palcsu, É. Svingor, M. Veres, T. Pintér, P. Tilky: Investigation of dissolved gases in the coolant of the cooling ponds and service pool No.1 of reactor No.2 of Paks Nuclear Power Plant, *Proceedings of the 6<sup>th</sup> International Seminar on Primary and Secondary Side Water Chemistry of Nuclear Power Plants* (CDROM) (2005) 1
- [45] M. Molnár, L. Palcsu, Z. Major, É. Svingor, M. Veres, T. Pintér, M. Veres: Dissolved gas measurements of the cooling ponds of Paks Nuclear Power Plant, Hungary, *Proceedings of International Conference on Water Chemistry of Nuclear Reactor System* (CDROM) (2006) 1
- [46] M. Molnár, S. Nagy, É. Svingor, I. Svetlík: Refining the  $\text{CO}_2$  absorption method for low level  $^{14}\text{C}$  liquid scintillation counting in the Atomki, *Proceedings of International Conference on the Advances in Liquid Scintillation Spectrometry, LSC 2005* (2006) 407
- [47] M. Molnár, L. Haszpra, I. Major, É. Svingor, M. Veres: Development of a mobile and high-precision atmospheric  $\text{CO}_2$  monitoring station, *Proceedings of European Geosciences Union General Assembly, Geophysical Research Abstract* CDROM 11 (2009) 10271
- [48] L. Rinyu, I. Futó, Á. Z. Kiss, M. Molnár, É. Svingor, G. Quarta, L. Calcagnile: Performance test of a new graphite target production facility in Atomki, *Radiocarbon* **49** (2007) 217
- [49] M. Molnár, L. Rinyu, I. Futó, É. Svingor, Á. Z. Kiss: Milligrammos minták radiokarbonos korméréseinek előkészítése az Atomki-ban (Preparation of radiocarbon measurements of samples of milligram size in the ATOMKI), *Proceedings of the 3<sup>rd</sup> Carpathian Basin Conference on Environmental Science* (2007) 106 (in Hung)
- [50] M. Molnár, L. Rinyu, T. Nagy, É. Svingor, I. Futó, M. Veres, A. J. T. Jull, G. S. Burr, R. Cruz, D. Biddulph: Developments and results from the new Hungarian graphite target line, *Nuclear Instruments and Methods in Physics Research Section B: Beam Interaction with Materials and Atoms* **268** (2010) 940
- [51] Á. Bihari, Z. Szűcs, M. Mogyorósi, T. Pintér: Combined determination of  $^{99}\text{Tc}$  and  $^{108\text{m}}\text{Ag}$  in L/ILW liquid wastes, *Journal of Radioanalytical and Nuclear Chemistry* **286** (2010) 759
- [52] H. A. Synal, S. Jacob, M. Suter: The PSI/ETH small radiocarbon dating system, *Nuclear Instruments and Methods in Physics Research Section B: Beam Interactions with Materials and Atoms* **172** (2000) 1
- [53] H. A. Synal, S. Jacob, M. Suter: New concepts for radiocarbon detection systems, *Nuclear Instruments and Methods in Physics Research Section B: Beam Interactions with Materials and Atoms* **161-163** (2000) 29
- [54] H. A. Synal, M. Stocker, M. Suter: MICADAS: A new compact radiocarbon AMS system, *Nuclear Instruments and Methods in Physics Research Section B: Beam Interactions with Materials and Atoms* **259** (2007) 7

## 1.1 Asymptotic properties of solvable $\mathcal{PT}$ -symmetric potentials

*G. Lévai*

The introduction of  $\mathcal{PT}$ -symmetric quantum mechanics generated renewed interest in non-hermitian quantum mechanical systems in the past decade.  $\mathcal{PT}$  symmetry means the invariance of a Hamiltonian under the simultaneous  $\mathcal{P}$  space and  $\mathcal{T}$  time reflection, the latter understood as complex conjugation. Considering the Schrödinger equation in one dimension, this corresponds to a potential with even real and odd imaginary components. This implies a delicate balance of emissive and absorptive regions that eventually manifests itself in properties that typically characterize real potentials, i.e. hermitian systems. These include partly or fully real energy spectrum and conserved (pseudo-)norm. A particularly notable feature of these systems is the spontaneous breakdown of  $\mathcal{PT}$  symmetry, which typically occurs when the magnitude of the imaginary potential component exceeds a certain limit. At this point the real energy eigenvalues begin to merge pairwise and re-emerge as complex conjugate pairs. Another unusual property of  $\mathcal{PT}$ -symmetric potentials is that they can, or sometimes have to be defined off the real  $x$  axis on trajectories that are symmetric with respect to the imaginary  $x$  axis.

After more than a decade of theoretical investigations a remarkable recent development was the experimental verification of the existence of  $\mathcal{PT}$ -symmetric systems in nature and the occurrence of spontaneous  $\mathcal{PT}$  symmetry breaking in them [1]. The experimental setup was a waveguide containing regions where loss and gain of flux occurred in a setout prescribed by  $\mathcal{PT}$  symmetry. These experimental developments require the study of  $\mathcal{PT}$ -symmetric potentials with various asymptotics, in which, furthermore, the complex potential component is finite in its range and/or its magnitude.

Having in mind that  $\mathcal{PT}$  symmetry allows for a wider variety of asymptotic properties than hermiticity, we studied three exactly solvable  $\mathcal{PT}$ -symmetric potentials and compared their scattering and bound states [2]. The ex-

amples included the Scarf II potential

$$V(x) = -\frac{V_1}{\cosh^2 x} + \frac{iV_2 \sinh x}{\cosh^2 x}, \quad (1)$$

the Rosen–Morse II potential

$$V(x) = -\frac{V_1}{\cosh^2(x)} + iV_3 \tanh(x) \quad (2)$$

and the Coulomb potential

$$V(x) = \frac{iZ}{t} + \frac{l(l+1)}{t^2}. \quad (3)$$

Potentials (1) and (2) are both defined on the real  $x$  axis, and their real components have the same form, while potential (3) is defined on a U-shaped trajectory running on both sides of the imaginary  $x$  axis encircling the origin.

Despite these circumstances, we found that the bound-state properties of potential (1) show more similarity with those of (3) than with those of (2). The former two systems possess strictly negative-energy bound states that are characterized by the  $q = \pm 1$  quantum number. Reaching a critical value of  $V_2 - V_1$  and  $l$  the spontaneous breakdown of  $\mathcal{PT}$  symmetry occurs and the bound states with opposite  $q$  merge pairwise and their energy eigenvalues turn complex for arbitrary value of the  $n$  principal quantum number. In contrast, the energy eigenvalues of potential (2) stay real for arbitrary value of  $V_1$  and  $V_3$  and do not carry the  $q$  quantum number. The spontaneous breakdown of  $\mathcal{PT}$  symmetry does not occur in this case, rather with increasing non-hermiticity the energy eigenvalues are gradually shifted to the positive domain. The properties of potential (2) are reminiscent of the purely imaginary  $ix^3$  potential, the classic example of  $\mathcal{PT}$ -symmetric quantum mechanics. The marked differences described above, which, however, do not show up in the scattering solutions, might be due to the asymptotically dominant and non-vanishing imaginary component in (2).

[1] C. E. Rüter *et al.*, Nature Physics **6** (2010) 192.

[2] G. Lévai, Int. J. Theor. Phys. **50** (2011) 997.

## 2.1 Renormalization of QCD<sub>2</sub>

*J. Kovács<sup>a)</sup>, S. Nagy<sup>a)</sup>, I. Nándori, K. Sailer<sup>a)</sup>*

Low dimensional fermionic models as toy models provide an excellent playground to try and develop new ideas and methods in quantum field theory. These models have only indirect physical meaning but they are much simpler than their 4-dimensional counterparts, and they usually show important characteristics of the original ones.

One usually takes the bosonized version of these models which are local self-interacting scalar theories, and can be investigated in an easier way. For example, the phase structure of the 2-dimensional quantum electrodynamics (QED<sub>2</sub>) with many flavors was mapped out from its bosonized version and it was shown that it exhibits only a single phase as opposed to the single-flavor QED<sub>2</sub>, which possesses weak and strong coupling phases.

The situation is a bit different in the case of the 2-dimensional quantum chromodynamics (QCD<sub>2</sub>). It is argued [1] that the single-flavor but multi-color QCD<sub>2</sub> possesses two phases, a weak coupling or quark phase, and a strong coupling or Bose phase. Elsewhere it is also argued [2] that the model has a single phase. This open question can be answered by considering the low-energy limit of the model, hence renormalization is required.

Our goal was in Ref. [3] to perform a renormalization group (RG) study of the bosonized multi-color (and single-flavor) QCD<sub>2</sub> in order to determine its low-energy behavior and to map out its phase structure. We showed [3,4] that both models, the bosonized multi-flavor QED<sub>2</sub> and the multi-color QCD<sub>2</sub> can be considered as the specific forms of a generalized layered sine-Gordon model which consists of 2-dimensional periodic scalar fields coupled by an appropriate mass matrix whose bare Lagrangian is written as

$$\mathcal{L} = \frac{1}{2}(\partial_\mu \Phi)^2 + \frac{1}{2}\Phi \mathcal{M}^2 \Phi + y \sum_{n=1}^N \cos(\beta \phi_n) \quad (4)$$

with the  $O(N)$  multiplet  $\Phi = (\phi_1, \dots, \phi_N)$ . For the specific choice  $\beta^2 = 4\pi$  with the mass

matrices (matrix elements)

$$(\mathcal{M}_{\text{QED}}^2)_{a,b} = (-1)^{a+b} G, \quad (5)$$

with  $a, b = 1, 2, \dots, N_f$ ,  $G = e^2/\pi$  (where  $e$  is the coupling constant of QED<sub>2</sub>) and

$$(\mathcal{M}_{\text{QCD}}^2)_{a,b} = (N-1)J\delta_{a,b} - J, \quad (6)$$

with  $a, b = 1, 2, \dots, N_c$ ,  $J \sim g^2$  (where  $g$  is the coupling constant of QCD<sub>2</sub>), one recovers the bosonized version of the  $N_f$ -flavor QED<sub>2</sub> for  $N = N_f$  and that of the  $N_c$ -color QCD<sub>2</sub> for  $N = N_c$ , respectively. The amplitude  $y$  of the periodic piece of the potential is identical for all component fields, and it is proportional to the fermion mass ( $y \sim m$ ).

We note that for  $N = 2$  the number of non-zero eigenvalues of mass matrices (5) and (6) coincide, consequently, the Bose forms of the 2-flavor QED<sub>2</sub> and the 2-color QCD<sub>2</sub> are similar. This implies the similar trivial phase structures of these models. The bosonized 3-color QCD<sub>2</sub> and 3-flavor QED<sub>2</sub> are, however, different, hence their phase structures are not necessarily the same. The bosonized 3-flavor QED<sub>2</sub> is known to be in the symmetry broken phase and represents a free massive theory. The low-energy behavior of the bosonized 3-color QCD<sub>2</sub> has been determined by the functional RG technique, and it was shown that the model exhibits a single phase similarly to the 3-flavor QED<sub>2</sub>. Thus, one can conclude that the 2-dimensional multi-color QCD<sub>2</sub> has a trivial phase structure, independently of the number of colors.

a) Department of Theoretical Physics, University of Debrecen, H-4032, Debrecen, Hungary

[1] V. Baluni, Phys. Lett. B **90**, 407 (1980).

[2] E. Abdalla, R. Mohayaee, A. Zadra, Int. J. Mod. Phys A **12**, 4539 (1997).

[3] J. Kovács, S. Nagy, I. Nándori, K. Sailer, JHEP **1101**, 126 (2011).

[4] I. Nándori, Phys. Lett. B **662**, 302 (2008).

## 2.2 Phase Structure and Compactness

*I. Nándori, S. Nagy<sup>a)</sup>, K. Sailer<sup>a)</sup>, A. Trombettoni<sup>b)</sup>*

The computation in a completely controlled way of renormalization group (RG) flows in gauge theories is at date a challenging issue. A major reason for such difficulties is the fact that, one must adopt a regularization scheme which incorporates a gauge invariant cutoff even for approximated treatments of exact RG equations. A related problem is the determination of critical properties and phases of compact field theories, since, compactness can be considered as one of the simplest realization of the gauge symmetry.

In order to study the influence of compactness on low-energy properties, it would be then relevant to compare the phase structure of a field theory with the fields being respectively compact and non-compact. In Ref. [1] we perform such comparison for the multi-frequency sine-Gordon (SG) model in  $1 + 1$  dimensions. Several reasons lead us to the choice and use of such a model for the purpose of studying the effects of compactness: first, the single-frequency SG is a paradigmatical example of integrable field theory, very well studied in the last four decades. Second, the rich phase structure of the compact double-frequency SG has been the subject of intense study, third, SG type scalar models have importance in two dimensions since they are the Bose forms of fermionic and gauge theories, and last but not least, a large variety of non-compact SG models have already been studied using non-perturbative RG methods [2,3].

Our goal was to consider the non-compact multi-frequency SG model by means of the functional RG approach and to compare our findings to those obtained by other methods for the compact model. The Lagrangian of the model reads

$$\mathcal{L} = \frac{1}{2} \partial_\mu \phi \partial^\mu \phi - \sum_i^n \mu_i \cos(\beta_i \phi + \delta_i) \quad (7)$$

which contains  $n$  cosine terms where  $\phi$  is a real

scalar field,  $\beta_i$  are the frequencies,  $\beta_i \neq \beta_j$  if  $i \neq j$ ,  $\mu_i$  are the coupling constants and  $\delta_i$  are the phases in the terms of the potential. It was shown by semiclassical analysis and by means of form factor perturbation and truncated conformal space approaches that (first and second order) phase transitions occur in the compact multi-frequency SG model as the coupling constants are tuned appropriately (assuming that  $n > 1$ ).

We showed that the high-energy scaling of the compact and the non-compact multi-frequency SG models coincides but their low-energy behaviors are different. In the high-energy limit, the quantum fluctuations (with high frequency and small amplitude) do not feel the difference between the models defined by compact and non-compact fields but the disagreement is expected to appear in the low-energy limit due to the large-amplitude quantum fluctuations of the low-energy domain. Therefore, on the one hand the critical frequency  $\beta_c^2 = 8\pi$  at which the SG model undergoes a topological phase transition is found to be unaffected by the compactness of the field since it is determined by high-energy scaling laws. On the other hand, while it is known that the compact model has first and second order (Ising) type phase transitions which are determined by the low-energy scaling, we showed that these are absent in the non-compact model.

a) Department of Theoretical Physics, University of Debrecen, H-4032, Debrecen, Hungary

b) SISSA and INFN, Sezione di Trieste, via Bonomea 265, I-34136 Trieste, Italy

[1] I. Nándori, S. Nagy, K. Sailer, A. Trombettoni, *JHEP* **1009**, 069 (2010).

[2] I. Nándori, S. Nagy, K. Sailer, A. Trombettoni, *Phys. Rev. D* **80**, 025008 (2009).

[3] S. Nagy, I. Nándori, J. Polonyi, K. Sailer, *Phys. Rev. Lett.* **102**, 241603 (2009).

### 3.1 Total reaction cross sections from elastic $\alpha$ -nucleus scattering angular distributions around the Coulomb barrier

*P. Mohr<sup>a)</sup>, D. Galaviz<sup>b)</sup>, Zs. Fülöp, Gy. Gyürky, G. G. Kiss, E. Somorjai*

The total reaction cross section  $\sigma_{\text{reac}}$  is a valuable measure for the prediction of  $\alpha$ -induced reaction cross sections within the statistical model and for the comparison of scattering of tightly bound projectiles to weakly bound and exotic projectiles. Here we provide the total reaction cross sections  $\sigma_{\text{reac}}$  derived from our previously published angular distributions of  $\alpha$ -elastic scattering on  $^{89}\text{Y}$  [1],  $^{92}\text{Mo}$  [2],  $^{112,124}\text{Sn}$  [3], and  $^{144}\text{Sm}$  [4] at energies around the Coulomb barrier. The measured angular distributions cover a broad angular range and thus allow the determination of  $\sigma_{\text{reac}}$  with small uncertainties of about 3%. The results are listed in Table 1.

**Table 1.** Total reaction cross sections  $\sigma_{\text{reac}}$  derived from the  $\alpha$ -elastic angular distributions of  $^{89}\text{Y}$  [1],  $^{92}\text{Mo}$  [2],  $^{112,124}\text{Sn}$  [3], and  $^{144}\text{Sm}$  [4].

target	$E_{\text{c.m.}}$ (MeV)	$\sigma_{\text{reac}}$ (mb)
$^{89}\text{Y}$	15.51	$678 \pm 20$
$^{89}\text{Y}$	18.63	$1004 \pm 30$
$^{92}\text{Mo}$	13.20	$238 \pm 7$
$^{92}\text{Mo}$	15.69	$578 \pm 17$
$^{92}\text{Mo}$	18.62	$883 \pm 26$
$^{112}\text{Sn}$	13.90	$93 \pm 3$
$^{112}\text{Sn}$	18.84	$695 \pm 21$
$^{124}\text{Sn}$	18.90	$760 \pm 23$
$^{144}\text{Sm}$	19.45	$404 \pm 12$

The data of the tightly bound  $\alpha$  projectile are compared to reaction cross sections induced by weakly bound projectiles ( $^{6,7,8}\text{Li}$ ) and the exotic projectile  $^6\text{He}$  with a neutron halo. A systematic behavior of the so-called reduced cross sections  $\sigma_{\text{red}}$  versus the reduced energy  $E_{\text{red}}$  (as defined in [5]) is found for all nuclei under study (see Figure 1).

The understanding of the energy dependence of  $\sigma_{\text{reac}}$  at low energies is the essential ingredient for the prediction of  $\alpha$ -induced reaction cross sections at energies far below the Coulomb barrier where the Gamow window for astrophysical reaction rates is located. The aim of the ongoing studies is to find a consistent  $\alpha$ -nucleus potential which is able to describe elastic  $\alpha$ -scattering and  $\alpha$ -induced reaction cross sections simultaneously.

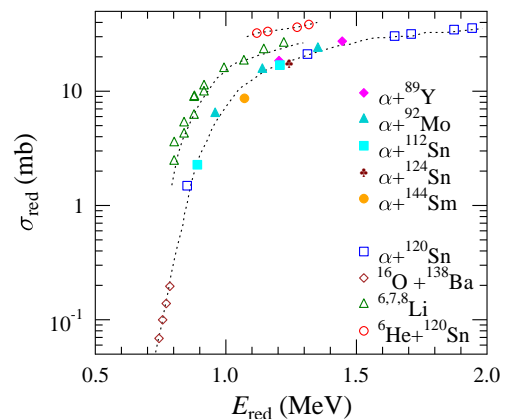


**Figure 1.** Reduced reaction cross sections  $\sigma_{\text{red}}$  versus reduced energy  $E_{\text{red}}$  for tightly bound  $\alpha$ -particles and  $^{16}\text{O}$ , weakly bound  $^{6,7,8}\text{Li}$  projectiles, and exotic  $^6\text{He}$  (see [5]). The error bars of the new data (full data points) are omitted because they are smaller than the point size. The lines are to guide the eye.

a) Diakonie-Klinikum Schwäbisch Hall, D-74523 Schwäbisch Hall, Germany

b) Centro de Fisica Nuclear, University of Lisbon, 1649-003 Lisbon, Portugal

[1] G. G. Kiss *et al.*, Phys. Rev. C **80**, 045807 (2009).

[2] Zs. Fülöp *et al.*, Phys. Rev. C **64**, 065805 (2001).

[3] D. Galaviz *et al.*, Phys. Rev. C **71**, 065802 (2005).

[4] P. Mohr *et al.*, Phys. Rev. C **55**, 1523 (1997).

[5] P. deFaria *et al.*, Phys. Rev. C **81**, 044605 (2010).

### 3.2 Nuclear structure study of $^{19,21}\text{N}$ nuclei by $\gamma$ spectroscopy

*Z. Elekes, Zs. Vajta, Zs. Dombrádi, T. Aiba<sup>a)</sup>, N. Aoi<sup>b)</sup>, H. Baba<sup>b)</sup>, D. Bemmerer<sup>c)</sup>, B. A. Brown<sup>d)</sup>, T. Furumoto<sup>e)</sup>, Zs. Fülöp, N. Iwasa<sup>f)</sup>, Á. Kiss<sup>g)</sup>, K. Kobayashi<sup>h)</sup>, Y. Kondo<sup>i)</sup>, T. Motobayashi<sup>b)</sup>, T. Nakabayashi<sup>i)</sup>, T. Nannichi<sup>i)</sup>, Y. Sakuragi<sup>e)</sup>, D. Sohler, M. Takashina<sup>j)</sup>, S. Takeuchi<sup>b)</sup>, K. Tanaka<sup>b)</sup>, Y. Togano<sup>b)</sup>, K. Yamada<sup>b)</sup>, M. Yamaguchi<sup>b)</sup>, K. Yoneda<sup>b)</sup>*

In the past years, new magic numbers far from stability have been discovered. One of the new subshell closures is at  $N=14$ , the strength of which was determined to be 4.2 MeV in  $^{22}\text{O}$ . Recently, disappearance of this  $N=14$  gap in carbon isotopes has been reported via the spectroscopy of  $^{20}\text{C}$ . Here, we investigated the interaction of a  $^{21}\text{N}$  radioactive ion beam with hydrogen and lead target. This allowed us to study the transition along the  $N=14$  line and to give spectroscopic information on the structure of the lighter neutron-rich nitrogen isotopes.

The experiment was performed at the Rikagaku Kenkyusho (RIKEN) Nishina Center by using a  $^{40}\text{Ar}$  primary beam of 63 MeV/nucleon energy and 700 pnA intensity. Other details of the setup and particle identification can be found elsewhere [1].

The Doppler-corrected spectra, which use the hydrogen target were produced with multiplicity (M) 1 and 2 of the  $\gamma$  ray detector array for all the nitrogen isotopes. Spectra for  $^{18}\text{N}$  served as a cross-check of the procedure because the low-energy excited states for this nucleus are well known. Two peaks were found for  $^{19}\text{N}$  in the neutron knockout reaction at 529(21) and 1137(26) keV. This is in good agreement with Ref. [2] where these transitions form a cascade. For  $^{21}\text{N}$ , the transition between the first excited and ground states [ $E_\gamma=1140(30)$  keV] dominates the proton inelastic scattering spectra with  $M=1$ , while the  $M=2$  spectra also contain events, which originate from the transition between the second and first excited states [ $E_\gamma=1210(33)$  keV]. This agrees well with the conclusion drawn in Ref. [2] on the level scheme where the two strongest peaks were found at 1177 and 1228 keV.

In addition to the level scheme, the inelastic scattering cross sections were also de-

duced for  $^{21}\text{N}$  both with hydrogen and with lead targets. The net counts in the nearby peaks for the spectra with liquid hydrogen were derived by fixing the known peak positions and the peak widths determined previously. The relative intensities deduced from the spectrum, which contain all the multipolarities are: 100(10) for the 1140 keV line and 65(6) for the 1210 keV line. The three excitation cross sections determined are  $\sigma(1140, \text{H}) = 6.6(8)$  mb,  $\sigma(2350, \text{H}) = 12.3(16)$  mb, and  $\sigma(1140, \text{Pb}) = 11.4(34)$  mb.

The cross sections were interpreted in terms of the collective model. The determination of the proton and neutron deformation lengths ( $\delta_p, \delta_n$ ) was performed in a similar manner described in detail in Ref. [3] and found to be  $\delta_n=0.95(5)$  fm and  $\delta_p=0.95(15)$  fm. With these values, we obtain the quadrupole neutron and proton transition matrix elements  $M_n^2=110(12)$  fm<sup>4</sup>,  $M_p^2=28(9)$  fm<sup>4</sup>, and the ratio  $M_n/M_p=2.0$ . This ratio is equal to  $N/Z$ , which shows the pure isoscalar character of the transition. These results are similar to those of the  $^{22}\text{O}$  nucleus, which has 14 neutrons, just one proton closer to stability, where small transition matrix elements together with  $M_n/M_p=1.4(5)$   $N/Z$  also were extracted.

According to the weak-coupling approximation, the sum of the E2 strengths from the ground state to the  $3/2^-$  and  $5/2^-$  states in the  $^{21}\text{N}$  isotope gives the  $B(E2; 0^+ \rightarrow 2^+)$  strength in its appropriate core. By using this assumption, the effective  $B(E2)$  value of the ground state transition in the core of  $^{21}\text{N}$  can be estimated as  $56(18)$  e<sup>2</sup>fm<sup>4</sup>. The shell model calculations give 54 e<sup>2</sup>fm<sup>4</sup> summed strength for  $^{21}\text{N}$  [2], which is about twice the  $^{22}\text{O}$  value and lies about halfway between the neighbouring oxygen and carbon  $B(E2; 0^+ \rightarrow 2^+)$  values. The shell model calculation gives 110 e<sup>2</sup>fm<sup>4</sup> for  $^{20}\text{C}$ , which is much larger than the experimen-

tal value ( $<18 \text{ e}^2\text{fm}^4$ ) because of the decoupling of the neutrons from the core in heavy carbon nuclei. This fact shows that the core structure of the nitrogen isotopes is softer than that of the singly-closed shell oxygen isotopes and is consistent with the 1.2 MeV reduction of the  $N=14$  shell closure when going from  $^{22}\text{O}$  to  $^{21}\text{N}$  as a result of the removal of a proton from the  $p_{1/2}$  orbit.

[1] Z. Elekes *et al.*: Phys. Rev. C **82** (2010) 027305.

[2] D. Sohler *et al.*, Phys. Rev. C **77** (2008) 044303.

[3] Z. Elekes *et al.*, Phys. Rev. C **78** (2008) 027301.

a) Niigata University, Japan

b) RIKEN, Japan

c) Forschungszentrum Dresden-Rossendorf, Germany

d) Michigan State University, USA

e) Osaka City University, Japan

f) Tohoku University, Japan

g) Eötvös Loránd University, Hungary

h) Saitama University, Japan

i) Tokyo Institute of Technology, Japan

j) RCNP, Osaka University, Japan

### 3.3 Parameters of the isobar analog resonance in complex optical potential

A. Rácz<sup>a)</sup>, T. Vertse<sup>a)</sup>

A simple description of the isobar analog resonances (IAR) can be done by using the coupled Lane-equations (CLE). In the CLE

$$\begin{aligned} [K_l + V_p - \mathcal{E}_p] \phi_p &= - \sqrt{\frac{1}{2}T_A V_1} \phi_n \\ [K_l + V_n - (\mathcal{E}_p - \Delta_c)] \phi_n &= - \sqrt{\frac{1}{2}T_A V_1} \phi_p, \end{aligned}$$

the interaction of the nucleon with the core is described by complex optical potentials  $V_0, V_{so}, V_1$ . The diagonal potentials in the proton/neutron channels are  $V_p = V_0 - \frac{V_1}{2}T_A + V_C + V_{so}$  and  $V_n = V_0 + \frac{V_1}{2}(T_A - 1) + V_{so}$ . In a recent publication the IAR of the  $^{208}\text{Pb} + p$  system were calculated in real nuclear potentials [1]. Now we extend the calculations for complex potentials. Our main goal is to check the accuracy of the complex energy shell model (CXSM) against the standard coupled channels (CC) approach for complex optical potentials. In the CC approach the calculated  $S(\mathcal{E}_p)$  val-

ues (along the real energy axis) are fitted by the one pole approximation form:

$$S(\mathcal{E}_p) = e^{2i\delta_p(\mathcal{E}_p)} \left(1 - i \frac{\Gamma_p}{\mathcal{E}_p - \mathcal{E}_{IAR}}\right),$$

where the complex energy of the resonance is  $\mathcal{E}_{IAR} = E_r - i\frac{\Gamma}{2}$ . In the CXSM approach we diagonalize the matrix of the CLE in Berggren-bases in the proton and neutron channels. The basis functions in these channels are the solutions of the diagonal parts of the CLE with real potentials:

$$\left[ K_l + \Re V_p - E_n^{(p)} \right] u_n^{(p)}(r) = 0,$$

$$\left[ K_l + \Re V_n - E_n^{(n)} \right] u_n^{(n)}(r) = 0.$$

One of the complex eigenvalues we get from the diagonalization belongs to the IAR. Here we present preliminary results for the  $g_{9/2}$  partial wave case with complex  $V_0$  potential.

**Table 1.** Comparison of the IAR parameters (the position  $E_r$  and the total width  $\Gamma$ ) calculated by using the CC and CXSM methods for different values of the imaginary part of the potential  $V_0$ .

$\Im V_0$	$E_r(\text{CXSM})$	$E_r(\text{CC})$	$\Gamma(\text{CXSM})$	$\Gamma(\text{CC})$
0.3	14.952	14.961	0.421	0.423
0.2	14.953	14.958	0.296	0.298
0.1	14.953	14.956	0.171	0.172
0	14.954	14.954	0.046	0.047
-0.1	14.954	14.955	-0.079	-0.078

One can observe that the results of the CC and CXSM methods agree well. Now  $\Im V_0 > 0$  means absorption from the proton channel. The IAR is the broadest at  $\Im V_0 = 0.3$  MeV. By taking  $\Im V_0 < 0$  we can simulate a source of protons in the elastic channel and with  $\Im V_0 = -0.1$  MeV we get negative total width for the resonance. The agreement between the results of the two methods is good even in this case.

#### Acknowledgements

This work has been partially supported by the TAMOP 4.2.1/B-09/1/KONV-2010-007/IK/IT. The project is implemented through the New Hungarian Development Plan co-financed by the European Social Fund, and the European Regional Development Fund.

a) University of Debrecen, Faculty of Informatics, H-4010 Debrecen, P. O. Box 12, Hungary

[1] R. Id Betan, A. T. Kruppa, T. Vertse, Phys. Rev. C **78**, 044308 (2008).

### 3.4 Towards a high precision astrophysical S-factor measurement for the ${}^3\text{He}+{}^4\text{He}$ reaction

*C. Bordeanu*<sup>a)</sup>, *Zs. Fülöp, Gy. Gyürky, Z. Halász, T. Szücs, E. Somorjai, J. Farkas*

The uncertainty of the  $S_{34}(0)$  value for the  ${}^3\text{He}+{}^4\text{He}\rightarrow{}^7\text{Be}+\gamma$  reaction is the nuclear physics biggest uncertainty contributing to the neutrino flux in the SSM (Standard Solar Model) from the decay of  ${}^7\text{Be}$  from the Sun [1]; so that a possible reduction of this uncertainty will significantly reduce the uncertainty in the calculated flux in the frame of the SSM and which the BOREXINO [2] and KamLAND [3] experiments are supposed to observe.

In the last 50 years, this experiment produced a lot of data somehow in conflict (see the prompt and delayed gamma rays measurements in [4]). For the last 10 years, new data was produced due to high precision measurements, new technology and new methods to reduce the background [5–8]. Theoretical models didn't yet solve the astrophysical factor fitting issue [9–13]. New perspectives [14–15] on the low-energy behavior investigations for the astrophysical S-factor for radiative captures have been recently introduced with extraordinarily good results for the reaction modern data. Controversy is still waiting for other similar experiments data and new experimental data on this reaction as well. In the new NuPECC Range Plan 2010 there is a recommendation for a future better absolute cross section measurement for this reaction [16].

The goal is to determine the astrophysical factor  $S_{34}(0)$  for the  ${}^3\text{He}+{}^4\text{He}$  reaction within a  $\pm 5\%$  error using the activation method for the radiative capture reaction. This experiment is planned to be fulfilled at ATOMKI in the next two years. Its accomplishment became a necessity after the last most recent results coming from LUNA, Seattle, ERNA and Weizmann.

The new approach consists in building a gas target chamber in ATOMKI for this experiment and all the enclosed systems required for a good operation, such as gas manipulation and gas pressure monitoring.

A first step had been done at the Van de Graaff accelerator for the contaminants check

using an alpha beam of 3.8 MeV energy and 200 nA intensity impinging on Cu and Al stopping foils of high purity. After several hours of gamma rays collection using the ORTEC Maestro detection system the data analysis revealed that the chance to create extra  ${}^7\text{Be}$  coming from parasitic reactions is under the background value in the energy region close to 478 keV.

#### *Acknowledgements*

This project is financially supported by OTKA and NKTH through the HUMAN–MB–08–B mobility project NKTH–OTKA–EU FP7 (Marie Curie). Many thanks to the accelerator people for their support.

a) on leave from NIPNE-HH, Magurele, Romania

- [1] J.N. Bahcall and M. H. Pinsonneault, *Phys. Rev. Lett.* **92**, 121301 (2004).
- [2] Borexino collaboration  
[http://arxiv.org/PS\\_cache/arxiv/pdf/0708/0708.2251v2.pdf](http://arxiv.org/PS_cache/arxiv/pdf/0708/0708.2251v2.pdf)
- [3] K. Eguchi *et al.* *Phys. Rev. Lett.* **90**, 021802(2003).
- [4] E. Adelberger *et al.* *Rev.Mod. Phys.* **70** (1998) 055502.
- [5] LUNA–Collaboration (Gyürky *et al.*), *Phys. Rev. C* **75**, 035805 (2007).
- [6] Brown *et al.*, *Phys. Rev. C* **76**, 055801 (2007).
- [7] Nara Singh *et al.*, *Phys. Rev. Lett.* **93**, 262503 (2004).
- [8] ERNA–Collaboration (Di Leva *et al.*), *Phys.Rev.Lett.***102** (2009) 232502.
- [9] Descouvemont *et al.*, *At. Data. Nucl. Data Tables* **88**, 203 (2004).
- [10] Kajino *et al.*, *ApJ* **319**, 531 (1987).
- [11] Csoto and Langanke, *Few-Body Systems* **29**, 121 (2000).
- [12] Nollett, *Phys. Rev. C* **63**, 054002, 2001.
- [13] Cyburt and Davids, *Phys. Rev. C* **78**, 064614 (2008).
- [14] A.M. Mukhamedzhanov *et al.* *Nucl. Phys. A* **708** (2002) 437.
- [15] T. Neff <http://arxiv.org/abs/1011.2869v1>
- [16] [http://www.nupecc.org/lrp2010/Documents/lrp2010\\_final.pdf](http://www.nupecc.org/lrp2010/Documents/lrp2010_final.pdf)

### 3.5 Alpha-induced reaction cross section measurements on $^{151}\text{Eu}$ for the astrophysical $\gamma$ -process

Gy. Gyürky, Z. Elekes, J. Farkas, Zs. Fülöp, Z. Halász, G. G. Kiss, E. Somorjai, T. Szücs, R. T. Güray<sup>a</sup>, N. Özkan<sup>a</sup>, C. Yalçın<sup>a</sup>, T. Rauscher<sup>b</sup>

The astrophysical  $\gamma$ -process is the main production mechanism of the p-isotopes, the heavy, proton-rich nuclei not produced by neutron capture reactions in the astrophysical s- and r-processes. The  $\gamma$ -process is a poorly known process of nucleosynthesis, the models are not able to reproduce well the p-isotope abundances observed in nature. Experimental data on nuclear reactions involved in  $\gamma$ -process reaction networks are clearly needed to provide input for a more reliable  $\gamma$ -process network calculation.

As a continuation of our systematic study of reactions relevant for the  $\gamma$ -process, the cross sections of the  $^{151}\text{Eu}(\alpha, \gamma)^{155}\text{Tb}$  and  $^{151}\text{Eu}(\alpha, n)^{154}\text{Tb}$  reactions have been measured. These reactions have been chosen because  $\alpha$ -induced cross section data in the region of heavy p-isotopes are almost completely missing although the calculations show a strong influence of these cross section on the resulting abundances. Since the reaction products of both reactions are radioactive, the cross sections have been measured using the activation technique.

The targets have been prepared by evaporating  $\text{Eu}_2\text{O}_3$  enriched to 99.2% in  $^{151}\text{Eu}$  onto thin Al foils. The target thicknesses have been measured by weighing and Rutherford Backscattering Spectroscopy. The targets have been irradiated by typically 1-2  $\mu\text{A}$  intensity  $\alpha$ -beams from the cyclotron of ATOMKI. The investigated energy range between 12 and 17 MeV was covered with 0.5 MeV steps. This energy range is somewhat higher than the astrophysically relevant one, but the cross sec-

tion at astrophysical energies is so low that the measurements are not possible there. The  $\gamma$ -activity of the reaction products has been measured by a shielded HPGe detector. The absolute efficiency of the detector was measured with several calibration sources. Since  $^{154}\text{Tb}$  has two long lived isomeric states, partial cross sections of the  $^{151}\text{Eu}(\alpha, n)^{154}\text{Tb}$  reaction leading to the ground and isomeric states could be determined separately.

The obtained results are compared with the predictions of the statistical model code NON-SMOKER<sup>WEB</sup> version v5.8.1 [2] which is widely used in  $\gamma$ -process network calculations. It is found that the calculations overestimate the cross sections by about a factor of two. A sensitivity analysis shows that this discrepancy is caused by the inadequate description of the  $\alpha$ +nucleus channel. A factor of two reduction of the reaction rate of  $^{151}\text{Eu}(\alpha, \gamma)^{155}\text{Tb}$  in  $\gamma$ -process network calculations with respect to theoretical rates using the standard optical potential by McFadden and Satchler (1966) [2] is recommended.

Further details of the experiment, the data analysis and the astrophysical discussion can be found in [3].

a) Department of Physics, Kocaeli University, TR-41380 Umuttepe, Kocaeli, Turkey

b) Department of Physics, University of Basel, CH-4056 Basel, Switzerland

[1] T. Rauscher, code NON-SMOKER<sup>WEB</sup>, <http://nucastro.org/websmoker.html>

[2] L. McFadden and G. R. Satchler, Nucl. Phys. **84**, 177 (1966)

[3] Gy. Gyürky *et al.* J. Phys. G **37**, 115201 (2010)

### 3.6 Shell or cluster structure

*N. Itagaki<sup>a)</sup>, J. Cseh<sup>b)</sup>, M. Ploszajczak<sup>c)</sup>*

The question of how much the states of  $N = Z$  nuclei are clusterized, or how much they have a shell-structure is an old and important problem of nuclear structure. Both the shell model and the cluster model provide us with a complete (or overcomplete) basis (in their general form, without simplifying assumptions), therefore, any nuclear state can be expanded in shell or cluster states. When performing these expansions for a specific nuclear state there are four possibilities. i) It is simple in the shell basis, but it is not simple in the cluster one. ii) It is simple in the cluster basis, but not in the shell one. iii) It is simple in both bases. iv) It is not simple in any of them. State of kind i) can be called a good shell-model state, ii) is a good cluster state, iii) is a good shell-model-like cluster state, and iv) is not a simple state.

In [1] we have investigated this question for the states of the ground-band of the  $^{20}\text{Ne}$  and  $^{24}\text{Mg}$  nuclei. A microscopic approach was applied (generator coordinate method with antisymmetrized quasicluster basis), in which the  $^{16}\text{O}+\alpha(s)$  state could be desolved into  $^{16}\text{O}+\text{nucleons}$ , by varying a parameter of the wavefunction. The physical reason for this change is the increasing importance of the spin-orbit interaction.

It turned out that in both nuclei the description of the experimental data requires wavefunctions which are close to category iii), i.e. good shell-model-like cluster states.

As for the physical content and the basic features of the different types of states the following can be added. A typical shell model state of type i) is the j-j coupled state, which corresponds to a strong spin-orbit force, and has an SU(2) symmetry. A state of type ii) is a rigid molecule-like cluster state, which has an O(4) symmetry. The shell-like cluster state iii) is an L-S coupled state having an SU(3) symmetry. In light of the recent phase-studies of the quantum systems they can be considered as different phases of the finite nuclear matter.

Our finding on the dominance of the shell-model-like clusterization is in line with the conclusion of the shell model studies on the approximate validity of the SU(3) symmetry.

[1] N. Itagaki, J. Cseh, M. Ploszajczak, Phys. Rev. C **83** (2011) 014302

<sup>a)</sup> *Yukawa Institute, Kyoto, Japan*

<sup>b)</sup> *ATOMKI, Debrecen, Hungary*

<sup>c)</sup> *GANIL, Caen, France*

### 3.7 Observation of $\gamma$ -band structure in $^{104}\text{Pd}$

*D. Sohler, J. Timár, I. Kuti, J. Molnár, A. Algora, Zs. Dombrádi, J. Gál, A. Krasznahorkay, L. Zolnai, P. Joshi<sup>a)</sup>, K. Starosta<sup>b)</sup>, D.B. Fossan<sup>c)</sup>, R. Wadsworth<sup>a)</sup>, P. Bednarczyk<sup>d)</sup>, D. Curien<sup>e)</sup>, G. Duchene<sup>e)</sup>, A. Gizon<sup>f)</sup>, J. Gizon<sup>f)</sup>, D.G. Jenkins<sup>a)</sup>, T. Koike<sup>g)</sup>, E.S. Paul<sup>h)</sup>, P.M. Raddon<sup>a)</sup>, G. Rainovski<sup>i)</sup>, J.N. Scheurer<sup>j)</sup>, A.J. Simons<sup>a)</sup>, C. Vaman<sup>b)</sup>, A.R. Wilkinson<sup>a)</sup>*

Low-lying cascades built on the second  $2^+$  state have been observed in several Pd and Ru isotopes in the  $A \approx 100$  mass region. Recently, such a structure has been identified also in  $^{102}\text{Ru}$  and it was interpreted as a quasi- $\gamma$  band associated with  $\gamma$ -soft triaxial deformation, which might be confined in a region away from axial symmetry. Since the nuclear structure of  $^{104}\text{Pd}$  shows similar characteristics than that of  $^{102}\text{Ru}$  having only 2 protons less, the existence of a quasi- $\gamma$  band is expected also in the studied nucleus.

The levels of the nonyrast low-lying positive-parity structure established in the present work were grouped into a  $\gamma$ -band which is built on the second  $2^+$  state of  $^{104}\text{Pd}$ . The band assignment is based on the observed decay pattern and on the similarities with the structure of  $^{102}\text{Ru}$ . A distinction between excitations in a  $\gamma$ -soft and a  $\gamma$ -rigid potential can be deduced from the energy sequence in the  $\gamma$ -band and can be expressed in the odd-even spin energy staggering function

$$S(I, I-1, I-2) = \frac{E(I) + E(I-2) - 2E(I-1)}{E(2_1^+)}$$

In the case of a triaxial rigid rotor this staggering gives positive values for even spins and negative ones for odd spins. For a  $\gamma$ -soft rotor it has an opposite phase, the values fall below 0 for even spins and above 0 for odd spins.

The experimental odd-even spin energy staggerings deduced for these bands are displayed in Fig. 1 together with the values extracted for  $^{102}\text{Ru}$ . The values obtained for  $^{104}\text{Pd}$  are in the same order of magnitude as in  $^{102}\text{Ru}$ . They vary between the negative values of  $-0.23$  and  $-0.53$  for even spins and they fall between the positive values of  $0.17$  and  $0.62$  for the odd spins. The resulted phase of the staggering is the same both in  $^{104}\text{Pd}$  and in

$^{102}\text{Ru}$ . Accordingly to the obtained odd-even spin energy staggerings in  $^{104}\text{Pd}$ , we can rule out the rigid triaxial rotor scenario and assign a  $\gamma$ -soft character to this nucleus. It is worth to note that the staggerings increase at higher spins of  $^{104}\text{Pd}$  unlike  $^{102}\text{Ru}$ , which might indicate a more  $\gamma$ -soft shape in  $^{104}\text{Pd}$  compared to  $^{102}\text{Ru}$ .

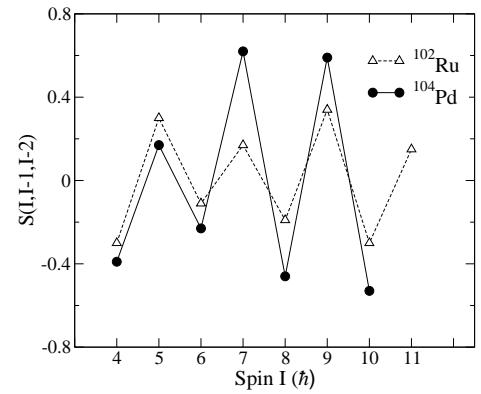


**Figure 1.** Experimentally observed odd-even spin energy staggerings in the nonyrast low-lying positive-parity band in  $^{104}\text{Pd}$  (filled circles, solid line) compared to the values of the quasi- $\gamma$  band in  $^{102}\text{Ru}$  (opened triangles, dashed line). The lines between the symbols are drawn to guide the eye.

- a) Department of Physics, University of York, York, YO10 5DD, UK
- b) NSCL, Cyclotron Laboratory, Michigan State University, East Lansing, MI 48824-1321, USA
- c) Department of Physics and Astronomy, SUNY, Stony Brook, New York, 11794-3800, USA
- d) GSI, Darmstadt, Germany
- e) IReS, 23 rue du Loess, Strasbourg, 67037, France
- f) LPSC, IN2P3-CNRS/UJF, F-38026 Grenoble-Cedex, France
- g) Department of Physics, Tohoku University, Sendai, Japan
- h) Oliver Lodge Laboratory, Department of Physics, University of Liverpool, Liverpool L69 7ZE, UK
- i) Faculty of Physics, St. Kliment Ohridski University of Sofia, BG-1164 Sofia, Bulgaria
- j) Université Bordeaux 1, IN2P3- CENBG - Le Haut-Vigneau BP120 33175, Gradignan Cedex, France

### 3.8 Rotational band structure of the chiral candidate $^{134}\text{Pr}$

*J. Timár, I. Kuti, D. Sohler, K. Starosta<sup>a)</sup>, D. B. Fossan<sup>b)</sup>, T. Koike<sup>b)</sup>, M. Cromaz<sup>c)</sup>, P. Fallon<sup>c)</sup>, I. Y. Lee<sup>c)</sup>, A. O. Macchiavelli<sup>c)</sup>, C. J. Chiara<sup>d)</sup>, A. J. Boston<sup>e)</sup>, H. J. Chantler<sup>e)</sup>, E. S. Paul<sup>e)</sup>, R. Wadsworth<sup>f)</sup>, A. A. Hecht<sup>g)</sup>*

Pairs of nearly degenerate dipole rotational bands with the same unique-parity configurations are known in several odd-odd nuclei. Such a structure was first studied in  $^{134}\text{Pr}$ , and it was considered as manifestation of chiral rotation of the triaxial nucleus. Later, considerably different quadrupole moments were measured for the two bands in this nucleus. This result strongly questioned the chiral interpretation, and new interpretation emerged emphasising the shape difference in the two bands. On the other hand, TRS calculations predict chiral band structure in this nucleus.

In order to collect more information on the structure of this key-nucleus among chiral candidates, we studied the rotational bands of  $^{134}\text{Pr}$  by in-beam  $\gamma$ -spectroscopic methods. Excited states of  $^{134}\text{Pr}$  were populated using the  $^{116}\text{Cd}(^{23}\text{Na},5n)$  reaction at a beam energy of 115 MeV and studied using the GAMMASPHERE array. The level scheme of  $^{134}\text{Pr}$  was deduced using  $E_{\gamma_1}-E_{\gamma_2}-E_{\gamma_3}$  triple coincidences,

which were sorted into Radware cubes.

On the basis of the observed  $\gamma\gamma\gamma$ -coincidence relations several new bands have been identified. One of them is linked to the previous chiral-candidate structure through many M1 and E2 transitions, has the same parity, and the equal-spin levels are nearly degenerate. According to this observation, there are three nearly degenerate  $\pi h_{11/2}\nu h_{11/2}$  bands in  $^{134}\text{Pr}$ , what may express a need for rethinking the interpretation of the previous chiral candidate structure.

- a) Department of Chemistry, Simon Fraser University, Burnaby, Canada
- b) State University of New York, Stony Brook, USA
- c) Lawrence Berkeley National Laboratory, Berkeley, California 94720, USA
- d) Washington University, St. Louis, USA
- e) Oliver Lodge Laboratory, University of Liverpool, Liverpool, United Kingdom
- f) University of York, Heslington, United Kingdom
- g) Wright Nuclear Structure Laboratory, Yale University, New Haven, USA

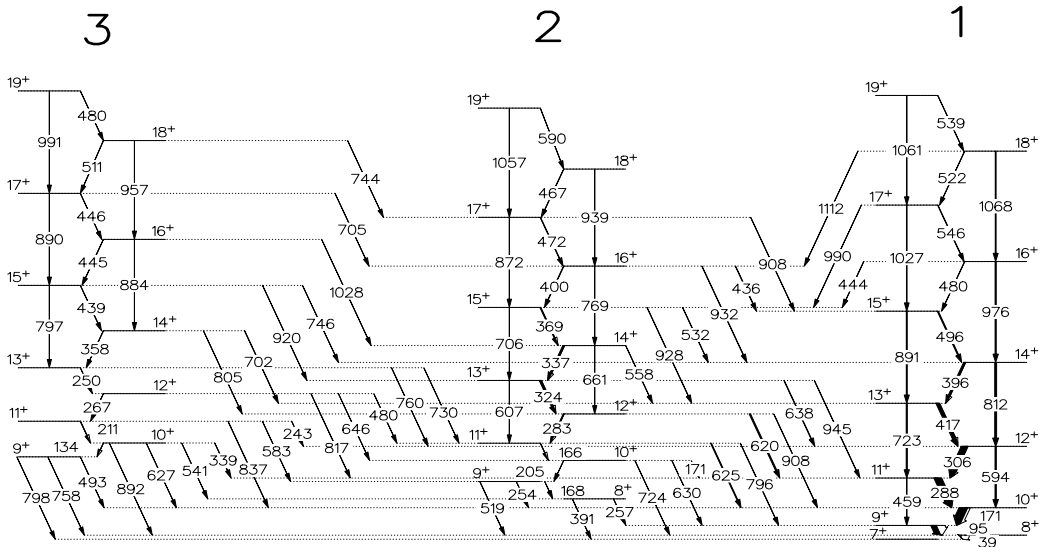


**Figure 1.** Partial level scheme of  $^{134}\text{Pr}$  containing the three  $\pi h_{11/2}\nu h_{11/2}$  bands up to spin  $19\hbar$ .

### 3.9 Electric dipole moments in $^{230,232}\text{U}$ and implications for tetrahedral shapes

*S. S. Ntshangase<sup>a,b)</sup>, R. A. Bark<sup>b)</sup>, D. G. Aschman<sup>a)</sup>, S. Bvumbi<sup>b,c)</sup>, P. Datta<sup>b)</sup>, P. M. Davidson<sup>d)</sup>, T. S. Dinoko<sup>e)</sup>, M. E. A. Elbasher<sup>b,e)</sup>, K. Juhász, E. M. A. Khaleel<sup>e)</sup>, A. Krasznahorkay, E. A. Lawrie<sup>b)</sup>, J. J. Lawrie<sup>b)</sup>, R. M. Lieder<sup>b)</sup>, S. N. T. Majola<sup>b,g)</sup>, P. L. Masiteng<sup>b,c)</sup>, H. Mohammed<sup>a)</sup>, S. M. Mullins<sup>b)</sup>, P. Nieminen<sup>d)</sup>, B. M. Nyakó, P. Papka<sup>e)</sup>, D. G. Roux<sup>h)</sup>, J. F. Sharpey-Shafer<sup>e)</sup>, O. Shirinda<sup>b,c)</sup>, M. A. Stankiewicz<sup>a)</sup>, J. Timár and A. N. Wilson<sup>d)</sup>*

Until recently, apart from the alpha cluster states in  $^{16}\text{O}$  [1], the most favored region to observe tetrahedral states was in the mass-160 region [2]. However, recent measurements of quadrupole moments of low-lying negative-parity bands in this region have not supported the tetrahedral hypothesis [3,4]. This leaves the actinide region as the next frontier. Of particular interest are  $^{230,234}\text{U}$ , as it is in the lowest-lying, negative-parity bands of these nuclei in which, with the exception of some tentative lines in  $^{230}\text{U}$ , no in-band E2 transitions have as yet been observed [5,6].

Ideally, a measurement of the quadrupole moments of these bands should be used as a simple test of the possibility of the existence of tetrahedral shapes. We have, rather measured  $B(E1)/B(E2)$  ratios in  $^{230,232}\text{U}$ , which can be compared with systematics in this region to obtain information on the likelihood of tetrahedral shapes in these nuclei.

The reactions used were  $^{232}\text{Th}(\alpha,6n)$  and  $^{232}\text{Th}(\alpha,4n)$  at energies of 61 and 42 MeV, respectively, with the beams being supplied by the Separated Sector Cyclotron (SSC) of the iThemba LABS facility.

Gamma rays were detected using the AFRODITE array of up to 9 clover and 8 segmented LEPS HPGe detectors in coincidence with evaporation residues identified by a special recoil detector [7]. Different combinations of HPGe detectors were used over the course of the experiment, while beam intensities were typically between 15 and 40 pnA.

The  $B(E1; I^- \rightarrow I^+ - 1)/B(E2; I^- \rightarrow I^- - 2)$  ratios are extracted from the data, and the magnitudes of the electric dipole moments  $|D_0|$ , were obtained from the  $B(E1)/B(E2)$  ratios using the strong-coupling limit of the rotational model:

$$D_0 \approx \frac{5(I-1)}{8(2I-1)} \frac{B(E1; I^- \rightarrow I^+ - 1)}{B(E2; I^- \rightarrow I^- - 2)}.$$

The close similarity in the energies and electric dipole moments of the negative-parity bands of the  $N = 138$  and  $N = 140$  isotones suggest a similar underlying structure, which by comparison with  $^{226}\text{Ra}$  in particular, imply an octupole vibrational picture instead of the tetrahedral interpretation.

- a) Dept. of Phys., Univ. of Cape Town, Rondebosch 7700, South Africa
- b) iThemba LABS, P.O. Box 722, Somerset West 7129, South Africa
- c) Dept. of Phys., Univ. of the Western Cape, Bellville ZA-7535, South Africa
- d) Dept. of Nucl. Phys., Res. School of Phys. Sci. and Eng., Australian Nat. Univ., Canberra ACT 0200, Australia
- e) Department of Physics, University of Stellenbosch, 7601 Matieland, South Africa
- f) Dept. of Inf. Technology, Univ. of Debrecen, Egyetem tér 1, H-4032 Debrecen, Hungary
- g) Dept. of Phys., University of Zululand, KwaDlangezwa 3886, South Africa
- h) Dept. of Phys., Rhodes University, Grahamstown 6140, South Africa

#### References:

- [1] J. P. Elliott, J. A. Evans, and E. E. Maqueda, Nucl. Phys. A **437**, 208 (1985).
- [2] J. Dudek, *et al.*, Phys. Rev. Lett. **97**, 072501 (2006).
- [3] R. A. Bark *et al.*, Phys. Rev. Lett. **104**, 022501 (2010).
- [4] M. Jentschel, *et al.*, Phys. Rev. Lett. **104**, 222502 (2010).
- [5] P. Zeyen *et al.*, Z. Phys. A **328**, 399 (1987).
- [6] B. Ackermann *et al.*, Nucl. Phys. A **559**, 61 (1993).
- [7] S. S. Ntshangase *et al.*, Phys. Rev. C **82**, 041305 (2010).

### 3.10 High resolution study of SDR in $^{40}\text{Sc}$ isotope

*L. Stuhl, A. Krasznahorkay, M. Csatlós, T. Adachi<sup>a</sup>, A. Algora<sup>b</sup>, J. Deaven<sup>c</sup>, E. Estevez<sup>b</sup>, H. Fujita<sup>a</sup>, Y. Fujita<sup>d</sup>, C. Guess<sup>c</sup>, J. Gulyás, K. Hatanaka<sup>a</sup>, K. Hirota<sup>a</sup>, H.J. Ong<sup>a</sup>, D. Ishikawa<sup>a</sup>, H. Matsubara<sup>a</sup>, R. Meharand<sup>c</sup>, F. Molina<sup>b</sup>, H. Okamura<sup>a</sup>, G. Perdikakis<sup>c</sup>, B. Rubio<sup>b</sup>, C. Scholf<sup>e</sup>, T. Suzuki<sup>a</sup>, G. Susoy<sup>f</sup>, A. Tamii<sup>a</sup>, J. Thies<sup>g</sup>, R. Zegers<sup>c</sup>, J. Zenihiro<sup>a</sup>*

The aim of the present work was to study the fragmentation of the dipole strengths into low-lying excited states in  $^{40-48}\text{Sc}$ . Here we present high resolution study of the relative dipole strength distribution excited in the ( $^3\text{He}, t$ ) reaction.

The experiment was performed at the Research Center for Nuclear Physics, Osaka University. The  $^3\text{He}$  beam of 420 MeV incident energy was transported to the self-supporting metallic  $^{40}\text{Ca}$  target with 1.63 mg/cm<sup>2</sup> thickness. The beam current was 25 nA. The energy of tritons was measured with the magnetic spectrometer Grand Raiden, using complete dispersion-matching techniques [1]. The spectrometer was set at 0° and 2.5°. The energy resolution was about 20 keV.

The spectra were analyzed with program package Gaspan. The level energies and intensities were deduced. The spectrum was studied in eight distinct angular regions. We determined the angular distributions for the newly identified peaks. The angular distributions of the newly identified levels are very similar to those of levels, which are known  $\Delta L = 1$  states from the literature. In case of  $^{40}\text{Sc}$  we have found 105 new levels, from these 92 were  $\Delta L = 1$  excited states.

The strength distribution for the  $\Delta L = 1$  ( $0^-$ ,  $1^-$ ,  $2^-$ ) dipole (spin-dipole) transition were analyzed. The distribution in  $^{40}\text{Sc}$  shows some interesting periodic feature, which is clearly seen in Fig. 1. It resembles to a soft, damped vibrational band with  $\hbar\omega = 1.8$  MeV. In a simple macroscopic liquid-drop model description of the vibration, the restoring force should be much softer compared to the one of the giant dipole resonance, which is located at around 22 MeV in  $^{40}\text{Ca}$ . In a paper published recently [2] the unique nature of the N=Z nuclei is expressed, in which enhanced correlations arise between neutrons and protons. The corresponding theoretical analysis of this inter-

esting periodical behaviour of this distribution is in progress.

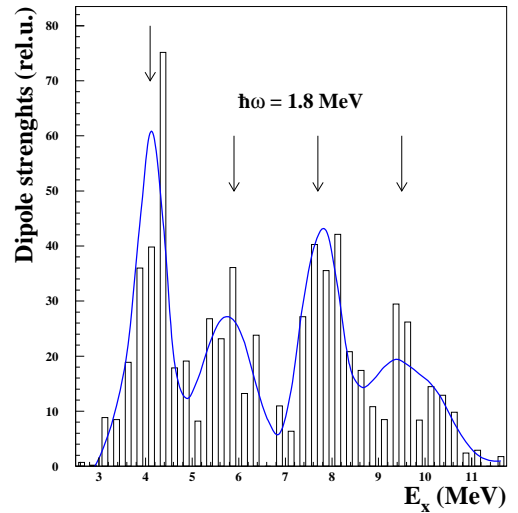


**Figure 1.** The distribution for  $^{40}\text{Sc}$  is shown separately with a smoothed curve produced by spline, and with arrows placed with equidistant energy gaps suggesting the presence of a dipole vibrational band.

#### Acknowledgements

The work has been supported by the Hungarian OTKA Foundation No. K 72566.

- a) RCNP, Osaka University, Ibaraki, Osaka 567-0047, Japan
- b) IFIC, CSIC-Universidad de Valencia, 46071 Valencia, Spain
- c) NSCL, Michigan State University, East Lansing, Michigan 48824, USA
- d) Department of Physics, Osaka University, Toyonaka, Osaka 560-0043, Japan
- e) Institut für Kernphysik, Universität zu Köln, 50937 Köln, Germany
- f) Istanbul Univ., Faculty of Sci., Phys. Dept., 34134 Vezneciler, Istanbul, Turkey
- g) Institut für Kernphysik, Universität Münster, 48149 Münster, Germany

[1] M. Fujiwara *et al.*, Nucl. Instrum. Methods Phys. Res. A **422**, 484 (1999).

[2] B. Cederwall *et al.*, Nature **469**, 68-71 (2011).

### 3.11 Determination of conversion coefficients in low-energy $\gamma$ rays of $^{132}\text{La}$

*I. Kuti, J. Timár, D. Sohler, K. Starosta<sup>a)</sup>, D. B. Fossan<sup>b)</sup>, T. Koike<sup>b)</sup>, M. Cromaz<sup>c)</sup>, P. Fallon<sup>c)</sup>, I. Y. Lee<sup>c)</sup>, A. O. Macchiavelli<sup>c)</sup>, C. J. Chiara<sup>d)</sup>, A. J. Boston<sup>e)</sup>, H. J. Chantler<sup>e)</sup>, E. S. Paul<sup>e)</sup>, R. Wadsworth<sup>f)</sup>, A. A. Hecht<sup>g)</sup>*

Level scheme of the chiral candidate  $^{132}\text{La}$  has been studied in fusion-evaporation reaction experiment using the Gammasphere array in order to obtain unambiguous spin and parity values of bands which were previously only tentatively known.

To derive the multiplicities of the  $\gamma$  transitions we mostly used DCO [1] and linear polarization analysis. However, linear polarization could not be determined for several important low-energy transitions. The electric or magnetic characters of these transitions were obtained by determining their internal conversion coefficients that were derived from coincidence-intensity balances.

Such transitions are the 96, 129 and 160 keV  $\gamma$  rays in the low-energy band in the left side of Fig. 1, and also the 67 keV transition that connects the chiral candidate rotational band, seen in the right side of Fig. 1, to the states with known spin-parities.

Our DCO measurements showed that these  $\gamma$  rays are stretched dipoles. Determination of the M1 or E1 characters was carried out by analysing coincidence intensities seen in double gated coincidence spectra setting the 294-(279+312+482) keV, 160-(231+557) keV, 160-(414+557) keV and 129-(231+557) keV gates for the 67, 96, 129 and 160 keV transitions, respectively.

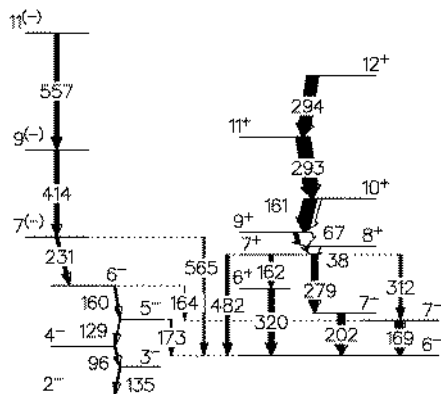


**Figure 1.** Part of the  $^{132}\text{La}$  level scheme.

Knowing that the reference 135 keV  $3^- \rightarrow 2^-$  and the 161 keV  $10^+ \rightarrow 9^+$   $\gamma$  rays have M1 characters, the relative total transition intensity in the cascade could be calculated, and the  $\alpha_{tot}$  conversion coefficients of the examined transitions could be deduced. This was done by measuring their relative  $\gamma$ -ray intensities in these spectra.

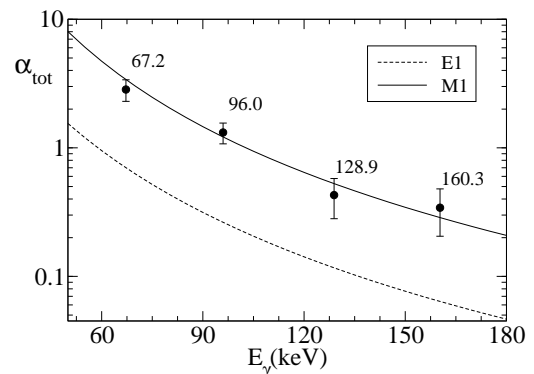


**Figure 2.** Experimental internal conversion coefficients of  $^{132}\text{La}$  transitions (data with error bars), as a function of  $\gamma$ -ray energy. Curves show theoretical values.

The obtained conversion coefficients, presented in Fig. 2. together with the theoretical E1 and M1 curves, show good agreements with the M1 theoretical values, hence the examined  $\gamma$  transitions of  $^{132}\text{La}$  have M1 multiplicities.

- a) Department of Chemistry, Simon Fraser University, Burnaby, Canada
- b) State University of New York, Stony Brook, USA
- c) Lawrence Berkeley National Laboratory, Berkeley, California 94720, USA
- d) Washington University, St. Louis, USA
- e) Oliver Lodge Laboratory, University of Liverpool, Liverpool, United Kingdom
- f) University of York, Heslington, United Kingdom
- g) Wright Nuclear Structure Laboratory, Yale University, New Haven, USA

[1] I. Kuti *et al.* Acta Phys. Debr. **XLI**, 11 (2010)

### 3.12 Mass and angular distribution of the fission fragments from $^{236}\text{U}$ hyperdeformed states studied with a new fission fragment detector called OBELISK

*T.G. Toronyi, J. Gulyás, A. Krasznahorkay, M. Csatlós, R.A. Bark<sup>a)</sup>, L. Csige, N.A. Kondratyev<sup>b)</sup>, L.V. Kondratyeva<sup>b)</sup>*

The measurement of the fission fragment angular distributions represents an important tool to investigate the properties of the triple-humped fission barrier and the spectrum of highly deformed states which is directly connected to the nuclear shapes [1]. On the other hand, fragment mass and energy distributions reveal interesting information on the fissioning system on its way from the outer saddle of the potential energy surface to the scission point [2].

In the present experiment we were aiming at a simultaneous measurement of both the fragment angular and mass distributions to study a possible correlation between the spin and deformation of the states lying in the third minimum (hyperdeformed states) and the fragment mass split (measured by the fragment times of flight (TOFs)).

A new double obelisk as a PPAC position sensitive detector [3] was upgraded recently at our institute for the above purposes. It has a large solid angle (nearly  $4\pi$ ), excellent time resolution ( $< 1$  ns), 2-dimensional position sensitive detectors, and good angular resolution.

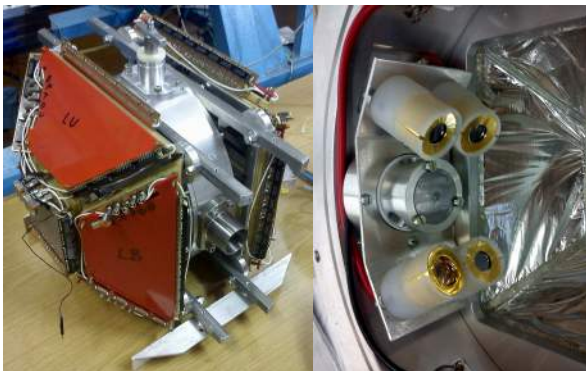


**Figure 1.** Photo of the OBELISK spectrometer and the inside part, which shows the four Si detectors and the beam collimator.

The left and right hemispheres (see in Fig.1.) are covered by five PPACs, each arranged like an obelisk, one square detector

and four trapezoidal detectors. The distance between the target and the outer detectors amounts to  $\approx 12.4$  cm. About 50% of the complete solid angle of  $4\pi$  is covered by the sensitive detector areas. The beam hits the target between the two hemispheres. This gas-filled counter is typically operated at a gas pressure of 4-5 mbar of isobutane.

An angular resolution  $< 1^\circ$  can be achieved. The excellent time resolution of the double-grid PPACs ( $< 0.4$  ns) enables to determine mass distributions applying the double TOF technique. The obtained mass resolution is mainly limited by the energy loss of the fragments and amounts to about 5 amu.

The  $^{236}\text{U}$  was excited in the  $^{235}\text{U}(\text{d,pf})^{236}\text{U}$  reaction using a 9 MeV deuteron beam from the Debrecen 103-cm isochronous cyclotron. Enriched (97.6%) and  $88 \mu\text{g}/\text{cm}^2$  thick target of  $^{235}\text{UO}_2$  was used.

The essence of the experiment was the measurement of the energy of the outgoing protons in coincidence with the two fission fragments flying in the opposite directions.

The energy of protons was analyzed by 4 high resolution silicon detectors having a thickness of  $500 \mu\text{m}$ , an energy resolution of 13 keV (for 5.1 MeV  $\alpha$ -particles) and a solid angle of 30 msr each. The start signal for the TOF measurement was provided also by the silicon detectors.

The analysis of the angular and mass distribution of the fission fragments as a function of the excitation energy is in progress.

a) iThemba LABS, P.O. Box 722, Somerset West, 7129 South Africa

b) Joint inst. for Nucl. Res., 141980, Dubna, Russia

[1] A. Krasznahorkay *et al.*, Phys. Rev. Lett. **80** (1998) 2073.

[2] S. Cwiok *et al.*, Phys. Lett. B**322** (1994) 304.

[3] W. Wilke *et al.*, Nucl. Instr. Meth. A**272** (1988) 785.

### 3.13 Target structure induced suppression of the ionization cross section for very low energy antiproton-hydrogen collisions

*H. Knudsen<sup>a)</sup>, H.A. Torii<sup>b)</sup>, M. Charlton<sup>c)</sup>, Y. Enomoto<sup>b)</sup>, I. Georgescu<sup>d)</sup>, C.A. Hunniford<sup>e)</sup>, C.H. Kim<sup>b)</sup>, Y. Kanai<sup>d)</sup>, H.-P.E. Kristiansen<sup>a)</sup>, N. Kuroda<sup>b)</sup>, M.D. Lund<sup>a)</sup>, R.W. McCullough<sup>e)</sup>, K. Tókési, U.I. Uggerhøj<sup>a)</sup> Y. Yamazaki<sup>d)</sup>*

Low energy antiprotons have been used previously to give benchmark data for theories of atomic collisions [1]. Here we present measurements of the cross section for single, nondissociative ionization of molecular hydrogen for impact of antiprotons with kinetic energies in the range 2-11 keV, i.e., in the velocity interval of 0.3-0.65 a.u. We find a cross section which is proportional to the projectile velocity [2], which is quite unlike the behavior of corresponding atomic cross sections, and which has never previously been observed experimentally.

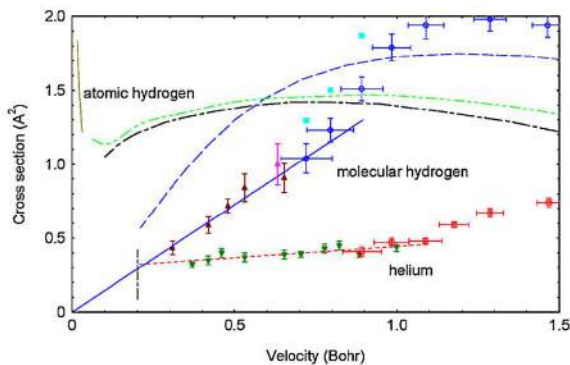


**Figure 1.** Experimental data and theoretical calculations of the cross section for single ionization by antiproton impact on atomic hydrogen, molecular hydrogen and helium as a function of the projectile laboratory velocity.

Figure 1 presents our experimental data [2] for the single ionization of helium and molecular hydrogen by antiproton impact with some theoretical calculations. For atomic hydrogen, we show as dashed-dotted black curves calculations by Lühr and Saenz [3] and by Igarashi *et al.* (green dash-dot-dot) [4]. Also shown as a brown solid curve is the low-velocity calculation of the total cross section for ionization by Cohen [5]. In the case of the molecular hydrogen target, we show the experimental data of the present work ( $\blacktriangle$ ) run in 2010,  $\triangle$  run in 2009 as well as previous data obtained by our group ( $\circ$ ), published in Hvelplund *et al.* [6]. The straight, solid line is a linear fit to these

data below a velocity of 1 a.u. The data points marked  $\blacksquare$  indicate the sum of the cross sections for nondissociative and dissociative ionization of molecular hydrogen by Hvelplund *et al.* [6]. The long-dashed dark blue curve shows a calculation of this cross section by Lühr and Saenz [3]. The vertical line indicates the projectile energy above which more than 90 % of the  $D_2$  ions created and more than 90% of the projectiles deflected in the collisions are collected by our apparatus. For the helium target, we show experimental data by Hvelplund *et al.*  $\square$  [6] and by Knudsen *et al.*  $\blacktriangledown$  [1].

#### Acknowledgements

We would like to thank our collaborators in the CERN ASACUSA Collaboration and the staff at the CERN AD for much help and support. Also thanks are due Poul Aggerholm for his tireless practical help. This work was supported by the Danish Natural Science Research Council, the U.K. Engineering and Physical Sciences Research Council, the Grant-in-Aid for Specially Promoted Research (19002004), MEXT, Japan, and the Hungarian Scientific Research Fund OTKA No. K72172.

- a) Department of Physics and Astronomy, University of Aarhus, DK 8000, Denmark
  - b) Institute of Physics, Komaba, University of Tokyo, 153-8902, Japan
  - c) Department of Physics, Swansea University, SA2 8PP, United Kingdom
  - d) Atomic Physics Laboratory, RIKEN, (Saitama) 351-0198, Japan
  - e) Department of Physics and Astronomy, Queens University Belfast, BT7-1NN, United Kingdom
- [1] H. Knudsen *et al.*, Phys. Rev. Lett. **101**, 043201 (2008).  
[2] H. Knudsen *et al.*, Phys. Rev. Lett. **105** (2010) 213201.  
[3] A. Lühr and A. Saenz, Phys. Rev. A **77** (2008) 052713.  
[4] A. Igarashi *et al.*, Nucl. Instrum. Methods Phys. Res., Sect. B **124** (2004) 135.  
[5] J. S. Cohen, Phys. Rev. A **56**, (1997) 3583.  
[6] P. Hvelplund *et al.*, J. Phys. B **27** (1994) 925.

### 3.14 Ionization of the hydrogen atom by short half-cycle pulses: dependence on the pulse duration

*D.G. Arbó<sup>a,b)</sup>, M.S. Gravielle<sup>a,b)</sup>, K.I. Dimitriou<sup>c,d,e)</sup>, K. Tókési, S. Borbély<sup>f)</sup>, J.E. Miraglia<sup>a,b)</sup>*

In the last decade short unidirectional electric pulses, called half-cycle pulses (HCPs), have had several applications like focusing of Rydberg wave packets, production of one-dimensional Rydberg atoms, and generation of quasiclassical Bohr-alike atoms. The aim of this work is to investigate the applicability of several quantum distorted wave and classical methods to describe the action of such HCP on atomic targets.

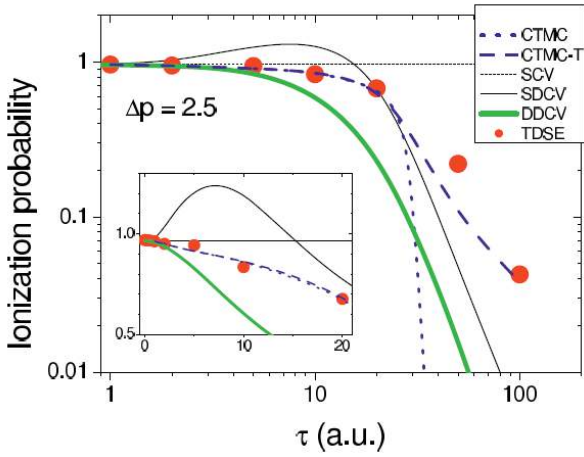


**Figure 1.** Total ionization probability as a function of the pulse duration after a pulse of momentum transfer  $\delta p = 2.5$  a.u. Dotted (blue) line: CTMC, dashed (blue) line: CTMCT, thin short-dashed line: SCV, thin black solid line: SDCV, and (green) gray thick solid line: DDCV. (Red) dots correspond to TDSE calculations.

Therefore in this work a theoretical study of the ionization of hydrogen atoms by short external half-cycle pulses (HCPs) as a function of the pulse duration, using different quantum and classical approaches, is presented [1]. Total ionization probability and energy distributions of ejected electrons are calculated in the framework of the singly-distorted Coulomb-Volkov (SDCV) and the doubly-distorted Coulomb-Volkov (DDCV) approximations. We also performed quasiclassical calculations based on a

classical trajectory Monte Carlo method which includes the possibility of tunneling (CTMC-T). Quantum and classical results are compared to the numerical solution of the time-dependent Schrödinger equation (TDSE). We find that for high momentum transfers the DDCV shows an improvement compared to the SDCV, especially in the low-energy region of the electron emission spectra, where SDCV fails (see Fig. 1). In addition, DDCV reproduces successfully the TDSE electron energy distributions at weak momentum transfers. CTMC-T results reveal the importance of tunneling in the ionization process for relative long pulses and strong momentum transfers but fails to overcome the well-known classical suppression observed for weak electric fields.

#### Acknowledgements

This work was carried out with financial support of CONICET, UBACyT X147, and ANPCyT PICT 2006-00772 of Argentina, the Argentine-Hungarian collaboration HU/08/02, the CNCSIS-UEFISCSU proj. No. PNII-IDEI 539/2007, the Hungarian National Office for Research and Technology and the Hungarian Scientific Research Found OTKA (K72172). SB and KT were also partially supported by the European COST Action CM0702.

- a) Institute for Astronomy and Space Physics, IAFE, CC 67, Suc. 28 (1428) Buenos Aires, Argentina
  - b) Department of Physics, FCEN, University of Buenos Aires, Argentina
  - c) Department of Physical Science and Applications, Hellenic Army Academy, Vari, Greece
  - d) Department of Informatics, Technological Educational Institution, Lamia, Greece
  - e) Institute of Theoretical and Chemical Physics, National Hellenic Research Foundation, Athens, Greece
  - f) Faculty of Physics, Babes-Bolyai University, Cluj-Napoca, Romania
- [1] D.G. Arbó, M.S. Gravielle, K.I. Dimitriou, K. Tókési, S. Borbély, and J.E. Miraglia, *Eur. Phys. J. D*, **59** (2010) 193.

### 3.15 Ionization of the water by intense ultrashort half-cycle electric pulses

*S. Borbély<sup>a)</sup>, K. Tókési, L. Nagy<sup>a)</sup>*

In the present work, the tunneling and over-the-barrier ionization of the water molecule by ultrashort half-cycle electric pulses is investigated theoretically, applying single active electron (SAE) and frozen core classical and quantum mechanical models. The period of the fastest oscillation in the water molecule, namely the asymmetrical stretching of the OH bonds, is 8.9 fs calculated from the vibrational frequency of  $3756\text{ cm}^{-1}$ . This is much larger than the duration of the longest half-cycle pulse (5 a.u.  $\approx 0.14$  fs) used in our calculations. Thus, during the action of the half-cycle pulse the geometry of the molecule is practically unchanged, which justifies the use of the frozen core approximation. During our calculations the electrons from the highest occupied molecular orbital (HOMO) 1b1 were considered. The ionization energy of the 1b1 orbital is experimentally known as 12.6 eV. In the simplest possible approach the  $\text{H}_2\text{O}$  molecule is modeled by a hydrogen-type atom (hydrogenic approximation) with one electron and an effective core charge ( $Z_{eff}$ ). This approximation was successfully used in the investigation of the charged particle impact of the  $\text{H}_2\text{O}$  molecule by several predictions and experimental data. This simplified approach can be efficient, if electrons from the 1b1 molecular orbital in the ionization process are involved. The 1b1 orbital is mainly constructed from the  $2p_z$  orbital of the  $O$  atom, and it can be described accurately by hydrogen type atomic orbitals, which provides us an accurate initial state wave function.

We found good agreement between the classical and quantum mechanical calculation at high intensities, where the over-the-barrier ionization mechanism is dominant. We found, furthermore, that the curve of the ionization probability densities has two maxima around the same electron momenta. This double structure shape can also be observed in the classical trajectory Monte Carlo (CTMC) model and can be explained as a result of the Coulomb

interaction between the core and the electron. As an illustration, Figure 1 shows typical classical electron trajectories. All of the electrons with momentum in the initial state parallel and in the same direction with the net momentum transfer can be directly ionized without approaching the core (Traj. A) leading to electrons with high energy. On the other hand, electrons with a momentum in the initial state, which leads in the opposite direction relative to the net momentum transfer, needs to *go around* the core leading to bound (Traj. C) or ionized trajectories with lower electron energies (Traj. B).

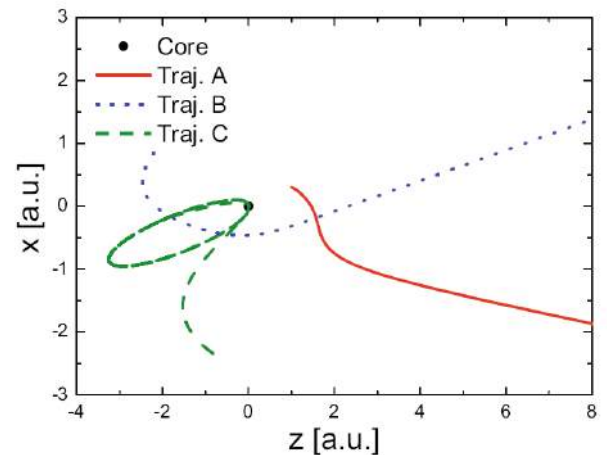


**Figure 1.** Typical classical trajectories of ionization with high (Traj. A) and low (Traj. B) ejection energies and typical trajectory excitation (Traj. C). The black dot is the core, and the net momentum transfer is along the Oz axis.

#### *Acknowledgements*

This work was supported by the Romanian National Plan for Research (PNII) under contract No. ID 539, the European COST Action CM0702, and the Hungarian Research Found OTKA (K72172). One of the authors (S. B.) is also grateful for the support of the Domus Hungarica Scientiarum et Artium.

a) Faculty of Physics, Babes-Bolyai University, Cluj-Napoca, Romania

[1] S. Borbély, K. Tókési, and L. Nagy, Eur. Phys. J. D59 (2010) 337.

### 3.16 The Newcomb–Benford law and nuclear half-lives

*J. Farkas, Gy. Gyürky*

The satisfaction of the Newcomb–Benford law (a.k.a. Benford’s first digit law) is a long standing issue in science, and has interesting mathematical and philosophical consequences. It was identified by Newcomb in 1881 and re-invented later by Benford in 1938. The law states that the distribution of the first digit of numbers taken from various sources like magazines, scientific publications, wealth statistics, etc. . . follows the law

$$P_d = \lg \left( 1 + \frac{1}{d} \right) \quad (d = 1, 2, \dots, 9),$$

where  $d$  is the given digit [1].

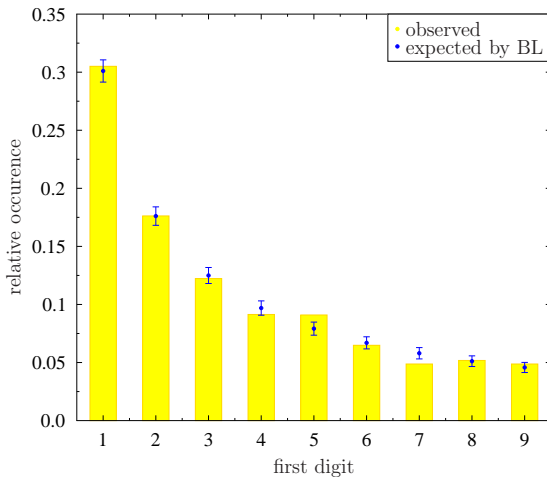


**Figure 1.** The distribution of the first significant digit of half-lives follows the Newcomb–Benford law.

It was reported recently that the satisfaction of the law was observed in nuclear decay half-life datasets [2,3]. Based on this fact, it was implied that the law is helpful as a test for

nuclear decay models, as well as it can be used to search for new physical phenomena (like self organized criticality) which can be responsible for the satisfaction of the law.

The mathematical conundrum of the Newcomb–Benford law has been solved in 2008 for numbers coming from a data set with a given distribution. The ‘Benford compliance theorem’ [1] uses the Fourier transform of the probability distribution function of the numbers to identify the characteristics of the distribution responsible for the satisfaction of the law.

In our work [4] we confirmed that the half-lives of radioactive nuclei satisfy the law by using two standard techniques: direct plotting and the ‘ones scaling test’ method. We also showed that the distribution of the half-life values closely resembles a log-normal distribution stretching through about 54 orders of magnitude. By using the Fourier transform of the distribution function we showed that the numbers with such a distribution automatically satisfy the Newcomb–Benford law, due to the compliance theorem. Thus we concluded that the satisfaction of the law provides no additional clue on whether a nuclear model is valid or not, given it produces a similar distribution of half-lives as observed.

- [1] S. W. Smith, *The Scientist and Engineer’s Guide to Digital Signal Processing*, California Technical Publishing, 1997, 2008, Ch.34, pp. 701–722
- [2] D. Ni, Z. Ren, *Eur. Phys. J.* **A38**, 251 (2008)
- [3] D. Ni, L. Wei, Z. Ren, *Commun. Theor. Phys.* **51**, 713 (2009)
- [4] J. Farkas, Gy. Gyürky, *Acta Phys. Pol. B* **41**, 6 (2010)

## 4.1 Classical trajectory Monte Carlo model calculations for ionization of atomic hydrogen by 75 keV proton impact

*L. Sarkadi*

The theoretical understanding of the collisional break-up of a three-body atomic system is one of the problems of fundamental importance in the physics of atomic collisions. For ion-atom collisions the simplest collision process leading to three free particles in the final state is the ionization of the hydrogen atom by proton impact.

Recently Laforge *et al.* [1] and Schulz *et al.* [2] measured doubly differential cross sections (DDCS) for ionization of atomic hydrogen by 75 keV proton impact as a function of the projectile scattering angle and energy loss. These experimental data are of particular importance, since they offer an accurate test of the three-body ionization theories. The authors compared their data with the predictions of various ionization models. A remarkable result of the experiments was that the distribution of DDCS as a function of the proton scattering angle showed a narrowing at energy loss of 53 eV. The latter value is special in that it corresponds to electron emission under the condition  $v_e = v_p$  ( $v_e$  and  $v_p$  are the velocity of the ejected electron and the projectile, respectively). At  $v_e = v_p$  strong post-collision interaction (PCI) takes place between the electron and the outgoing projectile which leads to the appearance of the well-known cusp peak in the energy spectrum of the forward-ejected electrons.

In our work [3] we compared the experimental data of Laforge *et al.* and Schulz *et al.* with the results of calculations carried out in the framework of the classical trajectory Monte Carlo (CTMC) method. The CTMC method is based on the numerical solution of the classical equations of motion for a large number of trajectories of the interacting particles under randomly chosen initial conditions. We mainly focussed on the narrowing effect. Surprisingly, our CTMC results showed only an enhancement of DDCS at the energy loss corresponding to  $v_e = v_p$  rather than narrowing of the

angular distribution of the scattered protons. At the same time, we observed the narrowing effect in that case when the scattering angle of the proton is measured relative to the direction of the center-of-mass velocity vector of the ejected electron and the outgoing proton (see Figure 1). We explained the experimentally observed narrowing effect (for *laboratory* scattering angle) by interference effects occurring between the scattering processes corresponding to the first- and second-order term of the Born perturbation series expansion.

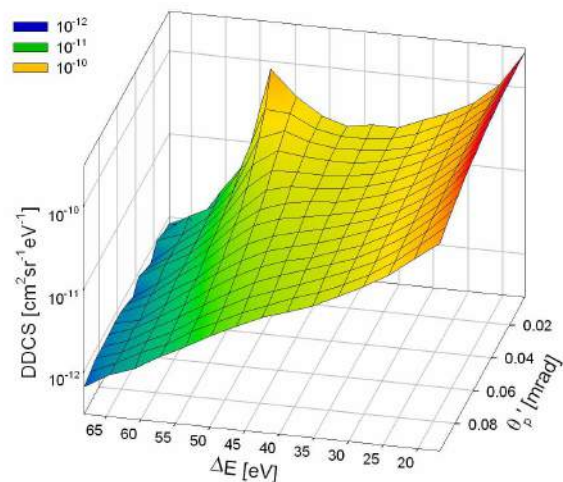


**Figure 1.** Result of the present CTMC calculations for DDCS as a function of the energy loss  $\Delta E$  and scattering angle  $\theta_p'$  of the outgoing protons in ionizing collisions of 75-keV protons with H atoms.  $\theta_p'$  is measured relative to the direction of the center-of-mass velocity vector of the electron-projectile subsystem.

- [1] A. C. Laforge, K. N. Egodapitiya, J. S. Alexander, A. Hasan, M. F. Ciappina, M. A. Khakoo, and M. Schulz, *Phys. Rev. Lett.* **103** (2009) 053201.
- [2] M. Schulz, A. C. Laforge, K. N. Egodapitiya, J. S. Alexander, A. Hasan, M. F. Ciappina, A. C. Roy, R. Dey, A. Samolov, and A. L. Godunov, *Phys. Rev. A* **81** (2010) 052705.
- [3] L. Sarkadi, *Phys. Rev. A* **82** (2010) 052710.

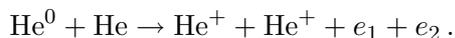
## 4.2 Two-electron cusp in the double ionization of helium

*L. Gulyás, L. Sarkadi, A. Igarashi<sup>a)</sup>, T. Kirchner<sup>b)</sup>*

The double ionization (DI) of helium has been investigated intensively in recent years by impact of photons, electrons and ions. The interest arises from the opportunity of studying the correlated motion of two electrons in the field of a heavy Coulomb particle. In the present work [1] we analyzed DI of He under the impact of 100 keV  $\text{He}^{2+}$  projectiles:



where  $\mathbf{k}_i$  denotes the momentum of the  $i$ th emitted electron with respect to the target nucleus. We paid special attention to the cusp region of the electron emission, i.e., to the case when the velocity of both ejected electrons matches the velocity of the projectile. Particularly, the present calculations were motivated by the observation of the two-electron cusp in a recent experiment carried out for 100 keV  $\text{He}^0 + \text{He}$  collisions [2]:



Our choice of the simpler collision system  $\text{He}^{2+} + \text{He}$  for the theoretical study of the two-electron cusp is justified by the similarity of the final states in the two collisions: Two repelling electrons move in the attractive Coulomb field of a heavy charged particle in the same direction with small relative velocity.

In the calculations we applied the impact parameter and frozen-correlation approximations where the one-electron events were treated by the continuum distorted wave method. Correlation between the emitted electrons, which plays an important role in forming the shape of the differential distribution of the electron emission, was described by the Coulomb density of states approximation (CDS) [3].

The main physical issue of the present work is the outcome of the competition between two interactions: (i) The repulsion between the two ejected electrons, and (ii) The strong final-state (Coulomb-focussing) interaction between the

electrons and the outgoing projectile. In the cusp region the correlated motion of the two electrons is influenced dominantly by the outgoing projectile, i.e., the correlation function of the CDS treatment is expected to depend on the electron momenta measured relative to the projectile, rather than to the target nucleus. A qualitative agreement with the experiment was achieved with a CDS model based on use of such a projectile-centered correlation function that applies effective charges as given in the dynamically screened 3-Coulomb wave function [4]. Our calculations support the existence of the two-electron cusp (see Figure 1), and give account of the strong correlation observed in the experiment between the energies of the electrons.

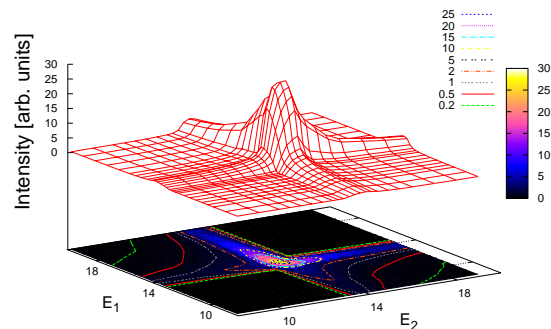


**Figure 1.** Calculated two-electron emission distribution following DI of He under 100 keV  $\text{He}^{2+}$  impact as a function of the electron ejection energies  $E_1$  and  $E_2$  at emission angles  $\theta_1 = \theta_2 = 0^\circ$ . The effect of the finite electron detection angles and energy resolution of the experiment [2] is included by a convolution procedure.

a) Department of Applied Physics, Faculty of Engineering, University of Miyazaki, Japan

b) Department of Physics and Astronomy, York University, Toronto, Ontario, Canada

[1] L. Gulyás, L. Sarkadi, A. Igarashi, and T. Kirchner, *Phys. Rev. A* **82** (2010) 032705.

[2] L. Sarkadi and A. Orbán, *Phys. Rev. Lett.* **100** (2008) 133201.

[3] M. McCartney, *J. Physics B* **30** (1997) L155.

[4] J. Berakdar and J. S. Briggs, *Phys. Rev. Lett.* **72** (1994) 3799.

### 4.3 $L_3$ -subshell alignment of Au and Bi in collisions with 12–55-MeV carbon ions

Ajay Kumar<sup>a)</sup>, A. N. Agnihotri<sup>b)</sup>, S. Chatterjee<sup>b)</sup>, S. Kasthurirangan<sup>b,c)</sup>, D. Misra<sup>b)</sup>, R. K. Choudhury<sup>a)</sup>, L. Sarkadi, L. C. Tribedi<sup>b)</sup>

We have measured the angular distribution of the L x-ray intensities of thin Au and Bi targets bombarded by 12–55-MeV carbon ions [1]. The  $L_\alpha$ ,  $L_\beta$ , and  $L_\gamma$  X-ray intensities were observed to be isotropic within the experimental uncertainty. The alignment parameter  $A_{20}$  of the  $L_3$  subshell was established from the angular distribution of the  $L_l$  x-ray intensity relative to the intensity of other L x-ray lines from the same spectrum.

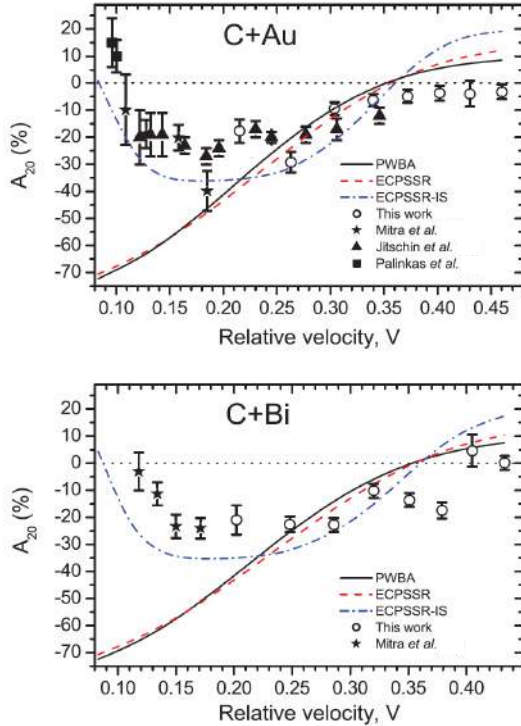


**Figure 1.** The measured and the calculated value of the alignment parameter  $A_{20}$  as a function of the relative velocity of the carbon projectile. Available experimental data for C + Au and C + Bi are also displayed.

We compared the measured  $A_{20}$  values with those obtained using theoretical models that involve: The plane-wave Born approximation (PWBA) [2]; the ECPSSR model [3] that accounts for the projectile’s energy loss and its Coulomb deflection from the straight-line trajectory, the perturbed-stationary-state effect,

as well as the electronic relativistic effect; and the ECPSSR-IS [4] model that includes a correction for the collision-induced intrashell transition of the primarily produced vacancies between the subshells.

Our data together with the  $A_{20}$  values measured by Pálincás *et al.* [5], Jitschin *et al.* [6], Mitra *et al.* [7], and the predictions of the theoretical models are shown in Figure 1. In the high-energy region, the PWBA and ECPSSR models reproduce the measured  $A_{20}$  values fairly well. In the low-energy region, the inclusion of IS correction in the ECPSSR model substantially improves the agreement between theory and experiment. For a better understanding of the ion-induced alignment, further angular distribution experiments have to be carried out with different heavy ions. High-resolution measurements of the L x-ray satellite lines are also required to elucidate the effect of the multiple ionization on the alignment parameter.

- a) Nuclear Physics Division, Bhabha Atomic Research Centre, Trombay, Mumbai, India
- b) Tata Institute of Fundamental Research, Colaba, Mumbai, India
- c) Institute of Chemical Technology, Mumbai, India

[1] Ajay Kumar, A. N. Agnihotri, S. Chatterjee, S. Kasthurirangan, D. Misra, R. K. Choudhury, L. Sarkadi, and L. C. Tribedi, *Phys. Rev. A* **81** (2010) 062709.

[2] M. Kamiya, Y. Kinefuchi, H. Endo, A. Kuwako, K. Ishii, and S. Morita, *Phys. Rev. A* **20** (1979) 1820.

[3] W. Brandt and G. Lapicki, *Phys. Rev. A* **23** (1981) 1717.

[4] L. Sarkadi, *J. Phys. B* **19** (1986) L755.

[5] J. Pálincás, L. Sarkadi, B. Schlenk, I. Török, and G. Kálmán, *J. Phys. B* **15** (1982) L451.

[6] W. Jitschin, R. Hippler, R. Shanker, H. Kleinpoppen, R. Schuch, and H. O. Lutz, *J. Phys. B* **16** (1983) 1417.

[7] D. Mitra, M. Sarkar, D. Bhattacharya, M. B. Chatterjee, P. Sen, G. Kuri, D. P. Mahapatra, and G. Lapicki, *Phys. Rev. A* **53** (1996) 2309.

## 4.4 Ab initio treatment of charge exchange in $\text{H}^+ + \text{CH}$ collisions

*E. Bene, G.J. Halász<sup>a)</sup>, Á. Vibók<sup>b)</sup>, L.F. Errea<sup>c)</sup>, L. Méndez<sup>c)</sup>, I. Rabadán<sup>c)</sup>, M.C. Bacchus-Montabonel<sup>d)</sup>*

Proton collision with the CH radical is interesting as a benchmark system to check approximations that can be applied to collisions with larger molecules, which are relevant in radiation damage of biological systems.

The aim of the present work was to check the validity of several approximations. In particular calculation at the Franck-Condon (FC) level was compared with more accurate calculations that employ the sudden approximation for rotation and vibration. We also discussed the extension of the calculation to energies below 50 eV [1].

The *ab initio* study of ion-molecule collisions at low and intermediate energies is carried out by employing a molecular expansion. This method requires the calculation of potential energy surfaces and dynamical couplings of the supermolecule formed during the collision, which was carried out by means of quantum chemistry techniques implemented in MOLPRO [2].

We have calculated total charge transfer cross sections with a fixed molecular orientation ( $\theta = 60^\circ$ )<sup>1</sup> and a 2-state basis ( $3^2\text{A}'$ ,  $4^2\text{A}'$ ). The eikonal calculation included both radial and rotational couplings, while only the radial coupling was included in the quantum mechanical calculation. Our results point out that the eikonal treatment is appropriate in the energy of this work. Besides, the approximation of neglecting the rotational coupling does not significantly modifies the total cross section. While the change of the cross section with  $\rho$  is relatively small for  $v > 0.1$  a.u. ( $E \approx 250$  eV), at lower velocities the energy difference becomes critical and we obtain very large cross sections for  $\rho < 1.9$  a.u. where

the two states are quasidegenerate in the limit  $R \rightarrow \infty$ . Although for  $v < 0.1$  a.u. the results of FC and sudden vibrational approximation agree, the strong dependence of the cross section on  $\rho$  indicates that the approximation is probably not accurate. In this respect, the decrease of the cross section at low velocities, which was also found in  $\text{H}_3^+$  [4], might be a consequence of the neglect of a vibronic resonant mechanism similar to that found in Ref.[5]. In practice, the extension of the present calculation to  $E < 250$  eV would require the use of regularized states and the use of a vibronic expansion [6].

### Acknowledgements

This work was supported by the Hungarian OTKA Grant No.K73703.

- a) University of Debrecen, Department of Information Technology, P.O. Box 12, H-4010 Debrecen, Hungary
  - b) University of Debrecen, Department of Theoretical Physics, P.O. Box 5, H-4010 Debrecen, Hungary
  - c) Departamento de Química, C-9, Universidad Autónoma de Madrid, 28049-Madrid, Spain
  - d) CNRS et Université de Lyon, Laboratoire de Spectrométrie Ionique et Moléculaire, 69622 Villeurbanne Cedex, France
- [1] E. Bene, G.J. Halász, Á. Vibók, L.F. Errea, L. Méndez, I. Rabadán, M.C. Bacchus-Montabonel, *Int. J. Quant. Chem* **111**, 487 (2011).
- [2] H.J. Werner and P. Knowles, MOLPRO (version 2002.1) package of ab-initio programs.
- [3] L.F. Errea, A. Macías, L. Méndez, I. Rabadán, and A. Riera, *Phys. Rev. A* **65**, 010701(R) (2001).
- [4] G. Niedner, M. Noll, J.P. Toennies, and C. Schlier, *J. Chem. Phys.* **87**, 2685 (1987).
- [5] L.F. Errea *et al.*, *Phys. Rev. A* **75**, 032703 (2007).

---

<sup>1</sup>  $R$  is the position vector of the projectile with respect to the molecule center of mass and  $\rho$  is the internuclear vector of the molecule with  $\cos\theta = \rho R$

## 4.5 Studying the electron components of the ECR plasma by plasma photographs

*R. Rácz, S. Biri, J. Pálincás*

An ECRIS (Electron Cyclotron Resonance Ion Source) is a magnetic trap that confines the electron component of the plasma. Electrons heated by microwave generate low or medium or highly charged ions. The electron part itself may artificially be grouped into three populations as cold, warm and hot electrons. Cold electrons are considered those which have not been heated by the microwave. Warm electrons have been energized by microwave and they are able to ionize atoms and further ionize ions. Electrons having much higher energy than necessary for an effective ionization are called hot electrons. Based on detailed study [1] cold electrons are considered with energy between 1-200 eV and warm electrons have several keV energy.

The interactions between the atom, electron and ion components of the ECR plasma cause radiation in the infra-red, visible light, ultra violet and X-ray regions of the electromagnetic spectrum. Thus visible light (VL) and X-ray (XR) photographs contain information about the density distribution of the electron components of the ECR plasma.

A comparison was made between the VL plasma photos and computer simulations (taken by TrapCAD code [2]) and consequences were withdrawn to the cold electron component of the plasma. The warm electron component of the similar simulation was compared with characteristic X-ray photos emitted by plasma ions. Through the example of 14.3 GHz argon ECR-plasma photos it was proved that the spatial distribution of the VL-photons correspond to the cold electrons simulated by computer code (fig. 1.). The simulated warm electrons were compared with argon XR-photos (fig. 2.), i.e with argon ions emitting characteristic XR-photons. Good agreement was found between them. Significant difference was found however between the spatial distribution of the cold and warm electrons [3]. Additionally detailed study was carried out to analyze and understand the

color of the ECR plasmas [4]

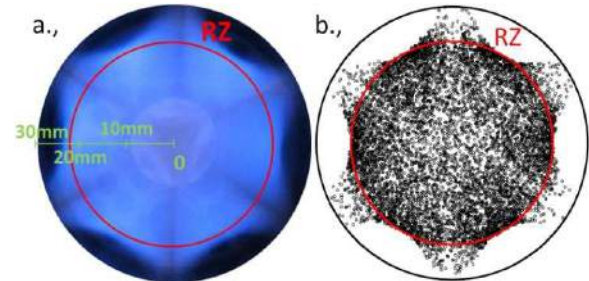


**Figure 1.** Typical argon plasma taken at 14.3 GHz microwave frequency with resonance zone (RZ) contour (a). Computer simulation of the cold electron cloud of a 14.3 GHz plasma with resonant zone contour (b). The external circles are the plasma chamber walls in both cases.

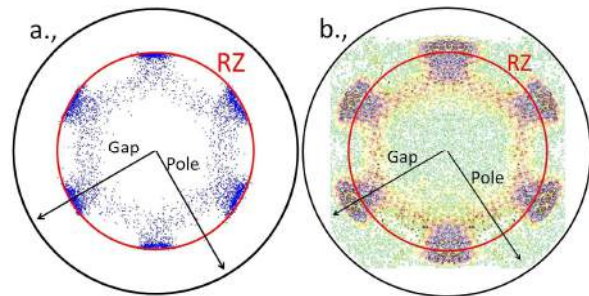


**Figure 2.** Computer simulation of the warm electron cloud of a 14.3 GHz plasma (a). X-ray photo of a 14.3 GHz argon plasma [5].

- [1] G. Shirkov and G. Zschornack, Nucl. Instrum. Methods **B95** (1995) 527.
- [2] S. Biri, A. Derzsi, É. Fekete, I. Iván, High Energy Physics and Nuclear Physics **31** (2007) 165.
- [3] R. Rácz, S. Biri, J. Pálincás, Plasma Sources Science and Technology (accepted for publication)
- [4] S. Biri, R. Rácz, J. Pálincás Proc. of 19th Int. Workshop on ECRIS. Grenoble, France, 23-26 Aug., 2010 (in progress)
- [5] S. Biri, A. Valek, T. Suta, E. Takács, Cs. Szabó, L. T. Hudson, B. Radics, J. Imrek, B. Juhász, and J. Pálincás, Rev. Sci. Instrum. **75** (2004) 1420.

## 4.6 The development of an electrostatic spectrometer for low energy ions

*Péter Herczku*

Molecular fragmentation by ion impact is a process of fundamental importance for ion-beam tumor therapy [ 1]. One of the main fragmentation mechanisms is the so called Coulomb explosion. When a collision removes electrons from a molecule, it may explode due to the repulsive forces between its positively charged atomic centers. The energy of the fragments falls typically in the range of 0-50 eV.

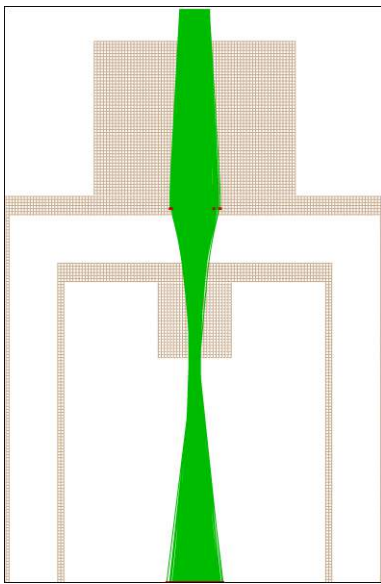


**Figure 1.** Calculated trajectories in the acceleration and deceleration lens of the spectrometer in acceleration mode. Acceleration voltage: 100 V, ion energy 20 eV.

For studying the energy and angular distribution of the low energy fragment ions, we need specific spectrometers. The path of the low energy ions should be as short as possible to avoid charge exchange with the background gases. Accordingly, we need a spectrometer with good resolution, brightness, accuracy, but small in size. Here I report about the development of such a specific spectrometer. In addition demand was to extend the angular range down to  $15^\circ$  observation angles relative to the

projectile ion beam. Moreover, the spectrometer should be applicable up to 10 kV/q ion energies, and capable to accelerate and decelerate ions before energy analysis. Accordingly, we had many constraints for the design. Finally, we decided to construct a so called  $45^\circ$  parallel plate spectrometer with a simple lens system. For calculating the ion trajectories within the small but rather complicated arrangement, we utilized the computer program Simion [2], an electrostatic field modeling program. Typical ion trajectories at the lens stage are shown in Fig. 1. The photo of the analyser part of the spectrometer is displayed in Fig. 2.

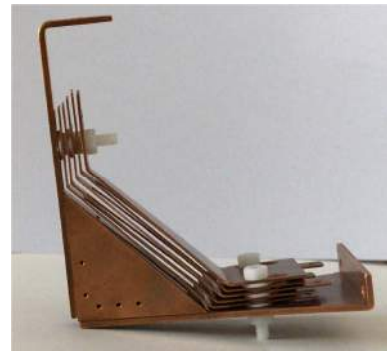


**Figure 2.:** The analyser part of the spectrometer

The first molecular fragmentation measurements with the use of the new spectrometer are expected in the second half of 2011.

### *Acknowledgements*

This work is supported by the OTKA Grant No 73703. I thank to Béla Sulik for supervising my work, Zoltán Pintye for the engineering plans and István Tassy for the careful construction of the spectrometer.

- [1] U. Amaldi, G. Kraft, Radiotherapy with beams of carbon ions, *Rep. Prog. Phys.* **68** (2005) 1861-1882
- [2] Dahl D. A. *International Journal of Mass Spectrometry*, **200** (200). 3-25.

## 4.7 Effusive molecular gas jet target for molecule fragmentation experiments

*S. T. S. Kovacs,*

Collisions between high energy ions and biological molecules have attracted an increasing attention in recent years. Such collisions often results in molecule fragmentation. Reliable knowledge of these interactions is essential in radiotherapy. As a first step it is important to study the fragmentation of water molecules, since water is the main constituent of tissues in living organs.

For measurements with molecules, we developed a special effusive gas jet target in Atomki. It consists of a vertically movable tube through a Wilson-seal and a nozzle, which is easily exchangeable. The nozzle is located at the end of the target tube (see Fig. 1). We designed two types of nozzles: a set of single capillary nozzles with 0,9 – 1,3mm diameter for the gas flow, and a special nozzle, where the gas flows through the tiny tubes of a microcapillary array (a piece of a micro-channel plate, MCP).



**Figure 1.** The elements of the gas jet target system.

All the nozzles are developed for working in the molecular flow range for providing a well collimated effusive gas beam with a target density in the  $7 \cdot 10^{12} \text{ cm}^{-3}$  to  $1 \cdot 10^{14} \text{ cm}^{-3}$  range, which allows to measure reasonably high count

rates, while a low background pressure in the chamber.

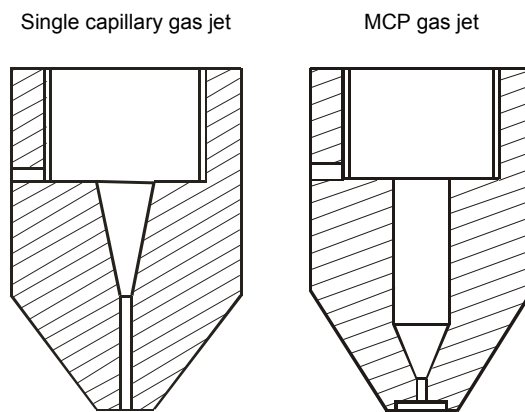


**Figure 2.** Cross sectional view of the two types of nozzles.

The molecular flow range is ensured by setting the geometry of the gas flow elements and the pressures. At the nozzle, the type of the flow depends on the main free path of the molecules, and on the length and diameter of the capillary nozzle [1]. The main free path can be controlled by a wad in the target tube and fine tuned by changing the pressure at the entrance of the target system. The wad is a capillary with adjustable length, and an inner wire with smaller diameter. Moreover, there is an other puffer. The pressure at the entrance is regulated by a control valve, which connects the clean water container with a steam pressure of cca. 20 mbar and the input buffer of the gas target with regulated pressure.

### *Acknowledgements*

This work was supported by the OTKA Grant No. 73703. I express my thanks to Zoltan Pintye, engineer, for his help in constructing the target system.

[1] S. Bohátka (2008): *Vákuumfizika és -technika in Hungarian* 2008

## 4.8 A new VdG-5 beamline for studying ion-atom and ion-molecule collisions

*S.T.S. Kovács, P. Herczku, Z. Juhász, L.L. Horváth, B. Sulik*

Studying energetic atomic and molecular collisions is a fundamental tool to understand processes relevant for plasma physics and materials sciences. In the past decades, atomic collisions have been studied in a wide range of impact energies and collision partners. Today, we understand the basic mechanisms and the most important collision scenarios (see e.g., [1] for electron emission). Due to the refined experimental methods, higher order processes have become routinely observable, and kinematically complete experiments can be performed providing fully differential cross sections. There is an increasing demand from the side of applications to utilize the results of the fundamental atomic collision research. At this point, we often face with the lack of sufficient knowledge about relevant processes, though similar systems and processes have already been investigated. A good example for this is cancer therapy by energetic ion impact, where e.g., the energy deposition is important, but not the most relevant quantity [2,3]. For optimizing the efficiency of the therapy, a multitude of collision mechanisms should be carefully considered in a wide impact energy range.

In this work, we report about a specific beamline for fundamental research on atomic and molecular collisions according to the demands of applications related to radiation damages. We focus on mechanisms which may significantly enhance the fragmentation yield of biomolecules (from water to DNA) by ion impact around the maximum and at the low energy side of the Bragg peak, by experiments in the ion energy range of 50-1000 keV/u at the beamline of the VdG-5 accelerator in Atomki, Debrecen.

The beamline consists of a 15° electrostatic

deflector chamber for the projectile ions, and a magnetically shielded universal experimental chamber of 1 m diameter. The electrostatic deflection is advantageous for heavier ions, and it also offers an easy way to chop the beam for time of flight experiments. In the chamber, there are two rotatable rings with angular calibration. The high vacuum system assures a background pressure of  $10^{-7}$  mbar. The main target is an effusive molecular gas jet which is designed for these experiments. The target gas density can be varied from  $7 \cdot 10^{12}$  cm $^{-3}$  to  $1 \cdot 10^{14}$  cm $^{-3}$  with a set of wads and nozzles. We developed a specific electrostatic spectrometer which is able to measure in the 15° - 165° observation angle range relative to the beam direction. This is a 45° parallel plate spectrometer, which can be used up to  $E/q=10$  keV. The spectrometer is equipped with an electrostatic lens for acceleration and deceleration. Time of flight spectrometers are under construction. We would like to measure double differential cross section of molecular fragments (both cations and anions) with and without coincidence conditions.

### *Acknowledgements*

This work was supported by the Hungarian National Science Foundation (OTKA, Grant No. 73703). We thank for the valuable help of engineers and operators of the VdG-5 accelerator of Atomki.

- [1] N. Stolterfoht, R.D. DuBois and R.D. Rivaola, *Electron Emission in Heavy Ion-Atom Collisions* (Springer, Berlin, 1997)
- [2] E.C. Montenegro, M.B. Shah, H. Luna et al., *Phys. Rev. Letters*, 99 (2007) 213201
- [3] M. Shah, invited talk at the XX. ISIAC, Aigos Nicolaos, Crete, Aug 1-3, 2007

## 4.9 Guided transmission of $\text{Ne}^{7+}$ ions through nanocapillaries in polymers: Dependence on the capillary diameter

*N. Stolterfoht<sup>a)</sup>, R. Hellhammer<sup>a)</sup>, Z. Juhász, B. Sulik, E. Bodewits<sup>b)</sup>, H.M. Dang<sup>b)</sup>, R. Hoekstra<sup>b)</sup>*

The capillary guiding phenomena is a result of a self-organizing process governing the charge deposition by the incident ions at the inner wall of the capillaries [1]. The ions are deflected by charge patches so they do not suffer close collisions with the capillary wall, even when the capillary axis is tilted with respect to the incident beam direction. This “fully elastic” guiding has been found to be significant in capillaries of different sizes and aspect ratios, made from different insulator materials, in a wide range of impact ion energies and charge states.

In this work [2], guiding 3-keV  $\text{Ne}^{7+}$  ions through nanocapillaries in insulating polyethylene terephthalate was investigated as function of the capillary diameter. The experiments were conducted at the ZERNIKE-LEIF facility at the KVI Groningen (Netherlands) [3]. Highly parallel capillaries with a density of  $4 \times 10^6 \text{ cm}^{-2}$  and diameters of 100, 150, 200, 300, and 400 nm were utilized.

The characteristic charges governing the charge evolution of the total ion yield were found to be independent of the capillary diameter. However, certain dynamic properties were found to change significantly with this diameter: The transmission profiles of the 100 nm capillaries are broad and structureless, whereas those for 300 nm are composed of three peaks and the mean angle oscillates with deposited charge. At equilibrium the total ion yield was studied as a function of the tilt angle. The results were used to evaluate guiding angles [2] (see Fig. 1 (b)), which were found to be almost constant near  $5.5^\circ$  with varying capillary diameter similarly as the characteristic charge governing the charge evolution.

Model considerations were applied to interpret the results. They have led to the conclusions that the effective potential and the capacity of the capillary samples are nearly independent on the diameter. These unexpected results imply the need for further investigations.

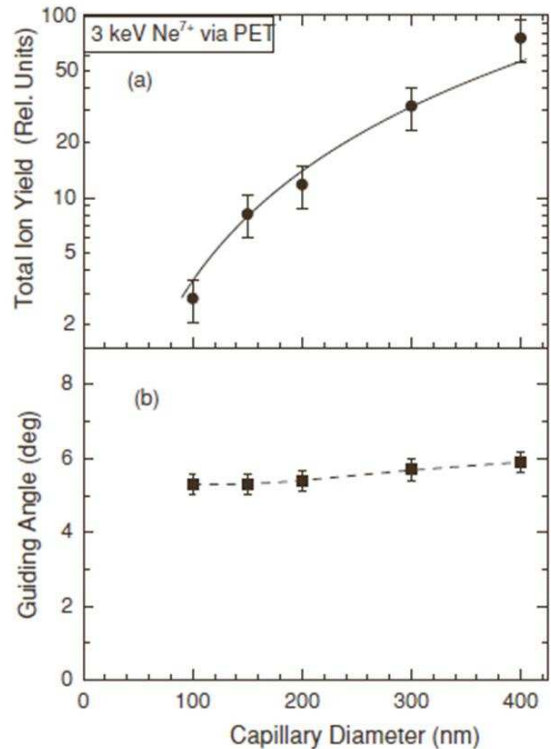


**Figure 1.** Transmission properties of 3-keV  $\text{Ne}^{7+}$  ions as a function of the capillary diameter  $d$ . In (a) the total ion yield  $Y_{min}$  at  $0^\circ$  tilt angle is displayed (as points) in comparison with a curve (as solid line) proportional to  $d^2$ . In (b) the guiding angle  $\Psi_c$  is plotted. The dashed line is merely to guide the eye. [2]

### Acknowledgements

B.S. and Z.J. were supported by the Hungarian National Science Foundation OTKA (No. K73703 and No. PD050000). The work was financially supported by the European Network ITS-LEIF RII3-026015.

a) Helmholtz-Zentrum Berlin für Materialien und Energie, Glienickerstr. 100, D-14109 Berlin, Germany

b) KVI Atomic Physics, University of Groningen, NL-9747 AA Groningen, The Netherlands

[1] N. Stolterfoht *et al.* Phys. Rev. Lett. **88**, 133201-1 (2002).

[2] N. Stolterfoht *et al.*, Phys. Rev. A **82**, 052902 (2010).

[3] M. Unipan *et al.*, Phys. Rev. A **74**, 062901 (2006).

## 4.10 Ion guiding accompanied by formation of neutrals in PET polymer nanocapillaries: Further insight into a self-organizing process

Z. Juhász, B. Sulik, S. Biri, K. Tőkési, R.J. Berezky, R. Rácz, Á. Kövér, J. Pálinkás<sup>a)</sup>, N. Stolterfoht<sup>b)</sup>

There is an increasing interest in the recently discovered ion guiding phenomena in nanocapillaries [1]. The phenomenon involves the charging up of inner capillary walls, which prevents a significant fraction of the ions getting close to the walls, i.e. they mostly preserve their initial charge state during the transmission.

Recently, systematic works have been started measuring and analyzing the time evolution of the angular transmission profiles [2-5]. A prospective way for gathering more information about the development of charge patches is to study the dynamic properties of the guided ions and those of charge-exchanging inelastic collisions simultaneously. This can be provided by the measurement of all ions with all charge states, as well as the neutralized atoms.

A detailed investigation of such type was recently performed at ATOMKI [6]. Part of the results is presented in Fig. 1. Relatively large yield for atoms formed by neutralization was observed when 3 keV  $Ar^{7+}$  ions were guided through polyethylene terephthalate (PET) nanocapillaries. We studied simultaneously the angular distribution of the guided ions and the formed atoms as a function of time.

The number of atoms strongly increased in time similarly to the number of ions but it reached saturation earlier. In accordance with earlier observations, oscillatory behavior of the mean emission angle for ions was observed [3]. For the atoms, it was much less pronounced.

The analysis shows that neutrals appear prior to the guided ions. Based on the results a tentative model for neutral formation was developed. Neutrals following straight line trajectories directly report on their places of origin, which provides us further insight into the guiding mechanism and charge patch for-

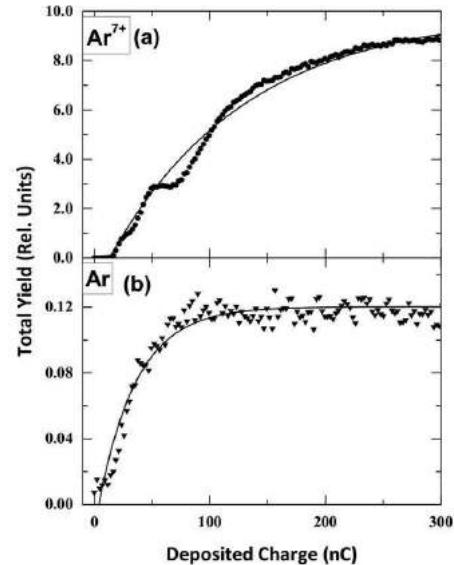


**Figure 1.** Total yield of  $Ar^{7+}$  (a) and  $Ar$  (b) transmitted through capillaries of 200 nm diameter as function of the deposited charge, which is also a measure of time. The tilt angle of the capillaries was  $5.5^\circ$ . Experimental data are shown as full symbols.

### Acknowledgements

This work received partial support from the Hungarian National Science Foundation OTKA (Grant No: K73703).

a) Dept. of Exp. Physics, University of Debrecen, Egyetem tér 1, H-4032 Debrecen, Hungary

b) Helmholtz-Zentrum Berlin für Materialien und Energie, Glienickerstr. 100, D-14109 Berlin, Germany

[1] N. Stolterfoht *et al.* Phys. Rev. Lett. **88**, 133201-1 (2002).

[2] Y. Kanai *et al.*, Phys. Rev. A **79**, 012711 (2009).

[3] N. Stolterfoht *et al.*, Phys. Rev. A **79**, 022901 (2009).

[4] P. Skog *et al.*, Phys. Rev. Lett. **101**, 223202 (2008).

[5] A. Cassimi *et al.*, Nucl. Instr. and Meth. B **267**, 674 (2009).

[6] Z. Juhász *et al.*, Phys. Rev. A **82**, 062903 (2010).

## 4.11 Emission of $H^-$ fragments from collisions of $OH^+$ ions with atoms and molecules

Z. Juhász, B.S. Frankland<sup>a)</sup>, F. Frémont<sup>a)</sup>, J. Rangama<sup>a)</sup>, J.-Y. Chesnel<sup>a)</sup>, B. Sulik

Detailed measurement of the kinematics of positive fragment ions from molecular collisions provide useful information about the collision dynamics (see e.g. [1-3] and references therein). In the present work, we turn our attention to negative fragments. Double differential emission spectra of negative charged particles have been measured in collisions of  $OH^+$  ions with gas jets of Ar atoms and acetone ( $CH_3-CO-CH_3$ ) molecules at 7 keV impact energy. Among the emitted electrons, a relatively strong contribution of  $H^-$  ions has been observed in both collision systems. According to a kinematic analysis, the observed  $H^-$  ions were produced in close atom-atom collisions. For acetone, these ions originated from both the projectile and the target. The present ion-impact energy range falls in the distal region of the Bragg peak. Therefore, a non negligible  $H^-$  production in biological tissues could be relevant for ion therapy and for radiolysis in general.

The present experiments were conducted at the 14.5 GHz Electron Cyclotron Resonance (ECR) ion source of the ARIBE facility, at the Grand Accélérateur National d'Ions Lourds (GANIL) in Caen, France. The molecular  $OH^+$  ions were produced by introducing water vapor in the ECR plasma chamber. The extracted ions were collimated to a diameter of 2.5 mm before entering the collision chamber. In its center, the  $OH^+$  projectiles crossed an effusive gas jet of either argon atoms or acetone molecules. In the collision area, the density of the gas target was typically of  $10^{13} \text{ cm}^{-3}$ . The electrons and negative ions produced in the collision were detected by means of a single-stage spectrometer consisting of an electrostatic parallel-plate analyzer.

Spectra taken at  $30^\circ$  observation angle are shown in Figure 1. Contributions from  $H^-$  appear in clearly visible peaks. Kinematics shows that the peak at 410 eV in both panels is due emission of  $H^-$  ions moving with nearly the projectile velocity. An  $H^-$  ion is created when

an H center is detached from the projectile in collision with one of the heavy centers of the target. Ions in the second peak (lower panel) originate from close binary collisions between H atoms of the target and the O atoms of the projectile. We are working on absolute cross sections as well as theoretical models for understanding these, somewhat unexpected processes.

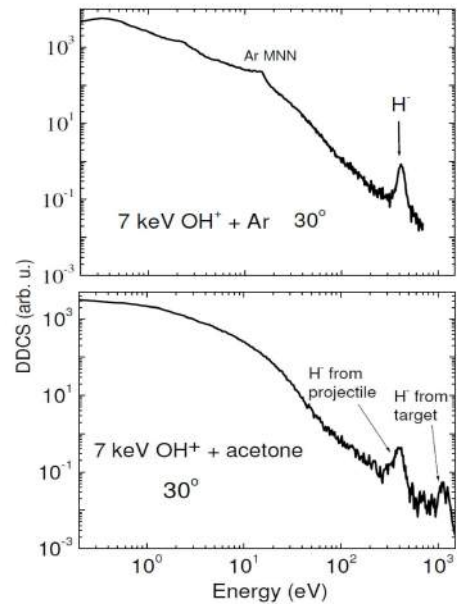


**Figure 1.** Double differential cross sections of negatively charged particles emitted in collisions of 7 keV  $OH^+$  with Ar atoms (upper panel) and acetone molecules (lower panel), at  $30^\circ$  observation angle.

### Acknowledgements

This work was supported by the Transnational Access ITS-LEIF, granted by the European Project HPRI-CT-2005-026015, and the Hungarian National Science Foundation OTKA (No. K73703).

a) Centre de Recherche sur les Ions, les Matériaux et la Photonique (CIMAP), Unité Mixte CEA-CNRS-EnsiCaen-Université de Caen Basse-Normandie, UMR 6252, 6 Boulevard Maréchal Juin, F-14050 CAEN cedex 04, France

[1] N. Neumann *et al* 2010 Phys Rev Lett **104** 103201

[2] Z. Juhász *et al* 2009 Nucl Instr Meth B **267** 326

[3] Z.D. Pesic *et al* 2009 J Phys B **42** 235202

## 5.1 Determination of hydrogen concentration in a-Si and a-Ge layers by elastic recoil detection analysis

*N.Q. Khánh<sup>a)</sup>, M. Serényi<sup>a)</sup>, A. Csik, C. Frigeri<sup>b)</sup>*

Hydrogenated amorphous Si and Ge films are of current interest in academic and industrial research due to their unique physical properties and important applications. The incorporation of hydrogen in the amorphous network is an accepted means for reducing the density of defect states in the midgap [1]. The passivation of dangling-bonds leads to a significant improvement in the electronic and optical properties of these layers. However, hydrogen is also suspected to degrade the performance of amorphous Si and Ge material and devices. Several studies related to hydrogen motion have been proposed to explain the light and thermal degradation effect in these layers. Thus to improve the performance and reliability of these devices, it is crucially important to understand the role of hydrogen in amorphous layers.

In our previous works [2,3] the structural changes of hydrogenated a-Si/Ge multilayers as a function of annealing condition was investigated. It was shown that during annealing the samples underwent significant structural changes. Due to the fast out-diffusion of hydrogen from the layers prepared with high (6 ml/min) H<sub>2</sub> flow rate, bubbles and craters were created on the surface. However, in the multilayer samples prepared with hydrogen flow rate lower than 6 ml/min the macroscopic degradation by formation bubbles and craters was more moderated. The diffusion measurement shows that in these samples the structural degradation and intermixing of layers was slower than in the non-hydrogenated samples. As it was suggested the hydrogen can inactivate the dangling bonds of amorphous layers and, as a result of this, the intermixing slows down. It was also predicted that the hydrogen first released from the Ge layers because of the lower binding energy [3].

In this work, we have studied the individual

a-Si and a-Ge hydrogenated layers prepared by RF sputtering on Si (100) substrates. The absolute value of atomic content of the H was determined by Elastic Recoil Detection Analysis (ERDA) using MeV He<sup>+</sup> ions. ERD is most frequently used for H detection, because it is simple, non-destructive method. The samples were annealed in high purity argon at 623 K for 1 and 4 hours. Non-hydrogenated samples sputtered and annealed under the same conditions of the hydrogenated ones were also investigated.

It was shown that hydrogen can diffuse out faster from Ge film than from the Si one during annealing. This result is in good agreement with literature and with our previous prediction concerning the thermal stability investigations of hydrogenated Si/Ge multilayers. As it follows from the ERDA results, the formation of bubbles on the surface of multilayers is due to release of hydrogen from the Ge layers. Breaking of the Si-H bonds is also possible but they play a minor role in the structural degradation of multilayers.

This work was supported by the Scientific Cooperation Agreement between MTA (Hungary) and CNR (Italy) (contract no.MTA 1102) and by the National Office for Research and Technology (NKTH, grant no.TFSOLAR2).

a) Research Institute for Technical Physics and Materials Science, Hungarian Academy of Sciences (MTA-MFA), H-1121 Budapest, Konkoly-Thege ut 29-33, Hungary

b) CNR-IMEM Institute, Parco Area delle Scienze, 37/A, 43010 Parma, Italy

[1] M.E. Gueunier *et al.*, *J. of Appl. Phys.* **92**(9) (2002) 4959

[2] A. Csik *et al.*, *Vacuum* **84** (2010) 137

[3] C. Frigeri *et al.*, *J. Mat. Sci. Mat. Electron.* **19** (2008) S289-S293

## 5.2 Effect of temperature on the mutual diffusion in Ge/GaAs and GaAs/Ge systems

*M. Bosti<sup>a)</sup>, G. Attolini<sup>a)</sup>, C. Ferrari<sup>a)</sup>, C. Frigeri<sup>a)</sup>, M. Calicchio<sup>a)</sup>, F. Rossi<sup>a)</sup>, K. Vad, A. Csik, Zs. Zolnai<sup>b)</sup>*

GaAs/Ge heterostructures are commonly used in high efficiency solar cells. The efficiency of multiple junction cells, such as InGaP/GaAs/GaAs or GaAs/Ge and triple junction InGaP/GaAs/Ge, is continuously improved. Heteroepitaxy of GaAs on Ge substrate is common for photovoltaic applications and electronic devices but Ge epitaxy on GaAs is much less studied. Ge junctions are usually made by diffusion for either photovoltaic or thermophotovoltaic purposes. Crystal growers make clever use of the diffusion of Ga, As, In and P atoms from GaAs or InGaP into Ge to dope the Ge substrate for the realization of photovoltaic converters for infrared light. However, this process results in a broad interface between n and p type regions of the diode. Instead, an epitaxial deposition of Ge could permit to obtain better doping control and sharper interfaces, resulting in a more abrupt dopant profiles and heterointerface that could enhance light conversion efficiency.

The interdiffusion in Ge/GaAs and GaAs/Ge heteroepitaxy is a known problem. Since Ge acts as dopant in GaAs, and vice versa, the film/substrate interdiffusion of Ge and GaAs is used to increase the carrier concentrations in the first hundred of nanometers of the layer and to obtain diffused p/n junctions. While this is useful for realizing p/n junctions, there are some cases in which this phenomenon must be suppressed. The use of low temperature buffer was used to effectively reduce the problem.

Despite the fact that GaAs deposition on Ge is widely employed in commercial devices, Ge epitaxy on GaAs was not widely studied, especially in Metal-Organic Vapor Phase Epi-

taxy (MOVPE), because until recent years it was difficult to obtain suitable Ge precursors. For this reason the interdiffusion phenomena in epitaxial Ge are much less understood. In order to assess this problem we grew Ge/GaAs and GaAs/Ge heterojunctions by MOVPE using iso-butylgermane (iBuGe), arsine and trimethylgallium in hydrogen atmosphere at low pressure, varying the deposition temperature. Element concentration profiles were obtained by Secondary Neutral Mass Spectrometry (SNMS) and the use of low temperature GaAs and Ge buffer layers was investigated in order to limit the interdiffusion.

We found that the use of a low temperature GaAs buffer layer reduced the diffusion in GaAs/Ge epitaxy at 600°C, while a Ge low temperature buffer layer was not effective in reducing the interdiffusion in Ge/GaAs epitaxy at 700°C. SNMS analysis of element diffusion in the Ge/GaAs system shows that the interface thickness has a logarithmic dependency on  $1/kT$ . An asymmetry was found between the GaAs/Ge and Ge/GaAs systems: as diffusion process in an epitaxial Ge on a GaAs substrate is higher with respect to that of a As in GaAs film deposited on a Ge substrate.

This work was supported by the National Office for Research and Technology (NKTH, grant no.TFSOLAR2) and by the Scientific Cooperation Agreement between MTA (Hungary) and CNR (Italy).

a) CNR-IMEM Institute, Parco Area delle Scienze, 37/A, 43010 Parma, Italy

b) Research Institute for Technical Physics and Materials Science, Hungarian Academy of Sciences (MTA-MFA), H-1121 Budapest, Konkoly-Thege ut 29-33, Hungary

### 5.3 Depth profile analysis of solar cells by Secondary Neutral Mass Spectrometry using conducting mesh

*R. Lovics, A. Csik, V. Takáts, K. Vad, G.A. Langer<sup>b)</sup>*

A silicon thin film solar cell is a preferable choice for the large-scale production of low-cost solar modules for a numerous reasons: i) abundance of cheap raw material; ii) non-toxic component in the technology; iii) shorter energy payback time; iv) low temperature technology. A new and promising way for photovoltaic application of  $\mu$ -Si is the so-called “micromorph tandem” structure, which is a serial combination of an amorphous and a microcrystalline cell. The development and implementation of that technology into industrial manufacturing line may result in the reduction of specific processing costs and increasing efficiency. On the other hand, not only the production, but the analysis of the produced layers is also important in order to increase the efficiency of energy conversion.

In this work we show that charge accumulation developing on the surface of insulating samples due to sputtering can be avoided by using a conducting mesh. By using a copper mesh and operating the SNMS in high frequency sputtering mode (HFM), the sputtering depth profiling of dielectric samples becomes possible with the same quality as it can be performed in conducting samples. We have applied this method for analysis of  $p-i-n$  : Si diodes, and the results confirm us that the measurements with mesh is more effective to determine the doping level of phosphorus (P) and boron (B) in 500-600 nm depth, than without a mesh. The effect of an electrically conductive mesh placed on to the sample surface during HFM sputtering proved to be excellent. While the crater shape and, in addition, the depth resolution is not acceptable without a mesh (Fig.1, blue line), their quality is much better in the case with mesh (Fig.1, red line). The grey part in Fig.1 represents the ideal shape of the crater produced by sputtering. It can be seen that the bottom of the crater is close to the ideal square-shape. In Fig.2 the distribution of boron (B)

also support the usefulness of a metal screen mesh in depth profile analysis of solar cells.

This work was supported by the National Office for Research and Technology (NKTH, grant no.TFSOLAR2).

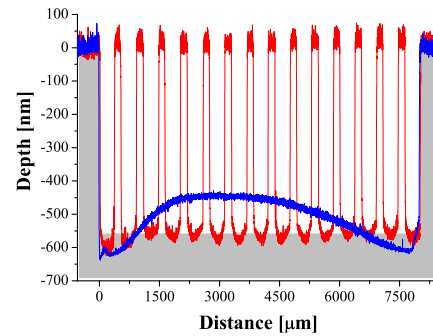


**Figure 1.** Sputtered crater shape without (blue) and with (red) copper mesh.

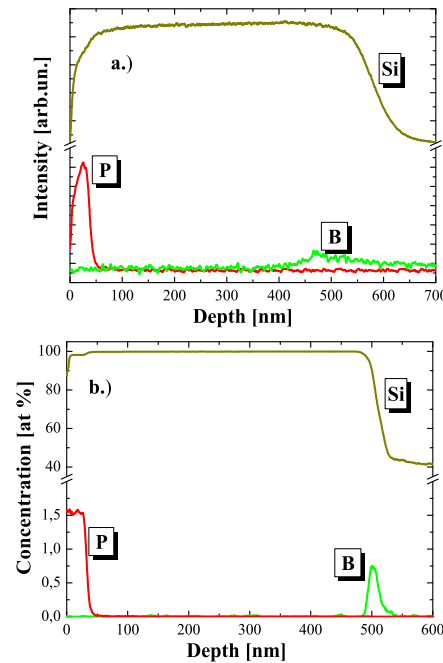


**Figure 2.** Depth profile of  $p-i-n$  : Si diode measured without (a) and with (b) copper mesh.

a) University of Debrecen, Department of Solid State Physics, H-4010 Debrecen, P.O. Box 2, Hungary

## 5.4 AR-HAXPES for determining Effective Attenuation Length of electrons

*L. Kövér, I. Cserny, A. Csik, W. Drube<sup>a)</sup>, S. Thiess<sup>a)</sup>*

In quantitative analysis of ultrathin films the effective attenuation length of electrons ( $EAL$ ) is a useful practical parameter accounting for inelastic and elastic scattering of electrons, depending weakly on the electron emission angle and film thickness in a wide range of angle and thickness [1]. The need of  $EAL$  values for HARD X-ray Photo-Electron Spectroscopy (HAXPES) is obvious. The “practical”  $EAL$  can be determined experimentally using its definition [1]:  $EAL = (1/\cos\theta)(d/(\ln I_0 - \ln I_d))$ , where  $d$  is the overlayer thickness,  $I_0$  and  $I_d$  the photoelectron peak intensities from the uncovered and covered substrate,  $\theta$  the emission angle of photoelectrons related to the surface normal of the sample. A disadvantage of this method is the use of samples with different surface conditions (e. g. roughness, etc.).  $I_0$  can be eliminated deriving  $EAL$  from the peak intensity ratios  $I_d^\theta/I_d^{\theta=0}$ .

Here angular resolved (AR-)HAXPES was used for determining the practical  $EAL$  [1] in  $Ni$  and its value was compared to estimated values from the formula [2] where  $\omega = \lambda_{in}/(\lambda_{in} + \lambda_{tr})$  and  $\lambda_{in}$  denotes the mean free path for inelastic scattering,  $\lambda_{tr}$  the transport mean free path [1] of the electrons. A  $Ni$  thin film was deposited by DC magnetron sputtering onto a Pd layer grown on a Si substrate. The thickness of the Ni overlayer was estimated to be  $(7.0 \pm 0.7)nm$ , using the sputtering rate calibrated by stylus profilometer. Angular resolved photoelectron spectra were measured with the Tunable High Energy XPS instrument [3] at the BW2 beamline of the DORIS III using a spectrometer energy resolution of 0.2 eV. A monochromated exciting photon beam of 5000 eV energy was used and  $\theta$  varied by tilting the sample. **Fig 1.** shows the linearized curve of the angular dependence of the measured relative  $Pd\ 3d$  peak intensities (corrected for changes in the irradiated sample area). The obtained value  $EAL = (3.9 \pm 0.4)nm$  agrees quite well with the estimated values based on

the  $\lambda_{tr}$  [4] value and  $\lambda_{in}$  values [5, 6] yielding  $EAL = 4.5\ nm$  [4,5] and  $4.2\ nm$  [4,6] showing that the effect of a possible hydrocarbon contamination top overlayer is small. Further studies are needed to account for this effect as well.

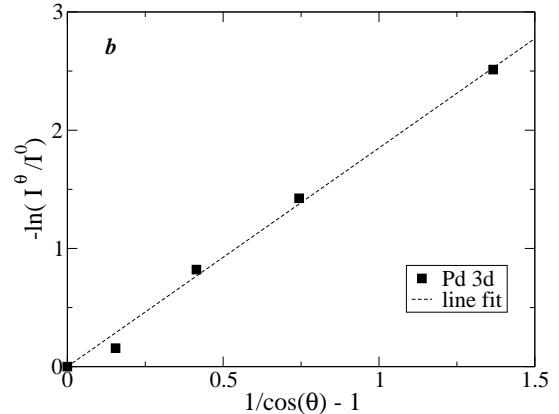


**Figure 1.** Linearized curve of the angular dependence of the measured relative  $Pd\ 3d$  peak intensities as a function of the sample tilting.

### Acknowledgements

The research leading to these results has received funding from the European Community’s Seventh Framework Programme (FP7/2007-2013) under grant agreement n° 226716 as well as from the Hungarian project OTKA 67873.

- a) HASYLAB/DESY, Notkestraße 85, D-22603 Hamburg, Germany
- [1] A. Jablonski and C. J. Powell, *J. Surf. Sci. Rep.* **47**, 33 (2002).
- [2] C. J. Powell and A. Jablonski, *J. El. Spectrosc. Rel. Phenom* **178-179**, 331 (2010).
- [3] W. Drube, T. M. Grehk, R. Treusch and G. Materlik, *J. Electron Spectrosc. Relat. Phenom.* **88-91**, 683 (1998).
- [4] NIST Standard Reference Database 64, <http://www.nist.gov/srd/nist64.cfm>
- [5] S. Tanuma, C. J. Powell and D. R. Penn, *Surf. Interface Anal.*, **43**, 689 (2011).
- [6] W. S. M. Werner, K. Glantschnig and C. Ambrosch-Draxl, *J. Phys. Chem. Ref. Data*, **38**, No. 4, 1013 (2009).

## 6.1 Transmission of electrons through a single glass macrocapillary: energy dependence

B. S. Dassanayake <sup>a)</sup>, R. J. Berezky, S. Das <sup>a)b)</sup>, K. Tókési, J. A. Tanis <sup>a)</sup>

In the last decade the transmission of charged particles through various types of capillaries has been in the center of interest. The interaction of charged particles with insulating capillaries first has motivated the development of nanotechnology. In recent years focus has been shifted to the more challenging and difficult transmission of charged particle through linear structures such as capillaries of nano- and macro-meter scales. These studies are important not only from the fundamental understanding of ion/electron insulator interactions view point, but also due to its potential applications in various fields.

In our work we investigated the transmission of 300 - 1000 eV electrons through a single glass macrocapillary [1, 2]. The measurements focused on the energy and tilt angle dependence of the transmitted electrons intensity [1]. The experiments were carried out in the tandem Van de Graaff accelerator laboratory at Western Michigan University in Kalamazoo. The borosilicate glass capillaries with a diameter of 0.18 and 0.23 mm, length 14.4 mm and 16.8 mm (aspect ratio 88 and 73) were prepared at the ATOMKI, in Debrecen. The samples and their holder were covered with graphite to carry away excess charge deposited on them, and to enable reading the current on the samples.

We have showed that electrons can be transmitted through a single glass microcapillary. The intensity of the transmitted particles decreases with increasing tilt angles. Due to the inelastic electron scattering with the inner surface the electrons lose energy but they can still pass through the capillary. Transmitted electron intensities were found to have two significant regions, a direct and an indirect transmission region. We found that the guiding angle of the capillary increased with increasing energy above 500 eV in the direct region for tilt

angles  $\Psi > 2.5^\circ$ . This is completely different what was observed in the case of slow positive ions and for fast electrons on nanocapillary foils and also deviates from the theoretical predictions. This can be caused by the presence of two different processes during the transmission of the electrons through the sample. The elastic scattering may be dominant at the lower energies, whereas Coulombic repulsion due to charge deposition overtakes it at higher energies.

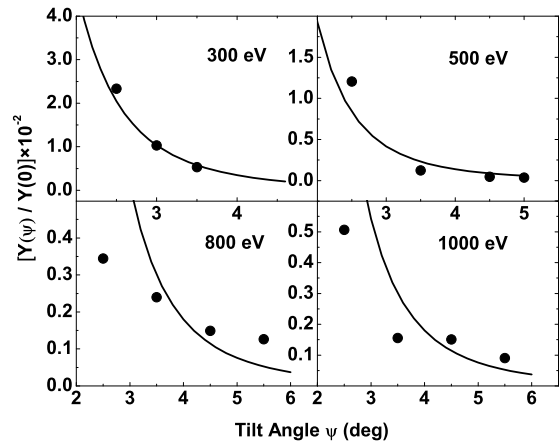


**Fig1.**  $Y(\Psi)/Y(0)$  of the obtained data vs. tilt angle for all energies, where  $Y(\Psi)$  is the yield at tilt angle  $\Psi$  and  $Y(0)$  is the yield at angle  $\Psi = 0^\circ$ . Dots indicate the experimental data points and the solid lines are the theoretical predictions of the Rutherford scattering cross section.

- a) Department of Physics, Western Michigan University, Kalamazoo, USA
  - b) Manne Siegbahn Laboratory, Stockholm University, Stockholm, Sweden
- [1] B. S. Dassanayake, S. Das, R. J. Berezky, K. Tókési and J. A. Tanis, Phys. Rev. A. **81**, 020701(R) (2010).
- [2] B. S. Dassanayake, R. J. Berezky, S. Das, A. Ayyad, K. Tókési and J. A. Tanis, Phys. Rev. A. **83**, 012707 (2011).

## 6.2 Time dependence of electron transmission through a single glass macrocapillary

R. J. Berezky , B. S. Dassanayake <sup>a)</sup>, S. Das <sup>a)</sup>, A. Ayyad <sup>a)</sup>, K. Tókési , J. A. Tanis <sup>a)</sup>

Transmission of charged particles through insulating nanoscale capillaries has been rigorously investigated in the last few years. Guiding of slow highly charged ions (HCI) and electrons through a single glass macrocapillary has been also studied, showing that guiding occurs even for macroscopic dimensions [1, 2]. It has been established that HCI transmission is caused by a self-organizing charge-up process of the inner wall of the capillary. After a characteristic charging time a well-tuned electric field is formed inside the tube. This field deflects ions enter later in the capillary. This allows the ions to be guided along the capillary, and inhibits further interactions of the transmitted ions with the capillary surface, preserving their initial charge state. Compared to the research for slow ions, a little has been done, both experimentally and theoretically, so far to investigate electron transmission dynamics.

In this work we present systematic measurements of the time evolution of electron transmission through a single glass macrocapillary for 500 and 800 eV electrons [3]. During the experiments borosilicate, cylindrically-shaped capillaries, with large aspect ratios ( $l/d = 80$  and  $73$ ) prepared at the Institute of Nuclear Research of the Hungarian Academy of Sciences, (ATOMKI) were used. The measurements were performed in the tandem Van de Graaff accelerator laboratory at Western Michigan University in Kalamazoo.

We have demonstrated that the electron transmission through a single glass macrocapillary has time- (charge-) dependent behavior, and it can be related to the competition among charge deposition, Coulombic repulsion, and discharge. Low transmission at the start of each angular measurement is mainly attributable to inelastically scattered electrons from interactions with the inner capillary surface. Charge deposition close to the entrance with time gradually creates a field distribution

on the inner surface, which elastically deflects further incoming electrons from the charging area toward the exit of the capillary. Transmission comes to equilibrium when compensation between charging and discharging processes is reached. It is emphasized, however, that stable equilibrium is never reached due to repeated sudden partial discharge of the charge patch from time to time. Such non-equilibrium has not been previously observed for electron or ion transmission in capillaries.

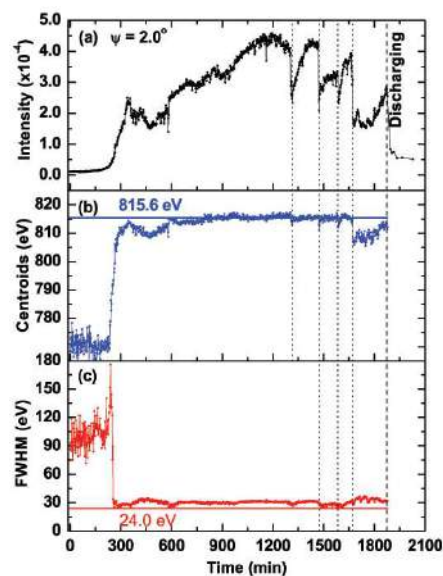


**Fig1.** Comparison of variation in transmitted beam intensity (a), centroid energy (b), and FWHM values (c) for 800 eV electrons at  $\Psi = 2^\circ$ . The blue solid line is the bare beam centroid (815.6 eV), and the red solid line is the bare beam FWHM (24.0 eV). The dotted lines indicate sudden discharging of the capillary.

a) Department of Physics, Western Michigan University, Kalamazoo, USA

- [1] R. J. Berezky, G. Kowarik, F. Aumayr and K. Tókési, NIM. B **267** 317 (2009).
- [2] B. S. Dassanayake, S. Das, R. J. Berezky, K. Tókési and J. A. Tanis, Phys. Rev. A. **81**, 020701(R) (2010).
- [3] B. S. Dassanayake, R. J. Berezky, S. Das, A. Ayyad, K. Tókési and J. A. Tanis, Phys. Rev. A. **83**, 012707 (2011).

### 6.3 Thin Layer Activation Technique under the Free Handling Limit

*F. Ditrói, S. Takács, F. Tárkányi, E. Corniani<sup>a)</sup>, M. Jech<sup>a)</sup>, T. Wopelka<sup>a)</sup>*

Thin Layer Activation (TLA) technique is extensively used in our laboratory for wear, corrosion and erosion measurements by using adequately high activities [1-2]. Because the production of radioactive isotopes and their application for wear measurements have been performed in different places/institutes/cities/countries, the delivery between the cooperating partners requires time consuming permission process, special packing and shielding and accredited transport companies. To avoid this complicated process a method was developed to use only activities below the Free Handling Limits (FHL) [3]. FHLs are determined for each radioactive isotope separately. In most cases we produce and use several isotopes in the same time. One must take care that the overall activity may not exceed the conditions given for the free handling limit for mixed isotopes. In this case one can legally deliver radioactive isotopes between countries by using only minimal shielding and regular post or courier services. The advantages of the method are demonstrated on real wear measurement tasks by using the most common isotopes used for Thin Layer Activation.

If one considers a real machine part made of steel, it may contain elements other than iron in reasonable amount. Even from pure iron more than one isotope is produced. In this case the conditions to fulfil the requirements for the Free Handling limit are determined according to the rule for mixed isotope:

$$\sum_1^n \frac{A_i}{FHL_i} \leq 1 \quad (8)$$

Where  $A_i$  is the measured/calculated activity of the  $i$ th isotope of the sample in the

time of delivery and  $FHL_i$  is the Free Handling limit of the same isotope,  $n$  is the number of measurable isotopes. The packages should be assembled in such a way that the condition of equation (8) must be fulfilled for every package.

Because of the fulfilment of the FHL condition the actual wear measurement can be performed in institutions and/or industrial plants without licence for handling radioactive materials, but the relative low activities might require the using of high efficiency scintillation detectors.

**Table 1.** The most frequently used radioactive isotopes

Isotope	Half-life hours	Gamma-energy keV	FHL kBq
<sup>55</sup> Co	17.53	931	1000
<sup>56</sup> Co	1854	847 1238	100
<sup>57</sup> Co	6523	122 136	1000
<sup>58</sup> Co	1701	811	1000
<sup>52</sup> Mn	134	744 935 1434	100
<sup>54</sup> Mn	7495	835	1000
<sup>51</sup> Cr	665	320	10000
<sup>48</sup> V	383	983 1312	100
<sup>65</sup> Zn	5862	1116	1000

a) Austrian Competence Center for Tribology, Wiener Neustadt, Austria

[1] F. Ditrói F., I. Mahunka: *Wear* **219** (1998) 78

[2] F. Ditrói, S. Takács, F. Tárkányi, M. Reichel, *et al.* *Wear* **261** (2006) 13974

[3] E. Corniani, M. Jech, F. Ditrói, T. Wopelka, F. Franek: *Wear* **267** (2009) 828

## 6.4 Optical properties of silver thin films, derived from REELS

Z.M. Zhang<sup>a)</sup>, T. Chen<sup>b)</sup>, Z.J. Ding<sup>b)</sup>, T. Tang<sup>b)</sup>, A. Csik, J. Tóth, K. Tőkési

The differential surface excitation probabilities (DSEPs) for medium-energy electrons traveling in Ag are extracted from reflection electron energy loss spectroscopy (REELS) spectra [1] by using the elimination-retrieved algorithm of Werner [2]. Based on a surface Kramers-Kronig dispersion relationship, the electronic structure and optical properties of Ag thin film are determined. The results show that the optical property curves between surface thin layer and bulk are similar in shape, whereas they deviate quantitatively for energies below 40 eV, which may be caused by the different electronic structures at surface and in bulk. The present data would be an appropriate approximation to the optical properties of thin film, whose thickness is characterized by the inelastic mean free path of the electrons in a REELS experiment.

Figure 1 shows the comparison on the surface energy loss functions (SELFs),  $\text{Im}\{-1/(1+\epsilon)\}$ , between the present result obtained from REELS spectra of Ag thin film and that derived from the optical data [3] for the surface of bulk specimen. It can be seen that the peak intensity of surface plasmon for thin film is lower than for the surface of bulk specimen but the peak width is broader. Furthermore, the obtained surface plasmon energy in a thin film (3.6 eV) is slightly lower than that at the surface of bulk specimen (3.65-3.7 eV). Ritchie had pointed out in 1957 [4] that for a quite thin film the electrostatic fields originating from both two interfaces overlap and results in the varied surface plasmon energy branches with thickness. With the REELS spectra measured for low-energy electrons, the complex dielectric functions as well as optical constants of the surface layer can be determined if the surface and bulk excitations could be successfully separated from each other in a REELS spectrum. Since the reflection energy loss process takes place in a space region of the order of the inelastic mean free path, it is possible, in

principle, to apply this procedure to probe the electronic structure and physical properties of individual nanostructures with REELS.

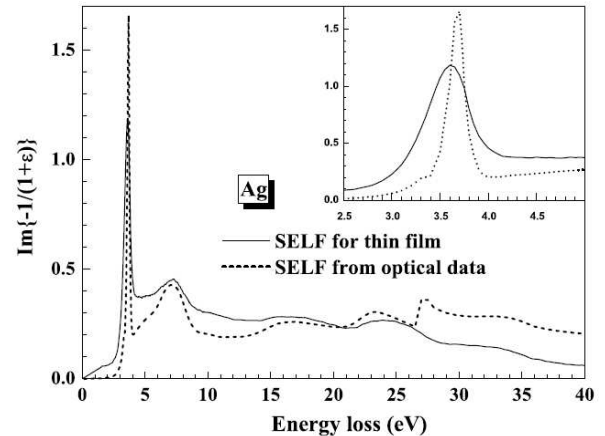


**Figure 1.** Comparison of the surface energy loss function,  $\text{Im}\{-1/(1+\epsilon)\}$ , between the present result obtained from REELS spectra of Ag thin film and that derived from the optical data [3] for the surface of bulk specimen.

### Acknowledgements

This work was supported by the National Natural Science Foundation of China (grant no. 10874160), National Basic Research Program of China (2007CB925004), 111 Project, Chinese Education Ministry and Chinese Academy of Sciences, the grant Bolyai from the Hungarian Academy of Sciences and TeT grant no. 554 CHN-28/2003.

- a) The Centre of Physical Experiments, University of Science and Technology of China, Hefei, Anhui 230026, P. R. China
- b) Department of Physics, University of Science and Technology of China, Hefei, Anhui 230026, P. R. China
- [1] Z.M. Zhang, T. Chen, Z.J. Ding, T. Tang, A. Csik, J. Tóth, and K. Tőkési, *Surf. Interface Anal.* **42** (2010) 1303.
- [2] W.S.M. Werner, *Surf. Sci.* **588** (2005) 26.
- [3] E. D. Palik, *Handbook of Optical Constants of Solids*, Academic Press, New York, 1985.
- [4] R.H. Ritchie, *Phys. Rev.* **106** (1957) 874.

## 6.5 Interaction potentials for fast atoms in front of Al surfaces probed by rainbow scattering

*P. Tiwald<sup>a)</sup>, A. Schüller<sup>b)</sup>, H. Winter<sup>b)</sup>, K. Tőkési, F. Aigner<sup>c)</sup>, S. Gräfe<sup>c)</sup>, C. Lemell<sup>c)</sup>, J. Burgdörfer<sup>c)</sup>*

Scattering of atoms off solid surfaces has developed into a versatile tool for the investigations of surface structure, of nonadiabatic dynamical processes, and of quantum diffraction effects. As early as 1929, Stern and collaborators demonstrated the wave nature of hyperthermal He atoms diffracting off alkali-halide surfaces. Thermal energy atom scattering is nowadays employed to accurately probe properties of surfaces. At higher collision energies, grazing-angle incidence of atoms allows one to probe surface potentials at relatively large distances in soft collisions.

We have presented a joint experimental and theoretical study of atom-surface potentials probed by rainbow scattering for axial surface channeling at different crystal faces and different groups of atomic projectiles (see Fig. 1). For low perpendicular energies ( $E_{\perp} \approx 10$  eV) and total kinetic energies ( $E_0 \leq 1$  keV/amu) such that the adiabatic limit of potential surfaces applies, we have shown that conventional pair potentials fail to reproduce several characteristic trends of our experimental data. *Ab initio* calculations of the combined collisional complex of atom plus Al surface are required to achieve good agreement of classical-trajectory Monte Carlo scattering simulations with experimental data. At high (parallel) projectile energies the onset of nonadiabatic effects can be observed. For atoms with large electron affinities and transient negative-ion formation, the breakdown of the adiabatic approximation following of electronic polarization sets in at energies  $E_0 \approx 1$  keV/amu while for rare gases deviations become noticeable at  $E_0 \approx 5$  keV/amu. These dynamic effects cannot be modeled by the present method, as potential calculations refer the limit of  $E_0 \rightarrow 0$ . Investigation of such dynamical effects in terms of effective surface potentials via TDDFT is an interesting topic for future investigations.

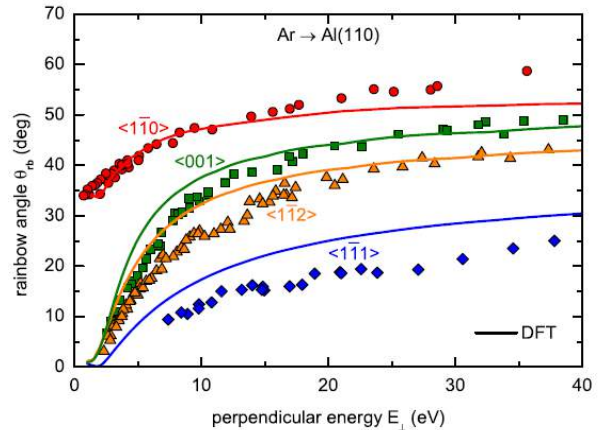


**Figure 1.** Rainbow angles of Ar atoms scattered from Al(110) along low-indexed directions. Experimental results: solid symbols; simulations using ab initio DFT potentials: solid curves.

### Acknowledgements

We thank Konrad Gärtner, Friedrich-Schiller-Universität Jena, for providing HF potentials. The assistance of S. Wethekam and K. Maass in the preparation of the experiments is gratefully acknowledged. This work was supported by DFG Proj. Wi 1336, the Austrian Fonds zur Förderung der wissenschaftlichen Forschung Projects SFB41 VICOM, No. 17449 and No. 17359, and the TeT under Grant No. AT-7/2007. One of us K.T. was also partially supported by the grant Bolyai from the Hungarian Academy of Sciences and the Hungarian National Office for Research and Technology.

a) Institute for Theoretical Physics, Vienna University of Technology, Wiedner Hauptstraße 8-10, A-1040 Vienna, Austria, EU

b) Institut für Physik, Humboldt-Universität zu Berlin, Newtonstr. 15, D-12489 Berlin-Adlershof, Germany, EU

[1] P. Tiwald, A. Schüller, H. Winter, K. Tőkési, F. Aigner, S. Gräfe, C. Lemell, and J. Burgdörfer, *Phys. Rev.* **B82** (2010) 125453.

## 7.1 Groundwater dating down to the milliliter level

*M. Molnár, R. Janovics, L. Rinyu, L. Wacker<sup>a)</sup>, H.A. Synal<sup>a)</sup>, M. Veres<sup>b)</sup>*

A novel method was developed for AMS C-14 measurement of carbonate samples using He carrier gas flushing in septum sealed test tubes. The new and powerful pretreatment method can be applied for normal size (0.1-1.0 mg C) and ultra small size (10-100  $\mu\text{g}$  C) carbonate samples. In this study we investigated the applicability of the new method for dissolved inorganic carbonate (DIC) samples for groundwater radiocarbon analysis.

The developed pretreatment method does not require vacuum during sample preparation, which significantly reduces the complexity. Reaction time and conditions can be easily controlled as carbon-dioxide content of water samples is extracted by acid addition in He atmosphere using a simple septum sealed test tube. A double needle with flow controlled He carrier gas is used for CO<sub>2</sub> transfer out from the test tube (Fig. 1).

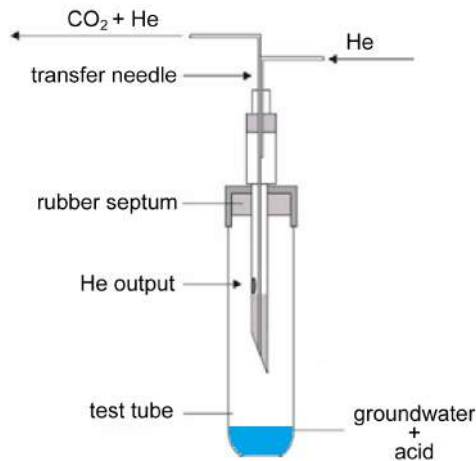


**Figure 1.** The applied CO<sub>2</sub> transfer method with He carrier gas flushing using a double needle in a septum sealed test tube.

Carbon-dioxide is trapped on a zeolite without using liquid N<sub>2</sub> freezing. The new method can be combined with an automatized graphitization system like AGE from ETHZ giving a full automatizable water preparation line for AMS graphite targets [1]. This case the needed typical sample size is between 5-12 ml of water sample.

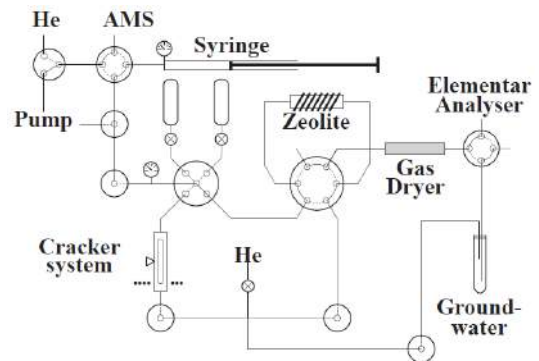


**Figure 2.** Layout of the connection of ground-water preparation line to the existing ETHZ AMS gas ion source interface.

The most powerful application of the new groundwater pretreatment method is to connect it directly to an AMS using gas ion source interface (Fig.2). With a MICADAS type AMS system we demonstrated that you can routinely measure the C-14 content of 1 ml of water sample with better than 1% precision (for a modern sample). This direct C-14 AMS measurement including sample preparation of one water sample takes about 20 minutes.

a) Laboratory of ion Beam Physics, ETHZ Zürich, Switzerland

b) Isotoptech Zrt., Debrecen, Hungary

[1] L. Wacker *et al.*, Nucl. Instr. and Meth. in Phys. Res. B **268** (2010) 931

## 7.2 Rapid graphite target preparation with sealed tube zinc reduction method for C-14 dating by MICADAS

*L. Rinyu, M. Molnár, I. Major, T. Nagy<sup>a)</sup>, Á. Kimák<sup>b)</sup>, M. Veres<sup>a)</sup>, L. Wacker<sup>c)</sup>, H.A. Synal<sup>c)</sup>*

In most cases the last step of the sample preparation for  $^{14}\text{C}$  dating by AMS is to produce graphite from the pure  $\text{CO}_2$  gas samples. Catalytic reaction is generally used to produce graphite for which stabilized temperature reaction cells are developed in certain laboratories. The properties (e.g. purity, conductivity) of the produced graphite vitally influence the quality of the AMS measurement.

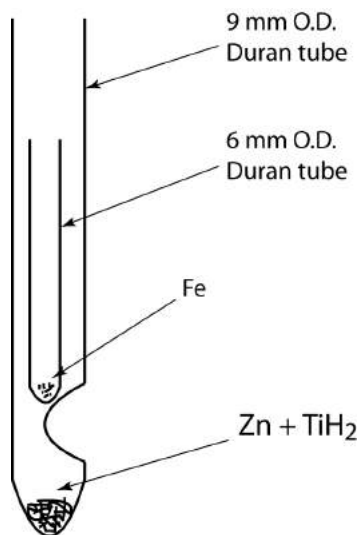


**Figure 1.** Reaction tube. 9 mm O.D. Duran reactor tube with reductants zinc (Zn) and titanium hydride ( $\text{TiH}_2$ ) in bottom and catalyst iron (Fe) in a 6 mm O.D. Duran tube sitting on a dimple from the base of outside tube.

Although the internationally validated hydrogen reduction graphitization line of Hertelendi Laboratory of ATOMKI is able to produce high quality graphite for AMS C-14 analyses, the throughput of the prepared targets is highly limited.

In this study we were looking for a rapid production and low cost graphitization method, whereby we are capable to handle numerous biomedical and environmental samples per day. The sealed tube zinc reduction method [1,2] mostly suits to these criteria (Figure 1).

We have adapted the method in ATOMKI and the goal of our study was to find out the proper conditions of the graphitization process. We have analyzed how does the graphitization time (240 - 3720 min) and the amount of zinc (30, 50 and 80 mg) and titanium hydride (7, 10 and 12 mg) reagents influence the value of the  $^{12}\text{C}$  ion current and the measured radiocarbon content of the sample and how big the caused isotope fractionation. Important task was to reach the achievable minimum background level and decrease the  $\delta^{13}\text{C}$  shift as minimal as possible.

We have also investigated the reproducibility of graphitization process and examined the radiocarbon content of graphite targets made of oxalic acid standard (NIST-SRM-4990c).

All of the graphite targets were prepared in ATOMKI laboratory and the AMS measurements were carried out on the MICADAS type accelerator mass spectrometer, developed and hosted in ETHZ, Zürich.

The amount of  $\text{TiH}_2$  we have examined does not have any kind of influence on the important features of the produced graphite. On the other hand the smaller volume of the zinc decreased the ion current and increased the  $\delta^{13}\text{C}$  shifts of the sample. We have also observed that higher volume of the zinc increased the stability of the graphite target.

Further investigations are needed to determine the deeper relationships between the reagents and the quality of the produced graphite targets.

a) Isotoptech Zrt., Debrecen, Hungary

b) University of Debrecen, Debrecen, Hungary

c) Laboratory of ion Beam Physics, ETHZ Zürich, Switzerland

[1] J.S. Vogel, Radiocarbon **34** (1992) 344-350.

[2] X. Xu *et al.*, Nucl. Instr. And Meth. In Phys. Res. B **259** (2007) 320-329.

### 7.3 Investigation of radioisotopes in different organisms around Paks NPP

R. Janovics, Á. Bihari, Z. Major, L. Palcsu, L. Papp, T. Bujtás<sup>a)</sup>, M. Veres<sup>b)</sup>

The Paks Nuclear Power Plant is a pressurised water reactor, therefore, it requires a large amount of cooling water. Cooling water is pumped from the Danube, and used water is also discharged back to the river through the warm-water channel. In the study Danube water and various aquatic organisms (a snail, *Viviparus Acerosus*, a mussel *Unio Tumidus*, a predatory fish *Stizostedion lucioperca* and a non-predatory fish *Leuciscus idus*) were collected upstream and downstream of the inlet of the channel. After freeze-drying both from the interstitial water and the dry matter of the aquatic organisms collected, tritium measurements were performed by the T-<sup>3</sup>He method to gain information about the ratio of the tritium concentration of the organically bound and the not-bound hydrogen, as well. The activity of the organically bound tritium reflects the mean activity of the environment of the organism, while the tritium activity of the interstitial water shows the actual activity of the aquatic environment [1,2]. The activity of gamma emitters in the dry matter was also measured by gamma spectrometry. In case of the mussel and snail samples gamma spectrometry measurements were performed separately from the calciferous skeleton and the tissues. Besides the aquatic organisms, soil and plant samples (Scots Pine *Pinus sylvestris*, Common Milkweed *Asclepias syriaca L.*, giant goldenrod *Solidago gigantea*) were collected in the vicinity of the nuclear power plant and in a background site, as well. These samples were analysed by

gamma spectrometry and for tritium concentration, and the results were compared with a background site. On the basis of the gamma spectrometry results significant amount of artificial gamma emitter isotopes do not get to the Danube through the warm-water channel. Only <sup>60</sup>Co occurred in certain mussel, snail and sludge in a measurable activity concentration, however, it is not of power plant origin, as it was present even in the background samples. The tritium activity concentration of the interstitial water of the aquatic organisms follows that of the surrounding water. Downstream of the inlet of the warm-water channel a slight increase in the tritium activity concentration of the Danube can be observed compared to the background values. The determination of the tritium organically bound in the interstitial water is the aim of our current research. In the soil and plant samples only gamma emitters of natural origin were identified.

a) Paks Nuclear Power Plant Co, Paks, Hungary

b) Isotoptech Ltd., Debrecen, Hungary

[1] J.-Baptiste *et al.*, The distribution of tritium in the terrestrial and aquatic environments of the Creys-Malville nuclear power plant (2002-2005). *Journal of Environ Radioact.* 2007 **94**(2) : 107-18.

[2] Stephan A. Ryba *et al.*, Effects of sample preparation on the measurement of organic carbon, hydrogen, nitrogen, sulfur, and oxygen concentrations in marine sediments. *Chemosphere* **48** (2002) 139-147

## 7.4 Development of procedure for the separation of $^{107}\text{Pd}$ from L/ILW radioactive waste material produced by the Hungarian NPP

*Á. Bihari, Z. Szűcs, M. Mogyorósi, and B. Kovács<sup>a)</sup>*

Palladium-107 is a beta emitter produced by the fission of  $^{235}\text{U}$  (yield: 0.16 %) and  $^{239}\text{Pu}$  (yield: 3.3 %). It is one of the radionuclides of interest in the management of nuclear waste repositories because of its long half life ( $6.5 \times 10^6$  y) [1]. Typical global activity of low- and intermediate level (L/ILW) liquid wastes of Paks NPP meant to deposition is in the range of  $10^5 - 10^7$  Bq L<sup>-1</sup>. In case of nuclear fuel with half as much  $^{239}\text{Pu}$  content as  $^{235}\text{U}$ , the yield of  $^{107}\text{Pd}$  is one-fifth that of  $^{99}\text{Tc}$ . Measurement of  $^{107}\text{Pd}$  is particularly difficult due to its low estimated activity concentration (about  $10^{-1}$  Bq L<sup>-1</sup>) in such waste matrixes. One of the main difficulty of the development of a separation procedure is that  $^{107}\text{Pd}$  is not available as a standard either in liquid or solid form. As a consequence, a “step by step” methodology was implemented to achieve the validation of the protocol where stable Pd and  $^{110m}\text{Ag}$  (gamma emitter) were

used as carrier and substitutive tracer, respectively, to estimate the chemical yields of the different steps.

We assume that palladium - similarly to other noble metals, including silver - is present in the samples in solid or colloidal form due to its strongly basic matrix. This way the first step of the separation procedure (after the addition of Pd and Ag carriers) is the filtration of 200 ml sample. (The liquid phase can be used for the parallel separation of  $^{79}\text{Se}$  [2]). The solid phase has been subsequently cleaned with 1M HCl and weak HNO<sub>3</sub> solutions. As Table 1 shows, these solutions removed significant amounts of interfering radionuclides while the loss in  $^{110m}\text{Ag}$  activity is  $\leq 10$  %. Applying hot *aqua regia* on the cleaned solid phase the noble metals (including palladium in the form of PdCl<sub>2</sub>) have been dissolved while the non-dissolveable parts have been removed by filtration (see last column of Table 1).

**Table 1.** Changes in the isotopic composition of sample 1151T2009 (filtration, cleaning and dissolution).

Isotope	Original sample (Bq)*	Solid phase (Bq)*	Cleaning solution 1+2 of solid phase (Bq)*	<i>Aqua regia</i> solution of solid phase (Bq)*	<i>Aqua regia</i> non-dissolvable parts (Bq)*
$^{94}\text{Nb}$	$(1.86 \pm 0.09) \times 10^2$	$(1.83 \pm 0.07) \times 10^2$	$(1.07 \pm 0.04) \times 10^2$	$(4.51 \pm 0.16) \times 10^1$	$(3.77 \pm 0.09) \times 10^1$
$^{106}\text{Ru}$	$(9.59 \pm 0.70) \times 10^4$	$(7.68 \pm 0.45) \times 10^4$	$(3.30 \pm 0.19) \times 10^4$	$(2.58 \pm 0.04) \times 10^4$	$(1.26 \pm 0.02) \times 10^4$
$^{125}\text{Sb}$	$(4.75 \pm 0.26) \times 10^3$	$(4.63 \pm 0.20) \times 10^3$	$(3.20 \pm 0.14) \times 10^3$	$(1.28 \pm 0.02) \times 10^3$	$(3.66 \pm 0.05) \times 10^2$
$^{134}\text{Cs}$	$(8.96 \pm 0.51) \times 10^3$	$(4.33 \pm 0.17) \times 10^3$	$(2.70 \pm 0.12) \times 10^3$	$(7.72 \pm 0.09) \times 10^2$	$< 5.56 \times 10^0$
$^{137}\text{Cs}$	$(5.72 \pm 0.30) \times 10^4$	$(2.47 \pm 0.10) \times 10^4$	$(1.71 \pm 0.07) \times 10^4$	$(5.55 \pm 0.10) \times 10^3$	$(3.51 \pm 0.12) \times 10^1$
$^{144}\text{Ce}$	$(2.41 \pm 0.15) \times 10^3$	$(2.38 \pm 0.11) \times 10^3$	$(2.09 \pm 0.10) \times 10^3$	$(4.84 \pm 0.32) \times 10^2$	$(2.43 \pm 0.61) \times 10^1$
$^{154}\text{Eu}$	$(5.26 \pm 0.22) \times 10^2$	$(5.23 \pm 0.17) \times 10^2$	$(4.89 \pm 0.16) \times 10^2$	$(9.89 \pm 0.26) \times 10^1$	$< 2.68 \times 10^0$
$^{155}\text{Eu}$	$(2.21 \pm 0.10) \times 10^2$	$(2.17 \pm 0.08) \times 10^2$	$(2.23 \pm 0.08) \times 10^2$	$(4.69 \pm 0.21) \times 10^1$	$(4.57 \pm 0.68) \times 10^0$
$^{54}\text{Mn}$	$(1.50 \pm 0.07) \times 10^3$	$(1.26 \pm 0.05) \times 10^3$	$(1.09 \pm 0.04) \times 10^3$	$(2.75 \pm 0.08) \times 10^2$	$< 1.11 \times 10^1$
$^{60}\text{Co}$	$(2.47 \pm 0.15) \times 10^4$	$(1.83 \pm 0.09) \times 10^4$	$(1.07 \pm 0.05) \times 10^4$	$(5.01 \pm 0.05) \times 10^3$	$(1.18 \pm 0.02) \times 10^3$
$^{108m}\text{Ag}$	$(2.50 \pm 0.41) \times 10^2$	$(2.47 \pm 0.32) \times 10^2$	$(1.63 \pm 0.21) \times 10^1$	$(1.90 \pm 0.03) \times 10^2$	$< 3.28 \times 10^0$
$^{110m}\text{Ag}$	$(2.12 \pm 0.23) \times 10^3$	$(2.11 \pm 0.18) \times 10^3$	$(1.98 \pm 0.17) \times 10^2$	$(1.85 \pm 0.02) \times 10^3$	$< 1.23 \times 10^1$
$^{241}\text{Am}$	$(8.77 \pm 0.43) \times 10^2$	$(8.64 \pm 0.33) \times 10^2$	$(7.00 \pm 0.27) \times 10^2$	$(1.62 \pm 0.06) \times 10^2$	$< 3.57 \times 10^0$

\* Decay-corrected to 2009.01.07.

The *aqua regia* solution was slowly evaporated to dryness and the evaporation residual has been dissolved in 1:1 HCl solution. Silver has formed AgCl<sub>2</sub> precipitation which was removed by filtration with 95% efficiency (see Table 2). In the 1:1 HCl solution, palladium is present as PdCl<sub>4</sub><sup>-2</sup> [1] which enables the reduction of the activity of cationic compounds with cation exchange resins. The total reduction of the interfering isotopes compared to the original sample is shown in the last column of

Table 2. Procedure for the selective removal of anionic interfering radionuclides (esp. <sup>106</sup>Ru and <sup>125</sup>Sb) is under development.

After the removal of all interfering radionuclides, the solution enriched for <sup>107</sup>Pd can possibly be measured with ICP-MS analytical technique. Based on background measurement and interpolated efficiency curve (from <sup>105</sup>Pd, <sup>106</sup>Pd and <sup>108</sup>Pd), the detection limit of <sup>107</sup>Pd is estimated to be 5 ppt which equals about 0.2 Bq kg<sup>-1</sup>.

**Table 2.** Changes in the isotopic composition of sample 1151T2009 (dissolution, filtration and cation exchange).

Isotope	1:1 HCl solution of <i>aqua regia</i> evaporation residual (Bq)*	1:1 HCl non-dissolvable parts (Bq)*	After AG50W-X12 cation exchange resin column (Bq)*	Reduction in activity compared to the original sample (%)
<sup>94</sup> Nb	$(3.62 \pm 0.27) \times 10^1$	$(1.05 \pm 0.21) \times 10^0$	$(1.24 \pm 0.27) \times 10^1$	93.3
<sup>106</sup> Ru	$(2.42 \pm 0.04) \times 10^4$	$< 3.75 \times 10^1$	$(2.23 \pm 0.03) \times 10^4$	76.8
<sup>125</sup> Sb	$(1.22 \pm 0.02) \times 10^3$	$< 6.49 \times 10^0$	$(9.34 \pm 0.09) \times 10^2$	80.3
<sup>134</sup> Cs	$(7.62 \pm 0.11) \times 10^2$	$< 1.95 \times 10^0$	$(4.21 \pm 0.04) \times 10^2$	89.6
<sup>137</sup> Cs	$(5.39 \pm 0.08) \times 10^3$	$(1.25 \pm 0.40) \times 10^0$	$(2.54 \pm 0.04) \times 10^3$	95.6
<sup>144</sup> Ce	$(5.00 \pm 0.48) \times 10^2$	$(3.30 \pm 0.42) \times 10^1$	$< 1.67 \times 10^1$	>99.3
<sup>154</sup> Eu	$(9.50 \pm 0.38) \times 10^1$	$< 1.13 \times 10^0$	$< 1.71 \times 10^0$	>99.7
<sup>155</sup> Eu	$(4.04 \pm 0.31) \times 10^1$	$< 1.08 \times 10^0$	$< 1.99 \times 10^0$	>99.1
<sup>54</sup> Mn	$(2.59 \pm 0.13) \times 10^2$	$< 2.86 \times 10^0$	$(1.74 \pm 0.03) \times 10^2$	88.4
<sup>60</sup> Co	$(4.85 \pm 0.04) \times 10^3$	$< 1.76 \times 10^0$	$(3.41 \pm 0.02) \times 10^3$	86.2
<sup>108m</sup> Ag	$< 8.25 \times 10^0$	$(1.97 \pm 0.03) \times 10^2$	$(8.89 \pm 0.42) \times 10^0$	96.4
<sup>110m</sup> Ag	$< 7.85 \times 10^1$	$(1.79 \pm 0.01) \times 10^3$	$(9.30 \pm 0.16) \times 10^1$	95.6
<sup>241</sup> Am	$(1.48 \pm 0.05) \times 10^2$	$< 1.33 \times 10^0$	$(2.04 \pm 0.39) \times 10^0$	99.8

\* Decay-corrected to 2009.01.07.

a) Institute of Food Science, Quality Assurance and Microbiology Centre for Agricultural Sciences and Engineering, University of Debrecen

[1] Hogdahl, O. T., 1961. The Radiochemistry of Palladium. National Academy of Sciences, National Research Council, NUCLEAR SCIENCE SERIES, NAS-NS 3052.

[2] Bihari, Á., Mogyorósi, M., Szűcs, Z., Kovács, B., 2010. Separation of <sup>79</sup>Se from L/ILW radioactive waste material produced by the Hungarian NPP. ATOMKI Annual Report 2009, 64.

## 7.5 Advancing the use of noble gases in fluid inclusions of speleothems as a palaeoclimate proxy: method and standardization

L. Papp, L. Palcsu, Z. Major, É. Svingor

Continental carbonates are essential archives of the past geological and climatological occurrences. Recently, fluid inclusions of carbonates have got into focus of palaeoclimate research.

A new approach using temperature-dependent gas solubilities might be a way that uses only physical laws, e.g. the Henry's law of solubility and gas partitioning models. The so-called noble gas temperature (NGT) can be calculated from the measured noble gas concentrations [1,2].

This report describes how our first advancing steps towards obtaining NGT's from fluid inclusions and tiny water amounts have been preformed. To extract the water inclusions from the carbonate matrix, the most suitable treatment is to crush the carbonate under vacuum. The water released from the inclusions is then collected in a cold finger by freezing. The amount of the liberated water is measured via its vapour pressure in a certain volume (Fig. 1).

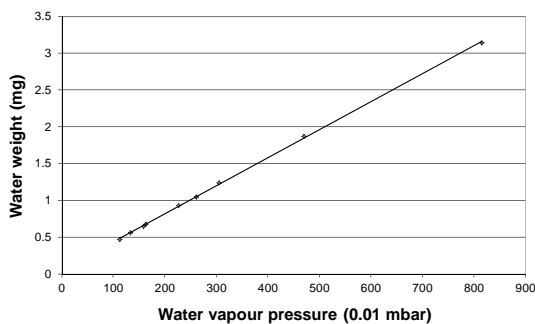


**Figure 1.** Calibration curve for water determination via vapour pressure

The liberated dissolved noble gases which were in the fluid inclusions are separated by a cryo system, and then admitted into the static mode noble gas mass spectrometer sequentially. The calibration of the noble gas mass spectrometric measurements is performed by means of well known air aliquots. To check the reliability of the whole measurement procedure standard water samples have to be mea-

sured. As for standard samples, first we have prepared air equilibrated water (AEW) in conditioned circumstances. We fill copper capillaries with AEW. Having completed the copper capillary assemblage, the AEW is letting flow through the capillary (Fig. 2).

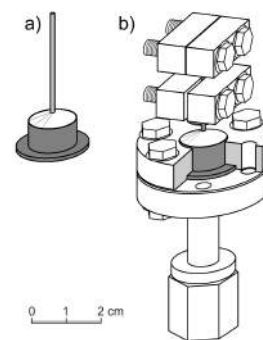


**Figure 2.** a) Copper capillary glued to a copper block, b) capillary assemblage with a CF-flange and a Swagelok VCR fitting

The error of such a water determination is less than 1 % in case of 1  $\mu$ l of liquid water (Fig. 1) that allows us to determine accurate noble gas concentrations. The reproducibility of  $^{40}\text{Ar}$  measurements is better than 0.6 %, while those of neon, krypton and xenon isotopes are 0.6-1.6 %, 0.9-2.2 % and 0.8-2.0 %, respectively. Theoretically, these precisions for noble gas concentrations obtained from sample measurements allow us to determine noble gas temperatures by an uncertainty of below 1  $^{\circ}\text{C}$ . In the measurement run we have performed six measurements. Four of these eight AEW samples show excess noble gases mainly in the heavier ones. Pre-treatment of the capillaries by helium flushing and heating have improved the AEW sample preparation. The measurements of other two AEW samples have given reasonable noble gas concentrations very close to the expected ones.

[1] Kluge T. *et al.* Earth & Planet. Sci. Lett. **269** (2008) 407.

[2] Scheidegger Y. *et al.* Chem. Geol. **272** (2010) 31.

## 7.6 A 9-year old record and analysis of stable isotope ratios of precipitation in Debrecen

G. Vodila, L. Palcsu, I. Futó, Zs. Szántó<sup>a)</sup>

The variability of the isotopic composition of precipitation is primarily driven by global trends, however, additional variability of several per mil is present at regional scales [1] creating the need to investigate  $\delta^{18}\text{O}$  and  $\delta\text{D}$  values of precipitation. In Debrecen the direct, event based measurement of the isotopic composition of the precipitation and the monitoring of the meteorological parameters has been being performed since January 2001.

The results showed that regional/local-scale processes control the isotopic composition of the local precipitation (both oxygen and hydrogen). Although temperature is an important parameter controlling year-to-year variability of stable isotopes in the precipitation, the interpretation of an isotope record solely with an isotope thermometer is incorrect. Based on our data it can be stated that  $\delta^{18}\text{O}$  values are more sensitive to indicate the extremities in the weather than  $\delta\text{D}$  values.

The local meteoric water line (LMWL) differs from the global meteoric water line [2] (GMWL) of  $\delta^2\text{H} = 8\delta^{18}\text{O} + 10$  in both slope and intercept showing the effect of secondary evaporation during the descent of precipitation from the cloud base to the ground (Figure 1). Differences in the slopes and intercepts of the single years' LMWLs are also a useful tool to monitor the given year regarding mainly secondary evaporation. A very important result of our research was that due to the significant difference between the data of the other continental stations and Debrecen, extrapolation of the data of the surrounding stations to Debrecen would be misleading.

Deuterium excess (d-excess;  $\delta^2\text{H} - 8\delta^{18}\text{O}$ ) is an isotopic parameter relevant for investigations on climatology concerning the identification of the air moisture source regions and thus the characterization of the air mass circulation patterns, and it seems to be an effective way to see the effects and extent of secondary evaporation in precipitation (Figure 2).

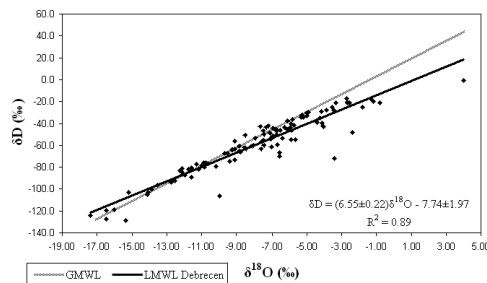


**Figure 1.** The LMWL of Debrecen shows a good correlation regarding  $\delta^2\text{H}$  and  $\delta^{18}\text{O}$  values of the precipitation based on the data of amount weighted monthly samples.

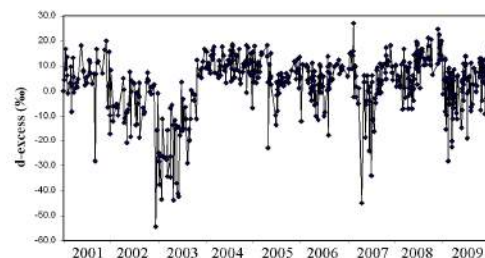


**Figure 2.** Event based deuterium excess values

Isotopic signatures ( $\delta^{18}\text{O}$ ,  $\delta^2\text{H}$ , d-excess, LMWL) of the three extreme years (2002, 2003 and 2007) deviate remarkably from the ones of the other six years. Depending of the regularity of extreme years it should be thought over whether the data of extreme years are to be omitted or not from the interpretation of the LMWL based on short datasets.

Observational data have displayed a good correlation of  $\delta^{18}\text{O}$  with the air temperature ( $\delta^{18}\text{O} = (0.32 \pm 0.03)T - 11.19 \pm 0.43$ ), validating the temporal (but not the spatial) isotope approach. The  $\delta^{18}\text{O}$ -T function has similar slope than reported for other continental stations, and is in the range characteristic for this climate.

a) University of Debrecen, Debrecen, Hungary

[1] G.J. Bowen, B. Wilkinson, *Geology* **30**, 315 (2002)

[2] H. Craig, *Science* **133**, 1702 (1961)

## 7.7 Investigation of indoor aerosols at educational institutions in Debrecen, Hungary

Z. Szoboszlai, E. Furu, A. Angyal, Z. Szikszai and Zs. Kertész

It is well known that the exposure to particulate matter (PM) during school-age, when children are in their growing stage, can have lifelong adverse effects on their health. Because of these facts it is important to analyse PM in such places where children stay in a limited space during long-term periods. An average schoolchild spends at least six to eight hours a day in an indoor environment. Thus the more detailed knowledge of the air parameters of scholastic environments is particularly important.

In this study our aim was to measure those parameters which might help the better estimation of the PM impact on the health of the children/students and teachers in autumn-winter season in different educational institutions in the centre of Debrecen, Hungary. Two schools (a primary and a secondary grammar) and a kindergarten were selected for the study. Coarse and fine mass concentrations, elemental composition and mass size distributions were determined in selected microenvironments. These were different classrooms, school yards, gymnasiums, a computer lab, a chemical lab and a so-called salt-room. The elemental composition (for  $Z \geq 13$ ) was determined by PIXE and the mass concentrations of particulate matter were determined by gravimetry. In the case of the kindergarten two cascade impactors were also deployed to provide size distribution.

vide size distribution.

In all cases the coarse concentrations of PM were higher inside the educational buildings than in the outer air, and every case the  $PM_{10}$  concentration exceeded the EU air quality standard (Fig. 1). The highest values were measured in the gymnasiums which could be explained by the activities. We observed increased PM concentrations in the lower educational levels. The fine concentration inside the buildings did not differ significantly from the air outside. We did not detect big differences between the indoor and outdoor elemental compositions, but found differences in the elemental concentrations.

Based on the mass size distribution values significant differences were found between the salt and the gymnastic room. In the salt room, where children were allowed only to sit, lower concentration values and smaller particle sizes were detected than in the other room where children did exercises and gymnastics. In the light of these results further aerosol characterization studies is needed to provide more accurate information about the sources and the possible health effects of ambient aerosol in educational environments.

### Acknowledgements

This work was supported by the Hungarian Research Fund OTKA and the EGT Norwegian Financial Mechanism Programme (contract no. NNF78829) and the János Bolyai Research Scholarship of the HAS.

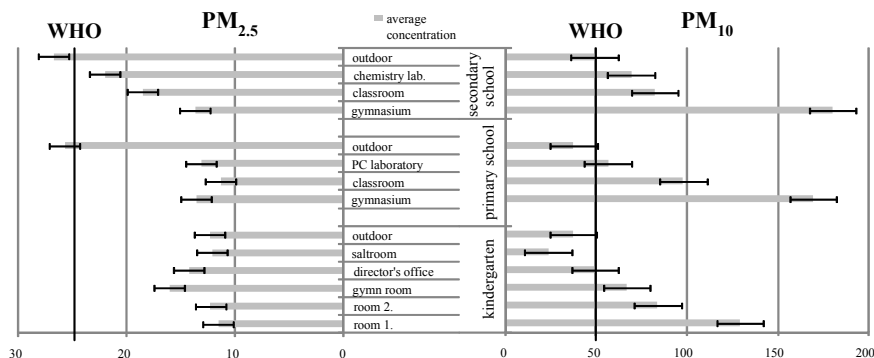


Figure 1.  $PM_{2.5}$  and  $PM_{10}$  average concentrations in  $\mu\text{g}/\text{m}^3$  at the three institutes.

## 7.8 Study of emission episodes of urban aerosol by ion beam analytical techniques

A. Angyal, Zs. Kertész, Z. Szikszai, Z. Szoboszlai, E. Furu, L. Csedreki, L. Daróczy<sup>a)</sup>

Aerosol pollution has impact on the climate and on human health. Thus investigation of atmospheric aerosol is important in urban environment such as Debrecen. One of the main goals of our study was to define the sources of the particles.

The hourly evolution of atmospheric aerosol concentration was used to identify sources of fine (aerodynamic diameter  $< 2,5 \mu\text{m}$ ) and coarse ( $10 \mu\text{m} \geq$  aerodynamic diameter  $\geq 2,5 \mu\text{m}$ ) urban particulate matter in Debrecen. In both size fractions sources were found which were characterized by high heavy metal content. In this study we provide accurate information of the sources of coarse mode heavy metals by using nuclear and scanning electron microscopy.

Single particle analysis of chosen samples was carried out on the ATOMKI Scanning Nuclear Microprobe Facility. Elemental composition for  $Z \geq 6$ , morphology and size of around 500 coarse mode particles were determined by Scanning Transmission Ion Microscopy, light-element PIXE and PIXE analytical methods. Furthermore Scanning Electron Microscopy (SEM) was used to investigate particles morphology.

The main components of the particles were Na, K, Ca, S, P and Fe with traces of Ti, V, Cr, Mn, Ni, Cu, Zn, Co, Pb. S-rich particles were enriched in one or more of the following elements: Na, Ca, K, Fe, Zn. Trace metals (Mn, Cu, Zn, Cr) occurred together Fe supposedly originated from industrial emission or traffic. P appeared in the Ca-rich particles. Particles with high concentration of Ni were rich in V, Fe and S. Thus this source was identified as residual combustion. V-rich particles occurred together with Fe, Mn and Cr. Their possible source was industry. Pb was attached to Ca, Fe, S containing particles.

As result of the SEM study the following particle types (Figure 1.) were identified: semi-transparent material (S-K-rich, S-Zn-rich, P-Ca-rich), spherical (FeO, Fe-Ni-Cr-V-rich), cubic (KCl, CaCl) and crystalline (S-Ca-rich).

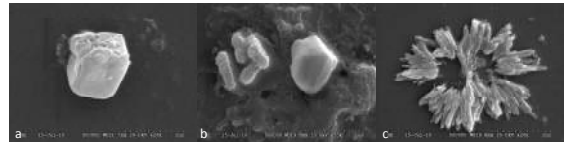


**Figure 1.** Particle type was determined by SEM a. cubic (Ca-Cl-rich) b. ZnO-rich (left), Zn-S-rich (right), c. crystalline (S-Ca-rich).

The main sources of atmospheric aerosol in Debrecen were biomass burning (S-K-rich particles), which in our case is domestic heating in winter and field burning in summer. Furthermore trace metals originated from traffic or industrial emission. Zn compounds could be abrasion products of brake and tire wear of cars. Ni and V originated from oil combustion. Pb was products of winter tyre abrasion, industrial emission or waste burning. Origin of salts was sea-salt, fertilizer or construction.

Single particle analysis in the combination of ion beam analytical methods and electron microscopy proved to be a powerful tool in the characterization of atmospheric aerosol particles in the micrometer size range.

### Acknowledgement

This work [1] was supported by the Hungarian Research Fund OTKA and the EGT Norwegian Financial Mechanism Programme (contract no. NNF78829) and the János Bolyai Research Scholarship of the Hungarian Academy of Sciences.

a) Department of Solid State Physics, University of Debrecen

[1] A. Angyal *et al.* Nucl. Instr. and Meth. B (2011)  
DOI: <http://dx.doi.org/10.1016/j.nimb.2011.02.057>

## 7.9 Study of the sap flow and related quantities of oak trees in field experiments

P. Kanalas <sup>a)</sup>, A. Fenyvesi, I. Ander, V. Oláh <sup>a)</sup>, E. Szöllősi <sup>a)</sup>, I. Mészáros <sup>\*a)</sup>

Climatology model calculations predict a drift of the transition zone between the wooden steppe and the forest regions in the Carpathian Basin in the next decades [1]. Climazonal forest communities in the mountainous regions will be affected severely. The sessile oak - Austrian oak forest of the Long Term Ecological Research (LTER) area of the Síkfőkút Project (Bükk Mountains, NE Hungary) is in the transition zone. Responses of oak tree species and their hybrids to climate change are studied there. In 2010 sap flow densities and changes of stem diameters were measured as a function of time for 20 trees. Photosynthetic photon flux density (PPFD), atmospheric pressure, temperature and relative humidity and vapour pressure deficit (VPD) of air, precipitation and soil moisture were recorded, too. The measured time series covered the whole unusually rainy vegetation season. The total amount of precipitation in the vegetation season was 22% more than the yearly average for the area.

For a *Quercus petraea-dalechampii* hybrid tree (ID: C141), as an example of the results, Figure 1 shows the values measured before and after a significant rainfall in July. The increase of soil moisture and refill of the water reser-

voirs of the trunks were very quick. The daily maxima of sap flow densities increased on the subsequent sunny days. Typically in the 12:00-15:00 (GMT + 2:00) periods the rate of water loss via transpiration exceeded water uptake leading to contraction of the trunks. During sunny days without rain the water consumption of the trees lead to decreasing soil moisture and reduced daily maxima of sap flow. The sap flow and water loss changed in correlation with the difference of the water potential of air and soil. Similar changes were observed for the other trees. These show that hydraulic conductances of the trees were mainly under well functioning stomatal control and there was no chance of drought stress.

### Acknowledgements

This work was supported by the Hungarian Research Found (OTKA K68397).

\* Corresponding author,  
e-mail: immeszaros@puma.unideb.hu

a) Dept. of Botany, Faculty of Science and Technology, Univ. of Debrecen, Egyetem tér 1., H-4032, Hungary.

[1] Mátyás, Cs., Czimer, K., In: Mátyás, Cs., Víg, P. (Eds.), Erdő és klíma IV., Sopron, NyME, 2004, pp. 35-44 (in Hungarian).

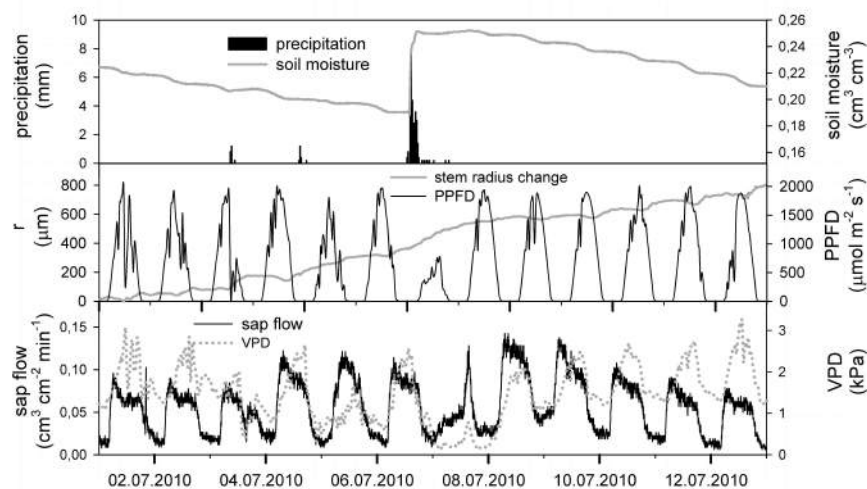


**Figure 1.** Time series of the measurements for the C141 *Quercus petraea-dalechampii* hybrid oak tree.

## 8.1 Status Report on the Accelerators Operation

*S. Biri, Z. Kormány, I. Berzi, I. Ander, Z. Gácsi, M. Hunyadi and R. Rácz*

2010 was the first full year in the short history of the Accelerator Center which was established in July 2009 [1]. After one year of experience it can be concluded that the new center works satisfactorily both from technical and human point of views. During the year all our main accelerators operated as scheduled, safely and without major or long breakdowns.

The utilization rate of the accelerators was diverse. The ECR ion source produced an average year (400 hour beamtime) while a remarkable demand was experienced for the cyclotron and the VdG-5 machines, resulted in record yearly beamtimes (around 2000 hours each) for both machines in the last 5 year. The VdG-1 accelerator however was used only for a short test in 2010 and the installation of the tandetron is still under progress. The isotope separator, as ion beam accelerator was utilized only for a few hours in 2010, since the research and development in this lab focused mainly on nano-particle synthesis. Nevertheless this special low-energy ion beam facility is available for research in surface physics requiring special deposition techniques, and sub-surface implantation, especially for isotope tracing studies. The Accelerator Center was one of the locations of a special half-animated scientific-entertaining film made in Atomki in 2010. Some of our facilities, target rooms, beamlines and ion source plasmas were shown in the film which was presented for different audiences throughout the year and finally broadcasted by the “m1” channel of the Hungarian Television [2]. In the next sub-chapters the 2010 operation and development details of the cyclotron, VdG-5 and ECR accelerators are summarized.

### Cyclotron operation

The operation of the cyclotron was concentrated to the usual 9 months because January, July and August were reserved for maintenance and holidays. The overall working time of the accelerator was 2741 hours; the time used for

systematic maintenance was 356 hours. The breakdown periods amounted only to 20 hours last year. So the cyclotron was available for users 2365 hours.

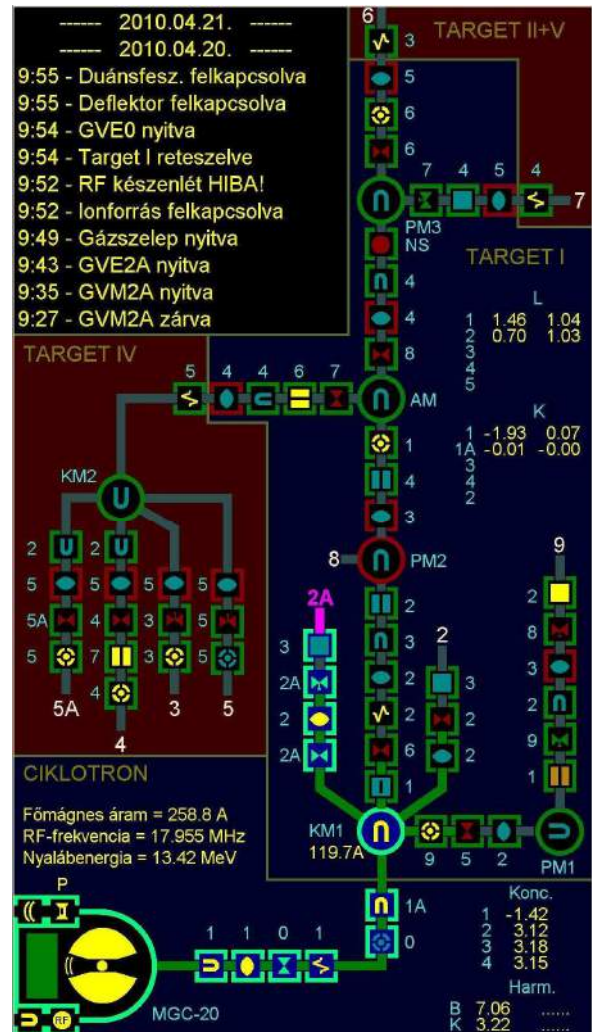


**Figure 1.** Typical screen output of the new cyclotron and transport system status display.

The distribution of the used beamtime is summarized in Table 1. A new status display has been developed for the cyclotron and the beam transport system. A wide-screen full HD TV was installed into the control rack, displaying the schematic layout of the accelerator and the beam lines. The actual status of the sys-

tem components is read from the main control program of the accelerator via interprocess communication (DDE) and is reflected on the status screen by different colors (Fig. 1). Important setting values like coil currents, RF-frequency, beam energy etc. are also displayed on screen in real time.

The project of building new power supplies for the low-current magnet coils of the cyclotron and the beam transport system has been continued. Based on the successful development of the prototype circuit, 10 new units have been constructed and installed during the shutdown periods in 2010. By now all the quadrupole lenses and half of the steering magnets are equipped with new power supplies. The remaining 5 units for the steering magnets are expected to be replaced during the winter shutdown in 2011.

**Table 1.** Time distribution of the cyclotron usage between different research groups.

Projects	Hours	%
Nuclear spectroscopy	348	18.4
Nuclear astrophysics	892	47.3
Radiation tolerance test	138	7.3
Medical isotope production	256	13.6
Thin layer activation (TLA)	252	13.4
<b>Total</b>	<b>1886</b>	<b>100</b>

### VdG electrostatic accelerators

At the VdG-5 machine we had more intense beam requirements than the preceding years: it was running 2054 hours in 2010. Due to the age of the accelerator and the increased operating hours, we had to open the accelerator tank 9 times during the year. We had three planned weekly maintenance work in January, April and September. In addition we had small machine failures throughout the year which required two or three days maintenance work each. With the 5 MV Van de Graff accelerator mainly (94%) proton particles were accelerated. There was little need (6%) for  $^4\text{He}^+$  particles. The beam time was distributed among different research subjects as shown in Table 2.

**Table 2.** Time distribution among different research activities at VdG-5.

Field	Hours	%
Nuclear physics	334	16.2
Nuclear astrophysics	72	3.5
Analytical studies	1425	69.4
Micromachining	170	8.3
Machine test	53	2.6
<b>Total</b>	<b>2054</b>	<b>100</b>

The development of several small-scale digital control systems started in the VdG-5 control room. A PC-based vacuum measurement software was written for the Pfeiffer Maxi-Gauge vacuum measurement and control units. A high-speed (500kbit/s) CAN-bus was built for controlling the electrostatic and magnetic quadrupole power supplies and for collecting information about the system. In 2010 the VdG-1 machine was working for only 74 hours. During February and March there were some test measurements with proton beam for a time-of-flight electron-spectrometer.

### ECR ion source

Table 3 shows the beamtime the ECRIS supplied in 2010 for users. Similarly to last years the “Hours” in the table mean the time when a plasma was generated in the ECRIS chamber. In most cases a positive or negative ion beam was extracted, of course, from this plasma.

In this year majority of the experiments and tests required very low beam energy provided by very low (usually several hundreds of volts) extraction voltage. As an important development, a very careful optical adjustment of the plasma chamber, extraction optics and beamline system (including the exchange of the bending magnet chamber from “C”-shape into an “X”-shape) was performed. A new Nd-FeB hexapole permanent magnet assembly was purchased and installed because the 15 years old magnet already partly lost its radial magnetic field strength during the years (the field strength decreased from 1.1 Tesla down to 0.7 Tesla and this decreasing accelerated in the past 2-3 years). The magnetic field of the new

hexapole (having the same geometry and structure as the old one) was 1.2 Tesla. The first beam tests with the new radial trap gave excellent results: we could reach or exceed our ever-obtained record highly charged beam intensities within a couple of days test time. Unfortunately, after 2-month of testing and normal, regular operation a small geometrical problem was discovered due to the weak gluing between the magnetic segments. The hexapole had to be sent back to the manufacturer for a guarantee repair. We expect to get it back around spring 2011. Close to the end of the year a

short test was performed to produce negative ion beams from the ECRIS. The experiment was successful: high intensity negative  $H^-$ ,  $O^-$ ,  $OH^-$  and  $C_{60}^-$  ion beams were easily obtained.

As mentioned in the introduction, the ECR Laboratory was one of the main locations of a film titled “Elementary dream” [2]. The ECR staff also got an opportunity taking part as actors in the film and the colorful star-shape ECR plasmas obtained from different gases became one of the highlights of that new style scientific-entertainment type movie.

**Table 3.** Positive and negative ion beams delivered by the ECRIS in 2010. The total energy of the beams is the product of the charge and the extraction voltage. DE: University of Debrecen, IEP: Institute of Experimental Physics, FD: Faculty of Dentistry, DAP: Division of Atomic Physics, ECR: ECR Group.

Research topic	User	Ion species	Extraction voltage(KV)	Hours	%
Ion guiding through capillaries	ATOMKI-DAP	$Ne^{7+}, Ar^{7+}$	0.4-0.9	130	32.1
Ti-coating with $C_{60}$	DE-FD, DE-IEP, ATOMKI ECR	$C_{60}^+$	0.05-0.4	80	19.8
Fullerene ( $C_{60}$ ) research	ATOMKI-ECR	$C_{60}^+, C_{60}^-$	0.3-0.5	83.5	20.6
New hexapole test	ATOMKI ECR	$O^{5+}, \dots, 7+$ $Ar^{7+}, \dots, 12+$	0.4-10	41.5	10.2
Beam development & maintenance	ATOMKI-ECR	$H^+, H^-, O^-, OH^-$ $Ar^{1+}, \dots, 16+$ $Ne^{4+}, \dots, 9+, C_{60}^+$	0.1-10	70.0	17.3
<b>Total</b>				<b>405</b>	<b>100</b>

[1] <http://www.atomki.hu/Accelerators>

[2] [http://videotar.mtv.hu/Videok/2010/11/04/17/Elemi\\_alom\\_2010\\_november\\_4\\_.aspx](http://videotar.mtv.hu/Videok/2010/11/04/17/Elemi_alom_2010_november_4_.aspx)

## 8.2 Laboratory background in an escape-suppressed germanium $\gamma$ -ray detector at a shallow underground laboratory

T. Szücs, D. Bemmerer<sup>a)</sup>, D. Degering<sup>b)</sup>, Z. Elekes, Zs. Fülöp, Gy. Gyürky, M. Köhler<sup>b)</sup>, and M. Marta<sup>a)</sup>

In many cases in nuclear astrophysics, the investigated quantity is proportional to the yield of the emitted  $\gamma$ -radiation. At relatively small energies, which occur in a stellar environment, this yield is tiny. If a study is performed close to these energies, the knowledge of the laboratory  $\gamma$ -ray background is crucial. It is important to keep the background as low as possible, to reach higher sensitivity. In this work, the effect of an active shield (veto detector), and a passive shield (underground location) on the background is shown.

For the present studies, a Clover detector [1] has been used. It is equipped with a surrounding bismuth germanate (BGO) scintillator. With anticoincidence electronics, the BGO is used as an escape-suppression veto detector. It can also act as an efficient veto against muons penetrating the germanium detector volume.

The underground site where the background measurements were performed is the Felsenkeller [2]. It is a shallow underground laboratory with 45 m thick rock cover (110 m water equivalent). As a comparison the spectra taken from [3] recorded at Laboratori Nazionali del Gran Sasso (LNGS) [4] are also shown. LNGS is a deep underground laboratory with 1400 m rock coverage (3400 m water equivalent).

For in-beam experiments, the counting rate in the high energy continuum is of paramount importance, because  $\gamma$ -rays from reactions with high  $Q$ -values can be emitted. In this region cosmic ray induced events dominate the laboratory background. On the Earth's surface and at the Felsenkeller, the main source of this background is the energy loss of penetrating muons in the germanium. Deep underground, because of the factor of  $10^6$  reduction in the muon flux, the main background sources are neutron reactions, producing high energy gammas.

In the present study, the BGO veto leads to a factor of 160 reduction in the continuum counting rates, which combined with the muon flux reduction (factor of 40) at Felsenkeller leads to a background counting rate comparable to that of LNGS. (Fig. 1.)

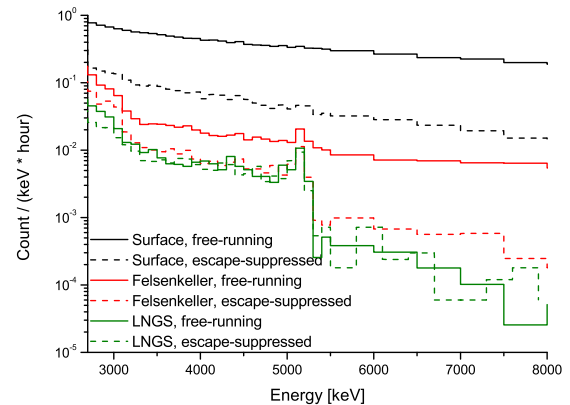


**Figure 1.** The high energy part (above the natural gamma lines) of the measured laboratory background spectra. LNGS spectra are taken from [3].

In summary, using an active shield in a shallow underground environment, a background level comparable to that of a deep underground laboratory can be reached.

Further details about the laboratory background investigations can be found in [5].

T.S. acknowledges a Herbert Quandt fellowship at Technical University Dresden.

a) Helmholtz-Zentrum Dresden-Rossendorf (HZDR), Dresden, Germany

b) Verein für Kernverfahrenstechnik und Analytik (VKTA), Dresden, Germany

[1] Z. Elekes *et al.*, Nucl. Inst. Meth. A **503**, 580 (2003)

[2] M. Köhler *et al.*, Applied Radiation and Isotopes **67**, 736 (2009)

[3] T. Szücs *et al.*, Eur. Phys. J. A **44**, 513 (2010)

[4] <http://www.lngs.infn.it>

[5] T. Szücs, AIP Conf. Proc. **1213**, 246 (2010)

### 8.3 Beam divergence of the proton microprobe

*L.Z. Tóth, I. Rajta*

The scanning ion microprobe focuses the ion beam by three quadrupole lenses to the typical spot size of  $1\mu\text{m}$  [1]. It was already known that the divergence of the focussed beam is small, but the exact value was not necessary for previous applications. For some recent [2,3] and other planned experiments we needed quantitative values of the beam divergence. Therefore, we have decided to determine the beam divergence at the image plane.

First we have observed the changes of the beam size on a fluorescent screen (mounted on the XYZ manipulator of the microprobe), using a camera with a microscope, when the screen moved along the  $z$  axis, which is parallel to the beam. Knowing the change in beam diameter and the distance from the focal point we can give the divergence by simple angle calculation. This is illustrated on *Figure 1*. The object slit size and the image on the target spot (in focus) can be assumed to be negligible, the collimator slit size and the quadrupole triplet focussing properties determine the divergence. The beam scanning was turned off.

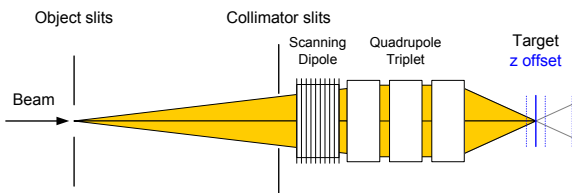


**Figure 1.** Schematic drawing of the experimental setup. The target was moved along the beam axis, the beam size and shape was recorded as a function of  $z$ .

We have performed the measurements in cases of the two most commonly used collimator slit sizes ( $50\mu\text{m}$  and  $400\mu\text{m}$ , i.e. the object plane divergence values of  $0.0005^\circ$  and  $0.004^\circ$ , respectively). The magnetic quadrupole lens produces different demagnifications and divergences in the  $x$  (horizontal) and  $y$  (vertical) di-

rections, so we have measured in both planes.

The evaluation has been carried out using a simple image-editing software. We have calculated the pixel size of the beam, and we also recorded a micrometer scale for calibration. The measurements showed that the divergence was so small that the maximum  $z$  offset of the target (about 9 mm) was not enough to determine the illuminated area accurately.

In the next series of experiments the fluorescent screen was placed at a fixed distance of 103.4 mm from the beam focal plane (i.e. the back flange of the target chamber), thus the beam was sufficiently expanded to perform a more accurate determination of the size of the rectangular illuminated area. The images clearly showed the  $y$  divergences being smaller than in the  $x$  plane, and the smaller collimator slit sizes resulting in smaller divergences. The results are summarized in *Table 1*.

**Table 1.** Beam divergence values for two typical collimator slit settings. The half divergence values are given.

	$\beta_x$	$\beta_y$
$50\mu\text{m}$	$0.0319\pm 0.0003^\circ$	$0.0103\pm 0.0003^\circ$
$400\mu\text{m}$	$0.2893\pm 0.0009^\circ$	$0.0886\pm 0.0003^\circ$

We have also performed theoretical model calculations by the PRAM software [4,5], and found a very good agreement.

- [1] I. Rajta et al, NIMB 109 (1996) 148
- [2] I. Rajta et al, Nanotechnology 21 (2010) 295704
- [3] I. Rajta et al, accepted for publication in NIMB
- [4] M.B.H. Breese, D.N. Jamieson, P.J.C. King: Materials Analysis using a nuclear microprobe, Wiley-Interscience, 1996
- [5] <http://www.ph.unimelb.edu.au/~dnj/research/pram/pramdist.htm>

## 8.4 The CHARISMA project in ATOMKI

*Z. Szikszai, L. Csedreki, E. Furu, Zs. Kertész, Á.Z. Kiss, I. Uzonyi and A. Simon*

CHARISMA (Cultural Heritage Advanced Research Infrastructures: Synergy for a Multidisciplinary Approach to Conservation / Restoration) is an EU-funded integrating activity project carried out in the FP7 Capacities Specific Programme “Research Infrastructures”. It started in 2009 and will end in 2013. The project provides transnational access (TNA) to advanced scientific instrumentations and knowledge allowing scientists, conservators-restorers and curators to enhance their research at the field forefront.

- **ARCHLAB** permits the access to the structured scientific information and analytical data, stored in the archives of the most prestigious European museums and conservation institutions.
- **MOLAB** offers access to a portable set of advanced analytical equipment, for in-situ non-invasive measurements on artworks.
- **FIXLAB** provides access to large and medium scale European installations, including the beamlines of one synchrotron radiation, one neutron source and two ion-beam analytical facilities.

Access to these facilities is offered free of charge to users working in the EC Member and Associated States, particularly to first-time users, and granted on the basis of project proposals which are reviewed and evaluated through a Peer Review selection. Calls are published twice a year on the CHARISMA website and the local websites of the institutions.

The Laboratory of Ion Beam Applications in ATOMKI-HAS is equipped with a

5 MV Van de Graaff electrostatic accelerator, as well as ion beam analytical facilities and instruments. The assortment of ion beams and their energy range makes it possible to apply most of the non-invasive ion beam analytical techniques used for the study of cultural heritage. The following methods are available: Particle Induced X-ray Emission technique (PIXE), Rutherford Backscattering Spectrometry (RBS), Particle Induced Gamma-ray Emission technique (PIGE), Nuclear Reaction Analysis (NRA), Elastic Recoil Detection Analysis (ERDA) and Scanning Transmission Ion Tomography (STIM). The expected fields of study are: a) materials alterations on samples (origin, products and mechanisms); b) provenance studies; c) characterization of micro-details of altered or unaltered materials e.g. to prevent further damage; d) studying of the manufacturing techniques for a contribution to art-historical studies; e) characterisation of the artwork conservation state or the effectiveness of a conservation treatment.

In 2010 seven projects were carried out within the CHARISMA TNA service in ATOMKI. The guest researchers arrived from Bulgaria, Germany, Greece, Finland and Romania. The investigated artefacts included nephrite axes and chisels from the Neolithic era, bronze and copper objects as well as gem stones (joint access project with the Budapest Neutron Centre) from the Bronze Age, antique pottery, decorative metal objects from the Middle Ages and pre-modern glass. In all cases major, minor and trace elements were quantified. In most of the cases the use of the ion microprobe was indispensable due to the heterogeneity and microstructure of the samples. The publication of the results is under way.

For further information about the CHARISMA project please visit:

<http://iba.atomki.hu/charisma/index.html>

or

<http://www.charismaproject.eu/transnational-access/fixlab/fixlab-welcome-desk.aspx>

## 9.1 Events

### **Physicists' Days** – Physics and Medicine

1-5 March 2010

Balázs Rózsa: *3D brain research*

Ervin Berényi: *Medical imaging from Atomki to the patients*

Zoltán Nusser: *How do nerves communicate*

Dezső Beke: *How can physics help in improving dental materials: nanoreactions between metals and ceramics*

### **RadiCal Workshop** Project No. 231753

Development of an Innovative, Accurate, Monolithic 2D CVD Diamond Based Radiation Dosimetry System for Conformal Radiotherapy Solutions.

11 May 2010

### **Researchers' Night**

24 September 2010

**Hungarian-Japanese Joint Working Seminar** on Studies of Fundamental Parameter Database and Atomic Processes for High Precision Quantitative Analysis using X-Ray Photoelectron Spectroscopy (in the frame of the bilateral MTA-JSPS scientific research cooperation project)

27 October 2010

**Informal workshop** on the  ${}^3\text{He}(\alpha,\gamma){}^7\text{Be}$  reaction

4 November 2010

## 9.2 Hebdomadal Seminars

January 20

Elementary composition study with the help of a secondary neutral mass spectrometer;  
Thermal stability and structural changes of hydrogenated amorphous Si/Ge multilayers  
(Institute habilitation)  
A. Csik

February 11

Novel  $^{11}\text{C}$ -radioisotope method for the study of heterogen catalysis;  
introduction of mini-PET-imaging to study chemically active surfaces  
É. Pribóczy

February 18

Supersymmetric particles and the LHC  
T. Fényes

February 25

The CHARISMA FP7 I3 project  
A. Simon

April 15

Anderson localisation on the quark-gluon plasma  
T. Kovács (University of Pécs)

April 19

State of affairs  
Zs. Fülöp, M. Pálinkás, B. Sulik, J. Molnár

May 20

Software methods and their applications on nuclear imaging  
on the fields of cardiology, small animal PET and education  
I. Valastyán

May 25

Comparison of the direct and indirect techniques for some CNO cycle reactions  
A.M. Mukhamedzhanov (Cyclotron Institute, Texas A&M University)

May 27

Optical applications in the cell physiology research  
L. Csernoch (University of Debrecen)

June 1

Specific structure of light neutron-rich nuclei  
N. Itagaki (Kyoto University)

June 8

Explosive hydrogen burning: experimental program at TUM  
S. Bishop (TU München)

June 10

Gravity on Earth and Moon - R. Eötvös and the outreach  
Gy. Radnai (Eötvös Loránd University, Budapest)

June 17

Basic and applied nuclear physics research program at iThemba LABS (National Research Foundation, South Africa)  
R. Newman (iThemba LABS, South Africa)

June 24

Radiopharmaceutical research at NECSA, South Africa  
Z. Szűcs

August 26

Electron scattering and transport in nanostructures  
K. Varga (Vanderbilt University, Nashville, Tennessee)

- August 31  
Asymmetrical photoelectron emission in the photon-atom and photon-H<sub>2</sub>-molecule interactions  
S. Ricz
- September 2  
Open session of the Atomki Advisory Board
- September 10  
Young scientists reports  
E. Bene, J. Farkas, P. Salamon
- September 16  
Climatic changes: data, magnitudes, models  
Z. Rácz (HAS Theoretical Physics Research Group at Eötvös Loránd University, Budapest)
- September 21  
Separation of nuclear reaction theory and spectroscopic factors  
A.M. Mukhamedzhanov (Cyclotron Institute, Texas A&M University)
- October 5  
Applications of symplectic symmetries in the nuclear structure  
A.I. Georgieva (Institute Of Nuclear Research And Nuclear Energy, Sofia)
- October 7  
Introduction of new colleagues in Atomki  
C. Bordeanu, E.B. Búzás, A. Bükki-Deme, P. Herczku, I. Hornyák, J. Karancsi,  
S. Kovács, I. Major, L. Stuhl, Zs. Török, Zs. Vajta
- October 13  
The ELI programme and its scientific challenges  
K. Osvay (University of Szeged)
- October 21  
Physics of hypernuclei  
T. Fényes
- October 28  
Mathematical resonance theory  
I. Horváth
- November 11  
Entropy, gravity and quantum  
T.S. Biró (Research Institute for Particle and Nuclear Physics, Budapest)
- November 23  
Information causality in the quantum world;  
Nonlocality of Werner states  
(Institute habilitation)  
T. Vértesi
- November 25  
In the tracks of alien worlds  
L. Kiss (HAS Konkoly Observatory)
- December 3  
Experimental determination of IMFP with EPES method in the energy range 0.2 - 5 keV in conducting polymers  
and III - V semiconductors;  
Determination of chemical state of very small surface atomic concentrations of different materials  
using electronspectroscopic techniques of XPS and XAES  
(Institute habilitation)  
J. Tóth
- December 16  
Physicists view of climatic changes - a second approach  
D. Berényi

### 9.3 Awards

Dénes Berényi

Honorary Degree (honoris causa), Babeş-Bolyai University, Cluj-Napoca (Kolozsvár), Romania

Sándor Biri

Roland Eötvös Physical Society: Pál Selényi Award

Zsolt Fülöp

Debrecen City Council: Hatvani Award

János Gál

Roland Eötvös Physical Society: Sándor Szalay Award

Rezső Lovas

Debrecen City Council: Honorary Freeman of the City of Debrecen (Debrecen Város Díszpolgára)

Mihály Novák

HAS Young Scientists' Award

László Palcsu and Péter Salamon

Atomki Young Scientists' Award

Zoltán Pécskay

Romanian Geological Society: Award of Merit

Romanian Academy of Sciences: Ludovic Mrazec Award

Endre Somorjai

HAS József Eötvös Wreath

Ferenc Tárkányi

Atomki: Sándor Szalay Award

## 9.4 List of Publications

The total number of publications in 2010 was 389, of which 203 SCI papers, 176 other papers and proceedings, 2 theses, 4 diploma works, 2 books or book chapters and 2 edited works.

The list of the Institute's publications can be found on-line at:  
<http://www.atomki.hu/p2/years/yea02010.htm>

### 9.4.1 Highlights

During the summer of 2010 we have decided to identify one paper every month as highlights. The first four papers in this series were the following:

5 July 2010

Nanochannel alignment analysis by scanning transmission ion microscopy

**Nanotechnology** 21, 295704 (2010)

*I. Rajta, G.A.B. Gál, S.Z. Szilasi, Z. Juhász, S. Biri, M. Mátéfi-Tempfli and S. Mátéfi-Tempfli*

30 August 2010

Interference effect in the dipole and nondipole anisotropy parameters of the Kr  $4p$  photoelectrons in the vicinity of the Kr  $(3d)^{-1} \rightarrow np$  resonant excitations

**Phys. Rev. A** 81, 043416 (2010)

*S. Ricz, T. Ricsóka, K. Holste, A. Borovik Jr., D. Bernhardt, S. Schippers, Á. Kövér, D. Varga, A. Müller*

15 October 2010

An exactly solvable Schrödinger equation with finite positive position-dependent effective mass

**Journal of Mathematical Physics** 51, 092103 (2010)

*G. Lévai, O. Özer*

24 November 2010

Reactor Decay Heat in  $^{239}\text{Pu}$ : Solving the  $\gamma$  Discrepancy in the 4–3000-s Cooling Period

**Phys. Rev. Lett.** 105, 202501 (2010)

*A. Algora, D. Jordan, J. L. Taín, B. Rubio, J. Agramunt, A. B. Perez-Cerdan, F. Molina, L. Caballero, E. Nácher, A. Krasznahorkay, M. Hunyadi, J. Gulyás, A. Vitéz, M. Csatlós, L. Csige, J. Äystö, H. Penttilä, I. D. Moore, T. Eronen, A. Jokinen, A. Nieminen, J. Hakala, P. Karvonen, A. Kankainen, A. Saastamoinen, J. Rissanen, T. Kessler, C. Weber, J. Ronkainen, S. Rahaman, V. Elomaa, S. Rinta-Antila, U. Hager, T. Sonoda, K. Burkard, W. Hüller, L. Batist, W. Gelletly, A. L. Nichols, T. Yoshida, A. A. Sonzogni, and K. Peräjärvi*

**A short summary of these papers can be found on the next pages.**

# Nanochannel alignment analysis by scanning transmission ion microscopy

*I. Rajta*<sup>1</sup>, *G.A.B. Gál*<sup>1</sup>, *S.Z. Szilasi*<sup>1</sup>, *Z. Juhász*<sup>1</sup>, *S. Biri*<sup>1</sup>,  
*M. Mátéfi-Tempfli*<sup>2</sup> and *S. Mátéfi-Tempfli*<sup>2</sup>

<sup>1</sup> Institute of Nuclear Research of Hungarian Academy of Sciences, Debrecen, P.O. Box 51, H-4001, Hungary

<sup>2</sup> Institutue of Condensed Matter and Nanosciences, Université Catholique de Louvain,  
Place Croix du Sud, 1, bâtiment Boltzmann a1, bte 3, B-1348 Louvain-la-Neuve, Belgium

**Nanotechnology 21, 295704 (2010)**

In this paper a study on the ion transmission ratio of a nanoporous alumina sample is presented.

The hexagonally close-packed  $\text{Al}_2\text{O}_3$  nanocapillary array, realized as a suspended membrane of  $15\ \mu\text{m}$  thickness, had pore diameters of  $\sim 215\ \text{nm}$  and interpore distances of  $\sim 450\ \text{nm}$ . The perfect hexagonal order is valid only inside typical domains of  $1\text{-}10\ \mu\text{m}$  lateral size. The scanning electron microscope (SEM) images reveal errors in this arrangement along the domain boundaries.

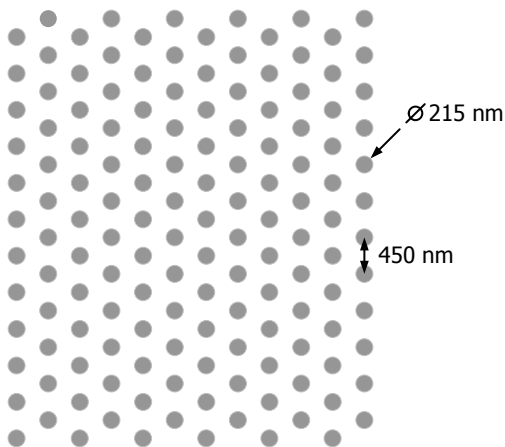


**Figure 1.** Schematic top view of the sample. The perfect hexagonal order is valid only inside  $1\text{-}10\ \mu\text{m}$  sized domains.

The sample has been investigated by scanning transmission ion microscopy (STIM) with

different beam sizes. When the proton beam size was limited to a single domain, a peak transmission ratio of 19% has been observed as is expected from the geometry ( $\sim 19\text{-}20\%$ ). This result points out an almost perfectly parallel alignment of the capillaries within one domain. However, for larger beam scanning areas (sampling multiple domains) the transmission ratio has been reduced to 5%. The STIM analysis over an area larger than the typical domain size has revealed an overall capillary angular spread of  $\sim 2^\circ$ .

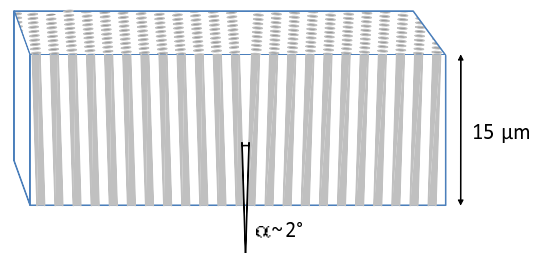


**Figure 2.** Schematic side view of the sample.

The video below [1] shows the STIM transparency as a function of sample tilt angle to the beam. The lighter pixels indicate higher transparency, i.e. the domains in which the nanocapillaries are aligned to the beam direction.

This paper started the “Highlights” (also known as “Paper of the month”) section of the Atomki website.

[1] <http://www.youtube.com/watch?v=u4y3sbi3b8I>

## Interference effect in the dipole and nondipole anisotropy parameters of the Kr $4p$ photoelectrons in the vicinity of the Kr $(3d)^{-1} \rightarrow np$ resonant excitations

*S. Ricz*<sup>1</sup>, *T. Ricsóka*<sup>1</sup>, *K. Holste*<sup>2</sup>, *A. Borovik Jr.*<sup>2</sup>, *D. Bernhardt*<sup>2</sup>, *S. Schippers*<sup>2</sup>, *Á. Kövér*<sup>1</sup>, *D. Varga*<sup>1</sup>, *A. Müller*<sup>2</sup>

<sup>1</sup> Institute of Nuclear Research of Hungarian Academy of Sciences, Debrecen, P.O. Box 51, H-4001, Hungary

<sup>2</sup> Institute for Atomic and Molecular Physics, Justus-Liebig University Giessen, D-35392 Giessen, Germany

**Physical Review A 81, 043416 (2010)**

In this paper we presented our new results on the angular distribution of the Kr  $4p$  photoelectrons. The photoelectrons were investigated in the photon energy range of the  $(3d)^{-1} \rightarrow np$  resonant excitations. The experimental dipole ( $\beta$ ) and non-dipole ( $\gamma$  and  $\delta$ ) anisotropy parameters were determined for the spin-orbit components of the Kr  $4p$  shell in function of the photon energy. A simple theoretical model was developed for the description of the photoionization and the resonant excitation processes. The measured dipole parameters were compared with the present model calculations. Both the measurement and the theoretical estimation show that the angular distribution of photoelectrons is strongly influenced by the excitation processes. The difference between the measured and calculated photon energy dependence of the dipole anisotropy parameters demonstrates the presence of interference between the direct ionization and the resonantly excited participator Auger decay processes. Similar effects were observed for the  $\gamma$  non-dipole anisotropy parameters where

the interference was more pronounced. This is the first study for the non-dipole anisotropy parameters where the interference between the direct and non-direct photoionization channels was observed.

The experiment was performed at the beam line BW3 of the third generation DORIS III storage ring at HASYLAB, Hamburg, Germany. The operating energy of this synchrotron is 4.45 GeV and both electrons and positrons can be used for creating synchrotron radiation. The emitted electrons, originated from photon-atom collisions, were analyzed using the ESA-22D electrostatic electron spectrometer developed in Debrecen. The spectrometer consists of a spherical and a cylindrical mirror analyzer. The spherical mirror focuses the electrons from the scattering plane to the entrance slit of the cylindrical analyzer which then performs the energy analysis of the electrons. The photoelectrons were detected simultaneously with 22 channeltrons between  $0^\circ$  and  $360^\circ$  (except  $90^\circ$  and  $180^\circ$ ) relative to the polarization vector.

## An exactly solvable Schrödinger equation with finite positive position-dependent effective mass

*G. Lévai*<sup>1)</sup>, *O. Özer*<sup>2)</sup>

<sup>1</sup> Institute of Nuclear Research of Hungarian Academy of Sciences, Debrecen, P.O. Box 51, H-4001, Hungary

<sup>2</sup> Department of Engineering Physics, Faculty of Engineering, University of Gaziantep, 27310 Gaziantep, Turkey

**Journal of Mathematical Physics 51, 092103 (2010)**

The exact solutions of the Schrödinger equation that describes the dynamics of quantum mechanical systems play an important role in the interpretation of the phenomena of the subatomic world. Typically exact solutions are obtained for problems modelled by one-dimensional potentials. Results obtained in this field have been applied recently to describe problems defined with position-dependent effective mass, which occur in various branches of physics. However, for most of these exactly solvable problems the formalism is compatible only with mass functions that take on zero and/or infinite value in certain points. This fact obviously limits the range of applicability of these models to realistic physical prob-

lems. We pointed out that by suitable generalization of the formalism exact results can be obtained also for problems associated with mass functions that are finite and positive everywhere. As an example we presented a four-parameter potential that carries the characteristics of both the harmonic oscillator and the Morse potential, while the mass function varies monotonously between two asymptotic values. We also discussed further possible generalizations of the method.

This work was supported by a three-month MTA-TÜBİTAK fellowship awarded to the Turkish co-author, after he initiated collaboration with the Hungarian side.

## Reactor Decay Heat in $^{239}\text{Pu}$ : Solving the $\gamma$ Discrepancy in the 4–3000-s Cooling Period

A. Algora<sup>1,2</sup>), D. Jordan<sup>1</sup>), J.L. Tañá<sup>1</sup>), B. Rubio<sup>1</sup>), J. Agramunt<sup>1</sup>), A.B. Perez-Cerdan<sup>1</sup>), F. Molina<sup>1</sup>), L. Caballero<sup>1</sup>), E. Nácher<sup>1</sup>), A. Krasznahorkay<sup>2</sup>), M.D. Hunyadi<sup>2</sup>), J. Gulyás<sup>2</sup>), A. Vitéz<sup>2</sup>), M. Csatlós<sup>2</sup>), L. Csige<sup>2</sup>), J. Áysto<sup>3</sup>), H. Penttilä<sup>3</sup>), I.D. Moore<sup>3</sup>), T. Eronen<sup>3</sup>), A. Jokinen<sup>3</sup>), A. Nieminen<sup>3</sup>), J. Hakala<sup>3</sup>), P. Karvonen<sup>3</sup>), A. Kankainen<sup>3</sup>), A. Saastamoinen<sup>3</sup>), J. Rissanen<sup>3</sup>), T. Kessler<sup>3</sup>), C. Weber<sup>3</sup>), J. Ronkainen<sup>3</sup>), S. Rahaman<sup>3</sup>), V. Elomaa<sup>3</sup>), S. Rinta-Antila<sup>3</sup>), U. Hager<sup>3</sup>), T. Sonoda<sup>3</sup>), K. Burkard<sup>4</sup>), W. Hüller<sup>4</sup>), L. Batist<sup>5</sup>), W. Gelletly<sup>6</sup>), A.L. Nichols<sup>6</sup>), T. Yoshida<sup>7</sup>), A.A. Sonzogni<sup>8</sup>) and K. Peräjärvi<sup>9</sup>)

<sup>1</sup> IFIC (CSIC-Univ. Valencia), Valencia, Spain

<sup>2</sup> Institute of Nuclear Research, Debrecen, Hungary

<sup>3</sup> University of Jyväskylä, Jyväskylä, Finland

<sup>4</sup> GSI, Darmstadt, Germany

<sup>5</sup> PNPI, Gatchina, Russia

<sup>6</sup> University of Surrey, Guildford, United Kingdom

<sup>7</sup> Tokyo City University, Setagaya-ku, Tokyo, Japan

<sup>8</sup> NNDC, Brookhaven National Laboratory, Upton, New York, USA

<sup>9</sup> STUK, Helsinki, Finland

### Phys. Rev. Lett. 105, 202501 (2010)

In a working nuclear reactor (normal operation) less than 10 % of the released energy is related to the beta decay of the fission products. This source of energy, commonly called “decay heat” becomes the dominant one after reactor shutdown.

Proper estimation of the decay heat is a very important factor in the design and operation of nuclear reactors as well as for the handling and disposing nuclear waste. It is interesting from the historical point of view that one of the first methods used to evaluate the decay heat is based on a work of Way and Wigner using statistical considerations (*Phys. Rev* 73, 1318 (1948)).

Nowadays the most extended method for decay heat calculations is the so-called summation calculations. In this method the decay heat is calculated summing the activities (decays/second) of the fission products (produced during the fission process and after shutdown) times the energy released in the beta decay. This apparently simple method depends on the available nuclear data.

Uncertainties in nuclear data used in sum-

mation calculations lead to excessive margins for safety. This is why it is important to have a precise assessment of decay energies. In our recent article, we have combined for the first time three techniques to study the beta decay of important contributors to the decay heat in  $^{239}\text{Pu}$  fuel. The used techniques were: 1) total absorption, which is a detection technique, that provides beta decay data free of the so-called Pandemonium systematic error, 2) the IGISOL technique, used to produce refractory elements that can not be obtained easily in conventional RIB facilities, 3) and finally the JYFLTRAP, a Penning Trap, that was used as a mass separator to provide radioactive beams of high purity for the measurements. With the combination of these techniques we have been able to solve a large part of a long-standing discrepancy that existed between experiment and summation calculations for the  $^{239}\text{Pu}$  fuel.  $^{239}\text{Pu}$  provides approximately 30-40 % of the total energy in a nuclear reactor.

A Viewpoint article has been published about this paper in *Physics* 3, 94 (2010).

## Index

- Agnihotri A.N., 52  
Agramunt J., 94  
Aiba T., 34  
Aigner F., 69  
Algora A., 40, 94  
Ander I., 79, 80  
Angyal A., 77, 78  
Aoi N., 34  
Arbó D.G., 47  
Attolini G., 62  
Äysto J., 94  
Ayyad A., 66
- Baba H., 34  
Bacchus-Montabonel M.C., 53  
Batist L., 94  
Bednarczyk P., 40  
Bemmerer D., 34, 83  
Bene E., 53  
Bereczky R.J., 65, 66  
Bernhardt D., 92  
Berzi I., 80  
Bihari Á., 1, 72, 73  
Biri S., 54, 59, 80, 91  
Bodewits E., 58  
Borbély S., 47, 48  
Bordeanu C., 37  
Borovik Jr. A., 92  
Bosi M., 62  
Boston A.J., 41, 44  
Brown B. A., 34  
Bujtás T., 72  
Burkard K., 94  
Burgdörfer J., 69
- Caballero L., 94  
Calicchio M., 62  
Chantler H.C., 41, 44  
Charlton M., 46  
Chatterjee S., 52  
Chen T., 68  
Chesnel J.-Y., 60  
Chiara C.J., 41, 44  
Choudhury R.K., 52  
Corniani E., 67  
Cromaz M., 41, 44  
Csatlós M., 94  
Csedreki L., 78, 85  
Cseh J., 39  
Cserny I., 64  
Csige L., 94  
Csik A., 61–64, 68  
Curien D., 40
- Dang H.M., 58  
Daróczy L., 78  
Das S., 65, 66  
Dassanayake, 65, 66  
Degering D., 83  
Dimitriou K.I., 47  
Ding Z.J. , 68  
Ditrói F., 67  
Dombrádi Zs., 34, 40  
Drube W., 64  
Duchene G., 40
- Elekes Z., 34, 38, 83  
Elomaa V., 94  
Enomoto Y., 46  
Eronen T., 94  
Errea L.F., 53
- Fallon P., 41, 44  
Farkas J., 37, 38, 49  
Fenyvesi A., 79  
Ferrari C., 62  
Fossan D.B., 40, 41, 44  
Frémont F., 60  
Frankland B.S., 60  
Frigeri C., 61, 62  
Fülöp Zs., 33, 34, 37, 38, 83  
Furu E., 77, 78, 85  
Furumoto T., 34  
Futó I., 1, 76
- Gácsi Z., 80  
Gál G.A.B., 91  
Gál J., 40  
Galaviz D., 33  
Gelletly W., 94  
Georgescu I., 46  
Gizon A., 40  
Gizon J., 40  
Gräfe S., 69

Gravielle M.S., 47  
 Gulyás J., 94  
 Gulyás L., 51  
 Güray R.T., 38  
 Gyürky Gy., 33, 37, 38, 49, 83  
  
 Hager U., 94  
 Hakala J., 94  
 Halász G.J., 53  
 Halász Z., 37, 38  
 Hecht A.A., 41, 44  
 Hellhammer R., 58  
 Herczku P., 55, 57  
 Hoekstra R., 58  
 Holste K., 92  
 Horváth L.L., 57  
 Hüller W., 94  
 Hunniford C.A., 46  
 Hunyadi M., 80, 94  
  
 Igarashi A., 51  
 Itagaki N., 39  
 Iwasa N., 34  
  
 Janovics R., 1, 70, 72  
 Jech M., 67  
 Jenkins D.G., 40  
 Jokinen A., 94  
 Jordan D., 94  
 Joshi P., 40  
 Juhász Z., 57–60, 91  
  
 Kanai Y., 46  
 Kanalas P., 79  
 Kankainen A., 94  
 Karvonen P., 94  
 Kasthurirangan S., 52  
 Kertész Zs., 77, 78, 85  
 Kessler T., 94  
 Khánh N.Q., 61  
 Kim C.H., 46  
 Kimák Á., 71  
 Kirchner T., 51  
 Kiss Á., 34  
 Kiss Á.Z., 85  
 Kiss G.G., 33, 38  
 Knudsen H., 46  
 Kobayashi K., 34  
 Köhler M., 83  
 Koike T., 40, 41, 44  
  
 Kondo Y., 34  
 Kormány Z., 80  
 Kovács B., 73  
 Kovács J., 31  
 Kovács S.T.S., 56, 57  
 Kövér Á., 92  
 Kövér L., 64  
 Krasznahorkay A., 40, 94  
 Kristiansen H.-P.E., 46  
 Kumar A., 52  
 Kuroda N., 46  
 Kuti I., 40, 41, 44  
  
 Langer G.A., 63  
 Lee I.Y., 41, 44  
 Lemell C., 69  
 Lévai G., 30, 93  
 Lovics R., 63  
 Lund M.D., 46  
  
 Macchiavelli A.O., 41, 44  
 Major I., 1, 71  
 Major Z., 1, 72, 75  
 Marta M., 83  
 Mátéfi-Tempfli M., 91  
 Mátéfi-Tempfli S., 91  
 McCullough R.W., 46  
 Méndez L., 53  
 Mészáros I., 79  
 Miraglia J.E., 47  
 Misra D., 52  
 Mogyorósi M., 1, 73  
 Mohr P., 33  
 Molina F., 94  
 Molnár J., 40  
 Molnár M., 1, 70, 71  
 Moore I.D., 94  
 Motobayashi T., 34  
 Müller A., 92  
  
 Náchér E., 94  
 Nagy L., 48  
 Nagy S., 31, 32  
 Nagy T., 71  
 Nakabayashi T., 34  
 Nándori I., 31, 32  
 Nannichi T., 34  
 Nichols A.L., 94  
 Nieminen A., 94

Oláh V., 79  
 Özer O., 93  
 Özkan N., 38  
  
 Palcsu L., 1, 72, 75, 76  
 Pálinkás J., 54, 59  
 Papp L., 1, 72, 75  
 Paul E.S., 40, 41, 44  
 Penttilä H., 94  
 Peräjärvi K., 94  
 Perez-Cerdan A.B., 94  
 Ploszajczak M., 39  
  
 Rabadán I., 53  
 Rác A., 36  
 Rác R., 54, 80  
 Raddon P.M., 40  
 Rahaman S., 94  
 Rainovski G., 40  
 Rajta I., 83, 91  
 Rangama J., 60  
 Rauscher T., 38  
 Ricz S., 92  
 Ricsóka T., 92  
 Rinta-Antila S., 94  
 Rinyu L., 1, 70  
 Rissanen J., 94  
 Ronkainen J., 94  
 Rossi F., 62  
 Rubio B., 94  
  
 Saastamoinen A., 94  
 Sailer K., 31, 32  
 Sakuragi Y., 34  
 Sarkadi L., 50–52  
 Scheurer J.N., 40  
 Schippers S., 92  
 Schüller A., 69  
 Serényi M., 61  
 Simon A., 85  
 Simons A.J., 40  
 Sohler D., 34, 40, 41, 44  
 Somorjai E., 33, 37, 38  
 Sonoda T., 94  
 Sonzogni A.A., 94  
 Starosta K., 40, 41, 44  
 Stolterfoht N., 58, 59  
 Sulik B., 57–60  
 Svingor É., 1, 75  
 Synal H.A., 70, 71  
  
 Szántó Zs., 76  
 Szikszai Z., 77, 78, 85  
 Szilasi S.Z., 91  
 Szoboszlai Z., 77, 78  
 Szöllősi E., 79  
 Szücs T., 37, 38, 83  
 Szűcs Z., 73  
  
 Taín J.L., 94  
 Takács S., 67  
 Takashina M., 34  
 Takáts V., 63  
 Tárkányi F., 67  
 Takeuchi S., 34  
 Tanaka K., 34  
 Tang T., 68  
 Tanis, 65, 66  
 Thiess S., 64  
 Timár J., 40, 41, 44  
 Tiwald P., 69  
 Togano Y., 34  
 Torii H.A., 46  
 Tóth J., 68  
 Tóth L.Z., 84  
 Tőkési K., 46–48, 59, 65, 66, 68, 69  
 Tribedi L. C., 52  
 Trombettoni A., 32  
  
 Uggerhoj U.I., 46  
 Uzonyi I., 85  
  
 Vad K., 62, 63  
 Vajta Zs., 34  
 Vaman C., 40  
 Varga D., 92  
 Veres M., 70–72  
 Vertse T., 36  
 Vibók Á., 53  
 Vitéz A., 94  
 Vodila G., 1, 76  
  
 Wacker L., 70, 71  
 Wadsworth R., 40, 41, 44  
 Weber C., 94  
 Wilkinson A.R., 40  
 Winter H., 69  
 Wopelka T., 67  
  
 Yalçın C., 38  
 Yamada K., 34

Yamaguchi M., 34

Yamazaki Y., 46

Yoneda K., 34

Yoshida T., 94

Zhang Z.M., 68

Zolnai L., 40

Zolnai Zs., 62